Mathematical Modeling of Novel Cancer Immunotherapies

by

Elpiniki Nikolopoulou

A Dissertation Presented in Partial Fulfillment
of the Requirements for the Degree
Doctor of Philosophy

Approved May 2020 by the
Graduate Supervisory Committee:

Yang Kuang, Chair
Carl Gardner
Jana Gevertz
Yun Kang
Eric Kostellich

ARIZONA STATE UNIVERSITY

August 2020

ABSTRACT

Immunotherapy has received great attention recently, as it has become a powerful tool in fighting certain types of cancer. Immunotherapeutic drugs strengthen the immune system's natural ability to identify and eradicate cancer cells. This work focuses on immune checkpoint inhibitor and oncolytic virus therapies. Immune checkpoint inhibitors act as blocking mechanisms against the binding partner proteins, enabling T-cell activation and stimulation of the immune response. Oncolytic virus therapy utilizes genetically engineered viruses that kill cancer cells upon lysing. To elucidate the interactions between a growing tumor and the employed drugs, mathematical modeling has proven instrumental. This dissertation introduces and analyzes three different ordinary differential equation models to investigate tumor immunotherapy dynamics.

The first model considers a monotherapy employing the immune checkpoint inhibitor anti-PD-1. The dynamics both with and without anti-PD-1 are studied, and mathematical analysis is performed in the case when no anti-PD-1 is administrated. Simulations are carried out to explore the effects of continuous treatment versus intermittent treatment. The outcome of the simulations does not demonstrate elimination of the tumor, suggesting the need for a combination type of treatment.

An extension of the aforementioned model is deployed to investigate the pairing of an immune checkpoint inhibitor anti-PD-L1 with an immunostimulant NHS-muIL12. Additionally, a generic drug-free model is developed to explore the dynamics of both exponential and logistic tumor growth functions. Experimental data are used for model fitting and parameter estimation in the monotherapy cases. The model is utilized to predict the outcome of combination therapy, and reveals a synergistic effect: Compared to the monotherapy case, only one-third of the dosage can successfully control the tumor in the combination case.

Finally, the treatment impact of oncolytic virus therapy in a previously developed and fit model is explored. To determine if one can trust the predictive abilities of the model, a practical identifiability analysis is performed. Particularly, the profile likelihood curves demonstrate practical unidentifiability, when all parameters are simultaneously fit. This observation poses concerns about the predictive abilities of the model. Further investigation showed that if half of the model parameters can be measured through biological experimentation, practical identifiability is achieved.

To my grandpa and the star in my sky, my grandma

ACKNOWLEDGMENTS

First and foremost, I would like to thank my advisor Dr. Yang Kuang for his continuous support throughout my PhD. Dr. Kuang you have been instrumental in my success. Thank you for helping me realize my capabilities and encouraging me to pursue my desired career path.

I am exceedingly thankful to Dr. Jana Gevertz for her encouragement, patience and guidance. Jana, I am deeply grateful for all the time you have dedicated to my success and for all that you have taught me. I have enjoyed every second of the way working with you even though it was through long-distance. A big thank you to the rest of my committee members, Dr. Carl Gardner, Dr. Yun Kang and Dr. Eric Kostellich. Thank you for all your support and useful suggestions throughout my academic path.

I was so fortunate to have met Dr. Steffen Eikenberry, Dr. Ioannis Sgourallis, Dr. Sara Jamous and Lauren Dickman. Steffen thank you for always being willing to help and answer my questions. You have taught me so much! Ioannis thank you for all your help and for all our insightful mathematical discussions. Sara thank you for always being by my side throughout this journey and for sharing all your experiences. Lauren from the day we sat next to each other the first day at TA training I knew we would get through this together. Thank you for being a great collaborator, an office mate but above all a good friend.

I would also like to acknowledge three very important people in my academic journey, Dr. Katalin Kolossa, Joelle Park and Rhonda Olson. Katie thank you for supporting my journey as a TA and helping me improve my teaching skills. Joelle thank you for being so helpful and patient. Rhonda you have made such a difference in the math department! I am so grateful to have met you!

Thank you Dr. Jason Yalim for helping me adjust during my first years in graduate

school and for teaching me how to use Agave and the Research Computing at Arizona State University for providing HPC and storage resources that have contributed to the research results reported within this thesis.

Finally, none of this would have been possible without the support of my family, my friends and George. George thank you for your tremendous support and for navigating this journey with me. Thank you for always being there when I needed you. I would like to express my deepest gratitude to my parents for always believing in me, for always inspiring me to do my best and to never give up. Thank you to my sister for her unconditional love and for always being my rock through my stressful days.

TABLE OF CONTENTS

CHAPTER Page

CHAPTER Page

LIST OF TABLES

LIST OF FIGURES

Figure Page

Figure Page

Chapter 1

INTRODUCTION

1.1 Immunotherapy

Cancer is a significant burden worldwide in the 21st century. Common approaches for fighting cancer include radiation therapy, chemotherapy, and surgery (Rius and Lyko, 2012; Sharma *et al.*, 2017). However, at the forefront of cancer treatment is immunotherapy, which has shown great promise for certain types of cancer (Kaufman *et al.*, 2019). Specifically, in 2018 the Nobel prize was awarded to James P. Allison and Tasuku Honjo "for their discovery of cancer therapy by inhibition of negative immune regulation" (Press release, 2018).

Immunotherapy was originally introduced by Dr. Coley over 100 years ago (McCarthy, 2006). Immunotherapy is an umbrella term for methods that increase the potency of the immune response against cancer. Unlike other treatment modalities that directly attack the tumor, immunotherapy depends on the interplay between two complex systems: the tumor and the immune system (Kaufman *et al.*, 2019). Immunotherapy targets to deactivate the underlying mechanisms that the tumor cells are utilizing to suppress the immune system response (Disis, 2014).

Although immunotherapy has demonstrated positive effects, certain challenges still remain. One of the major obstacles is the uncertainty of treatment efficacy observed across patients (Ventola, 2017). Therefore, the discovery of new biomarkers revealing patient's response to the treatment is of paramount importance (Bailey *et al.*, 2014). On that front, the emerging field of precision and personalized medicine is demonstrating pathways for individualized and thus more efficient treat-

ment strategies leveraging patients' genetic profiles (Dumbrava and Meric-Bernstam, 2018). Additional challenges for immunotherapy are the toxicity levels induced by the administered drugs, the increasing tumor resistance to immunotherapy, and the lack of targeted experimental studies (Ventola, 2017).

Mathematical modeling is of particular importance as it assists in facing some of the challenges by providing the critical link among clinicians, data, and biologists. It formulates quantitative frameworks to gain better insights on cancer growth treatment response. Underlying mechanisms of cancer can be identified, enabling informed treatment procedures. Mathematical models are used to not only make predictions of cancer evolution that contribute to the design of new experiments but also to track patient response to therapies (Blair *et al.*, 2012). When the developed mathematical models are fitted against experimental data, crucial parameters describing the dynamics of the system are determined (Santiago *et al.*, 2017). Particularly in the field of immunotherapy, several mathematical models of varying complexity have been developed with the goal of advancing our biological understanding.

Immunotherapy consists of different types of treatments, such as checkpoint inhibitors, CAR-T cell therapy and cancer vaccines to name a few. Oncolytic virus (OV) therapy is another way to kill cancer cells and can be considered as a form of immunotherapy as long as genetically-engineered viruses act as cytokine-delivery vectors (Prestwich *et al.*, 2008). This dissertation focuses mainly on two treatments: the immune checkpoint inhibitors (anti-PD1 and anti-PD-L1) and the oncolytic virus therapy.

1.2 Immune Checkpoint Inhibitors

Immune checkpoints act as regulators of the immune system. Their role is extremely important as they provide balance between co-stimulatory and inhibitory

signals. This enables the immune system not to attack its own cells. However, cancer cells use escape mechanisms resulting in antitumor immune response suppression (Darvin *et al.*, 2018). They essentially nullify T cells' mechanisms, which in turn allows the cancer cells to roam in the system without being detected. The checkpoint inhibitor therapy provides a solution to this problem by blocking the signals induced by the cancer cells and reactivating the immune system.

This observation was first discovered by Leach, Krummel, and Allison (1996), who found that the protein cytotoxic T-lymphocyte-associated protein 4 (CTLA-4), which is expressed on the surface of activated T cells, inhibits the antitumor immune response when binding to B7 ligands. Therefore, developed therapies that target CTLA-4 have proven to boost the antitumor immune response showing clinical success across different types of tumor, including melanoma and renal cell carcinoma (Yang *et al.*, 2007). This seminal research revealed the existence of alternative inhibitory T cell pathways (Sharma and Allison, 2015).

Such an additional inhibitory pathway is based on the cell programmed death 1 (PD-1) protein, which is mainly found on the surface of activated T cells and was discovered by Ishida *et al.* (1992). Its ligand PD-L1 is expressed on both tumor cells and T cells (Talay *et al.*, 2009; Maute *et al.*, 2015). The interaction between PD-1 and PD-L1 leads to the formation of the PD-1-PD-L1 complex, which suppresses immune activation by preventing T cell activation and proliferation (Alsaab *et al.*, 2017). To combat the PD-1-PD-L1 complex formation, immune checkpoint inhibitors (anti-PD-1 and anti-PD-L1) were developed. A sketch demonstrating the biological mechanism of the immune checkpoint inhibitor therapy is depicted in Figure 1.1. In recent years, several pharmaceutical companies developed anti-PD-1 drugs (pembrolizumab by Merck, nivolumab by Bristol-Myers Squibb and cemiplimab by Regeneron Pharmaceuticals) and anti-PD-L1 drugs (atezolizumab by Roche Genen-

tech, avelumab by Merck Serono and Pfizer and durvalumab by AstraZeneca). Both antibodies that target PD-1 and PD-L1 respectively showed great clinical success for tumors such as bladder cancer (Powels *et al.*, 2014), melanoma, and non-small-lunger cancer (Topolian *et al.*, 2012). However, immune checkpoint inhibitors therapies may induce an immune response imbalance, which can cause side effects resembling auto-immune diseases. Such effects named immune-related adverse events (irAEs) include dermatologic, gastrointestinal, hepatic, endocrine events, and other toxicities (Naidoo *et al.*, 2015).

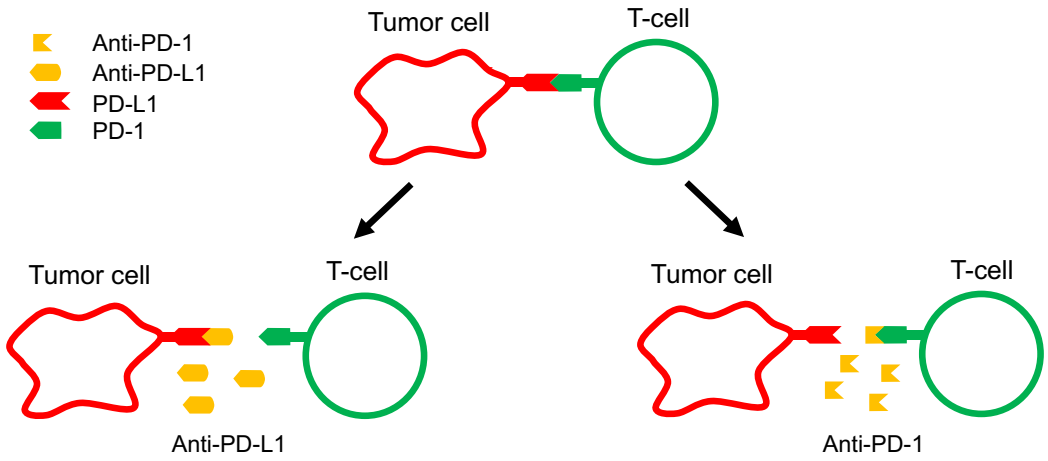

Figure 1.1: Immune checkpoint inhibitor therapy biological mechanism. Anti-PD-L1 drug is depicted on the left side and anti-PD-1 drug on the right side respectively. In the case of anti-PD-L1, antibodies bind to PD-L1, while in the case of anti-PD-1, antibodies bind to PD-1 with the goal to inhibit the PD-1/PD-L1 interaction.

1.3 Oncolytic Virus Therapy

The discovery of viruses as a potential way to destroy tumors originated at the beginning of the 19th century. However, great interest in this discovery was expressed over the past 30 years due to technological advancement (Kelly and Russel, 2007),

rendering oncolytic virus therapy a promising treatment strategy (Chiocca, 2002). Oncolytic virotherapy uses genetically engineered viruses that can infect both cancer and healthy cells. Once the healthy cells get infected, the inability of the virus to replicate results in sparing the healthy cells from the effects of the virus. On the contrary, the virus selectively replicates inside the cancer cells. Due to the exponential growth rate of the replication process, cancer cells are no longer able to support the viral load (Chiocca *et al.*, 2014). This causes the lysis effect, which bursts open the infected cells and allows the released virus to infect other cancer cells (Wond, Lemoine and Wang, 2010). This process is demonstrated in Figure 1.2.

One of the main drawbacks of oncolytic virus therapy is its temporary effectiveness due to the accelerated elimination of the virus by the immune system itself (Kim *et al.*, 2011). Recently, genetically engineered viruses are employed in a form of "Trojan Horses" delivering therapeutic molecules directly to the tumor site. Such therapies increase the ability of the immune system to identify tumor cells more efficiently (Melcher *et al.*, 2011). This significant progress has been observed in clinical trials, where a vast number of gene modified viruses such as adenovirus, measles, herpes simplex, Newcastle disease virus is utilized (Markert *et al.*, 2000; Csatary *et al.*, 2004; Garber, 2006).

1.4 Overview of Mathematical Modeling of Immune Checkpoint Inhibitor Therapy

The demonstrated potential of immune checkpoint inhibitor therapies has triggered several mathematical modeling efforts over the last few years (Azoury, 2015). The models focus on immune checkpoint inhibitors as a monotherapy and in combination with other treatments, which include radiation therapy, oncolytic virus therapy and dendritic cell vaccine (Serre *et al.*, 2016; Friedman and Lai, 2018; Radunskaya *et al.*, 2018).

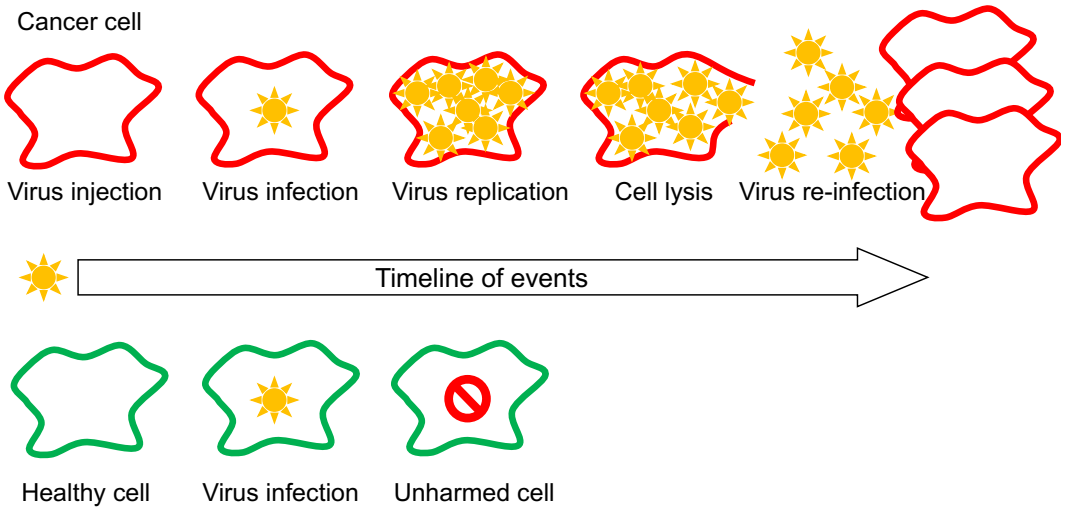

Figure 1.2: Oncolytic virus therapy biological mechanism. Once the virus is injected into the system, the cancer cells become infected in contrast to the healthy cells which are unharmed. Upon cancer cell infection, the virus replicates within the cancer cell. The viral replication load causes cancer cells to lyse. This results in the re-infection of other cancer cells.

Serre *et al.* (2016) first proposed a discrete time pharmacokinetic model, where they investigated the effects of combining immune checkpoint inhibitors with radiotherapy. The authors noted a synergistic effect between the combination treatments, and verified that their model resembles experimental studies qualitatively. Luksza *et al.* (2017) were one of the first to construct a fitness model that predicted immunotherapy success for both lung cancer and melanoma patients. The authors considered immune checkpoint inhibitors targeting neoantigens. Radunskaya *et al.* (2018) examined the combination of immune checkpoint inhibitors and dendritic cell vaccine with the goal of optimizing treatment.

Lai and Friedman have published a series of papers between $2017 - 2020$, where they investigated the combination of an immune checkpoint (anti-PD-1 or anti-PD-

L1) inhibitor with different treatments. These treatments include GM-CSF cancer vaccine (Lai and Friedman, 2017), BRAF/MEK inhibitor (Lai and Friedman, 2017a), oncolytic virus treatment (Friedman and Lai, 2018), BET and CTLA-4 inhibitors (Lai *et al.*, 2018), anti-VEGF inhibitor (Lai and Friedman, 2019) and radiation therapy (Lai and Friedman, 2020). Systems of partial differential equations were used to model these combinations. In the majority of their work they determined whether synergistic or antagonistic effects occurred for the different combinations, and demonstrated appropriate dosage levels required for tumor volume shrinkage (Lai and Friedman, 2019, 2017; Lai *et al.*, 2018).

1.5 Overview of Mathematical Modeling of Oncolytic Virus Therapy

Several mathematical modeling approaches have been carried out over the past years focusing on oncolytic virus therapy (OV), with a major inflection point happening in 2001 (Novozhilov *et al.*, 2006; Tian, 2011; Eftieme *et al.*, 2011; Wodarz, 2001). Particularly, Wodarz (2001) developed a simple ordinary differential equation model, where the author examined the effects of both virus-specific and tumor-specific cytotoxic T-lymphocytes (CTLs). The author established mathematical conditions and identified key parameters associated with the success of OV.

Two-dimensional differential equation systems that are studying the effects of OV therapy are also found in the literature. These models solely consider the population of uninfected and infected tumor cells (Novozhilov *et al.*, 2006; Wodarz and Komarova, 2009; Komarova and Wodarz, 2010). Using Wodarz (2001) work as basis, Karev, Novozhilov and Koonin (2006) presented a system of differential equations which accounted for tumor heterogeneity and identified the need for a heterogeneous population of oncolytic viruses. Both Wodarz and Komarova (2009) and Komarova and Wodarz (2010) mathematically analyzed the general case of the proposed model

seeking intuition into virus therapy success. They examined the effects of the rate at which the virus infects the tumor cells and concluded that potential tumor elimination can only be accomplished with "fast spread".

Although an increasing amount of mathematical models were proposed between $2001 - 2013$, none of the models accounted for intracellular viral lytic cycle delay. Wang, Tian and Wei (2013) was one of the first modeling efforts that more realistically described the viral lytic cycle in their model. The authors found that the viral lytic cycle is mainly influenced by the viral burst size. Wang, Guo and Smith (2019) not only incorporated the intracellular viral life-cycle employing a delay parameter but also added the virus-specific CTL response similar to Wodarz (2001). Using mathematical analysis, the authors obtained necessary conditions and strategies to decrease the total tumor size.

A limited amount of modeling attempts that include the syncytia formation are found in the literature. Syncytia are cells with multiple nuclei formed when mononucleated neighboring cells fuse together (Burton and Bartee, 2019). Examples of such models include Bajzer *et al.* (2008); Dingli *et al.* (2009). Dingli *et al.* (2006) work served as a basis for incorporation of syncytia formation term in Bajzer *et al.* (2008) model. A year later Dingli *et al.* (2009) added an equation to their model that accounted for the syncytia formation and used experimental data for validation. The common denominator between these models is that they revealed the possibility for tumor eradication and in some cases oscillatory behavior dependent on parameter ranges.

Finally, a series of mathematical models have been developed to boost the efficacy of OV response in combination with other treatments (Walker and Enderling, 2016). Specifically, Bagheri *et al.* (2011) explored the pairing of oncolytic adenovirus with MEK inhibitor and predicted that simultaneous administration of the treatments

increased efficacy. Wares *et al.* (2015) proposed a model that examines the combination between immuno-enhanced OV and a dendritic cell (DC) vaccine. The authors specifically examined the effects of varying the dosage levels of both therapies and additionally established the optimal sequence of administrating the drugs given constraints on dosage. In a more recent work, Gevertz and Wares (2018) simplified the model shown in Wares *et al.* (2015) and verified that the predictions and dynamics of the models are similar. A recently published work by Storey, Lawler and Jackson (2020) investigated the combination of OV with an immune checkpoint inhibitor (anti-PD-1) for glioblastoma including the innate and adaptive immune interactions. A combination therapy was proven to enable more immune conditions that support tumor size decrease or elimination compared to a single OV therapy.

1.6 Thesis Overview

The main motivation behind Chapter 2 originated from Lai and Friedman (2017). The authors presented a system of partial differential equations investigating the combination between the immune checkpoint inhibitor anti-PD-1 and the GM-CSF cancer vaccine. Their model provided insights on the synergistic administration of the two drugs. However, due to the complexity of the partial differential equations system proposed, any type of mathematical analysis is extremely difficult to perform.

This limitation has seeded my research presented in Chapter 2, where a simplification of Lai and Friedman (2017) using a system of ordinary differential equations is presented. Chapter 2 focuses on a monotherapy using the immune checkpoint inhibitor anti-PD-1. The objective is to achieve a simpler but adept model that allows mathematical analysis to be performed. The latter will lead to an increased biological understanding of the underlying mechanisms of the PD-1/PD-L1 pathway, as well as to other meaningful insights. As a starting point, the model is mathematically ana-

lyzed without the use of the immune checkpoint inhibitor anti-PD-1 and simulations are carried out to support the findings. Sensitivity analysis is employed to determine the parameters associated with tumor growth. Finally, the effect of intermittent and continuous dosage of anti-PD-1 on tumor-immune dynamics are studied. The results of this effort presented in Chapter 2 are used as the groundwork for the following investigations.

In Chapter 3, the combination of an immune checkpoint inhibitor with an alternative treatment is analyzed, since the monotherapy case is inadequate for sufficient T cell activation. The latter was confirmed by the work presented in Chapter 2 and is in line with clinical observations (Kang *et al.*, 2016). In Chapter 3, a modified version of the model in Chapter 2 is presented with two main differences: a) a combination treatment employing avelumab, an anti-PD-L1 drug, and the immunostimulant NHS-muIL12, and b) the use of anti-PD-L1 instead of anti-PD-1 treatment. The model validation and parameter estimation was performed utilizing the experimental data in Xu *et al.* (2017). At first, a generic form of the model without any treatments is constructed and this model is mathematically analyzed. Employing the conditions of the mathematical analysis of the generic model, two cases are further analyzed and their dynamics are studied: the logistic and the exponential tumor growth functions. Lastly, the synergistic effect between the two drugs (avelumab and NHS-muIL12) is investigated.

Data fitting of mathematical models presents challenges, due to limited and noisy experimental data. Some of these challenges were faced during the data fitting process in Chapter 3, which are explored in mode detail in Chapter 4. Using the model found in Wares *et al.* (2015) and Gevertz and Wares (2018) the goal is to comprehend the treatment impact of oncolytic virus therapy. However, in order to make reliable predictions, practical identifiability of all model parameters is vital. First, the fitting

methodologies for accurate parameter estimations are explored. Although Wares *et al.* (2015) uses a hierarchical fitting approach, the method has some disadvantages as error gets accumulated in every step. Therefore, parameter fitting is conducted using an alternative approach, namely the Quasi Monte Carlo sampling method with Sobol sequences in combination with a simplified version of the simulated annealing method (Kucherenko, 2015). Finally, practical identifiability analysis is conducted using the profile likelihood method (Murphy and Van Der Vaart, 2000; Venzon and Moolgavkar, 1988). Different series of simulations are carried out with the goal of obtaining a practically identifiable model.

Chapter 2

TUMOR-IMMUNE DYNAMICS WITH AN IMMUNE CHECKPOINT INHIBITOR

2.1 Abstract

The use of immune checkpoint inhibitors is becoming more commonplace in clinical trials across the nation. Two important factors in the tumor-immune response are the checkpoint protein programmed death-1 (PD-1) and its ligand PD-L1. We propose a mathematical tumor-immune model using a system of ordinary differential equations to study the dynamics with and without the use of anti-PD-1. A sensitivity analysis is conducted, and a series of simulations are performed to investigate the effects of intermittent and continuous treatments on the tumor-immune dynamics. We consider the system without the anti-PD-1 drug to conduct a mathematical analysis of the model to determine the stability of the tumor-free and tumorous equilibria. Through simulations, we found that a normally functioning immune system may control tumor. We observe treatment with anti-PD-1 alone may not be sufficient to eradicate the tumor cells. Therefore it may be beneficial to combine single agent treatments with other therapies to obtain a better antitumor response.

2.2 Introduction

The immune system works to differentiate between healthy cells and abnormal cells. Immune cells, known as T cells, fight the abnormal cells while leaving the healthy cells untouched. In accomplishing this, the use of "checkpoints", molecules on immune cells that enhance or suppress an immune response, is employed (Mahoney,

Freeman, and McDermott, 2015).

Two important factors in the tumor-immune response are programmed death-1 (PD-1) and its ligand PD-L1. PD-1 is a protein expressed on activated T cells (Simon and Labarriere, 2017). PD-L1, found mainly on various types of tumor cells and T cells (Maute *et al.*, 2015; Talay *et al.*, 2009), is one of PD-1's ligands. When PD-1 binds to PD-L1, the PD-1-PD-L1 complex is formed, allowing the cell expressing PD-L1 to be unrecognized as a danger when detected. In response to an immune attack, tumor cells may overexpress PD-L1 which can bind to PD-1 receptors on T cells, reducing or eliminating the effectiveness of T cells' attacks (He, Y. Hu, M. Hu, and Li, 2015).

Recently, scientists have worked to exploit the immune system through targeting the checkpoints and thus allowing the T cells to recognize tumor cells (Mahoney, Freeman, and McDermott, 2015). Drugs targeting PD-1 or PD-L1 can prevent the formation of the PD-1-PD-L1 complex. In particular, many PD-1 inhibitors (anti-PD-1s), including pembrolizumab and nivolumab, have been developed and shown positive results in over 270 international clinical trials (Liu and Wu, 2017). A 2012 clinical trial demonstrated the value of PD-1 inhibitors, as treated patients saw increases to their overall survival (Topolian *et al.*, 2012). Therapies involving immune checkpoint inhibitors are being developed to treat a wide array of tumor types (Alsaab *et al.*, 2017).

Low response rates have been observed across patients with the use of a single immune checkpoint inhibitor (Mahoney, Rennert anf Freeman, 2015). Instead, single agent treatments in combination with therapies such as chemotherapy, radiotherapy, and other forms of immunotherapy have shown greater promise through ongoing clinical trials (Hamanishi *et al.*, 2016). Combination therapies are proposed with the objective to increase the antitumor response effects.

2.3 Mathematical Model Proposed by Lai and Friedman (2017)

An influential mathematical model that investigates the combination of anti-PD-1 and a tumor vaccine (GVAX) was first developed by Lai and Friedman (2017). The authors propose a system of 13 partial differential equations, which are depicted below. The variables of the model and their biological description are presented in Table 2.1. A tumor-immune interaction network of the model is shown in Figure 2.1.

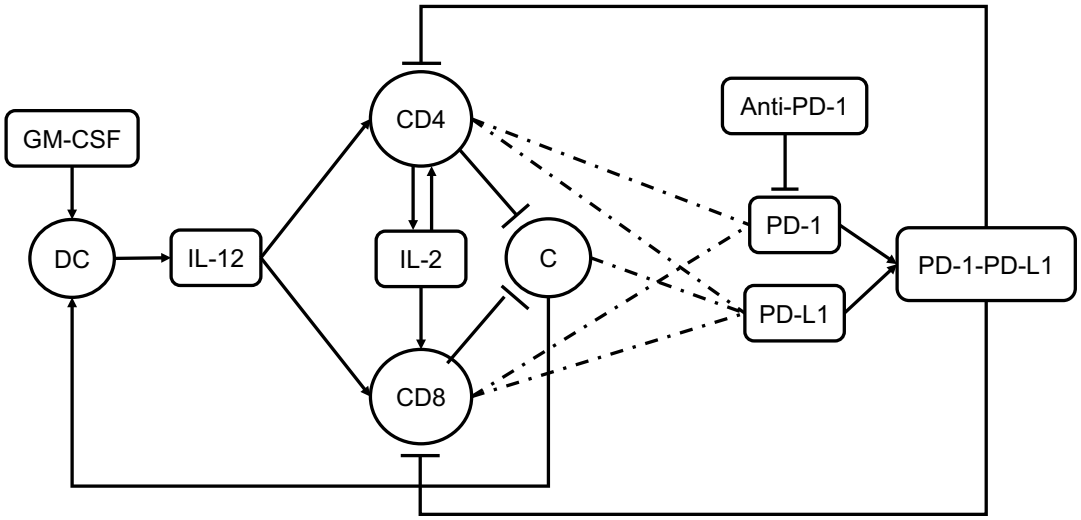

Figure 2.1: The tumor-immune interactions network represented in Lai and Friedman (2017). Proliferation/activation is demonstrated by sharp arrows. Killing/Blocking is demonstrated by blocked arrows. Proteins on the tumor or T cells are demonstrated by dashed lines. Once GM-CSF is inserted, dendritic cells are activated, which in turn produce IL-12. $CD4^+$ and $CD8^+$ T cells are activated by IL-12. IL-2 is produced by activated $CD4^+$ T cells resulting in the proliferation of $CD4^+$ and $CD8^+$ T cells. PD-L1 is found on tumor cells, and both PD-1 and PD-L1 are found on activated $CD4^+$ and $CD8^+$ T cells. The PD-1-PD-L1 complex is formed upon binding of PD-1 and PD-L1 resulting in inhibition of the activation of $CD4^+$ and $CD8^+$ T cells. Once anti-PD-1 binds to PD-1 the complex formation is prevented.

Table 2.1: Description of variables in the model system (2.3.1)-(2.3.13) adapted from Lai and Friedman (2017).

Variable	Meaning	Biological Description
N_C	density of necrotic tumor cells	Dead tumor cells
H	high mobility group B1 (HMGB-1) concentration	Protein released during the necrosis process of tumor cells.
D	density of dendritic cells	Antigen presenting cells activated by the necrosis function of tumor cells
T_1	density of activated $CD4^+$ cells	T helper cells that directly kill cancer cells by releasing cytokines
T_8	density of activated $CD8^+$ cells	T cells that kill cancer cells
C	density of tumor cells	Abnormal cells growing and dividing without control
I_2	interleukin-2 concentration	Interleukin produced by $CD4^+$ cells resulting in proliferation of T cells
I_{12}	interleukin-12 concentration	Interleukin produced by dendritic cells that activates $CD4^+$ and $CD8^+$ cells
P	PD-1 concentration	Protein expressed on activated T cells
L	free PD-L1 concentration	PD-1's ligand
Q	PD-1-PD-L1 concentration	Complex formed once PD-1 binds to PD-L1 that inhibits T cell function
A	anti-PD-1 concentration	Drug that blocks PD-1 and enables T cell activation
G	GM-CSF concentration	Cancer vaccine causing dendritic cell activation

$$\frac{\partial N_C}{\partial t} + \underbrace{\nabla \cdot (\mathbf{u} T_1)}_{\text{Velocity}} - \underbrace{\delta_{N_C} \nabla^2 N_C}_{\text{Diffusion}} = \underbrace{\lambda_{N_C C} C}_{\text{derived from life cancer cells}} - \underbrace{d_{N_C} N_C}_{\text{removal}} \tag{2.3.1}$$

$$\frac{\partial H}{\partial t} - \underbrace{\delta_H \nabla^2 H}_{\text{diffusion}} = \underbrace{\lambda_{N_H N_C} N_C}_{\text{released from necrotic cancer cells}} - \underbrace{d_H H}_{\text{degradation}} \tag{2.3.2}$$

$$\frac{\partial D}{\partial t} + \underbrace{\nabla \cdot (\mathbf{u} D)}_{\text{Velocity}} - \underbrace{\delta_D \nabla^2 D}_{\text{Diffusion}} = \underbrace{\lambda_{DC} D_0 \frac{C}{K_C + C}}_{\text{activation by HMGB-1}} - \underbrace{\lambda_{DG} D_0 \frac{G}{K_G + G}}_{\text{promotion by GM-CSF}} - \underbrace{d_D D}_{\text{death}} \tag{2.3.3}$$

$$\frac{\partial T_1}{\partial t} + \nabla \cdot (\mathbf{u} T_1) - \delta_T \nabla^2 T_1 = \left(\underbrace{\lambda_{T_1 I_{12}} T_{10} \frac{I_{12}}{K_{I_{12}} + I_{12}}}_{\text{activation by IL-12}} + \underbrace{\lambda_{T_1 I_2} T_1 \frac{I_2}{K_{I_2} + I_2}}_{\text{IL-2 induced proliferation}} \right) \times \underbrace{\frac{1}{1 + \frac{Q}{K_{TQ}}}}_{\text{inhibition by PD-1-PD-L1}} - \underbrace{d_{T_1} T_1}_{\text{death}} \tag{2.3.4}$$

$$\frac{\partial T_8}{\partial t} + \nabla \cdot (\mathbf{u} T_8) - \delta_T \nabla^2 T_8 = \left(\underbrace{\lambda_{T_8 I_{12}} T_{80} \frac{I_{12}}{K_{I_{12}} + I_{12}}}_{\text{activation by IL-12}} + \underbrace{\lambda_{T_8 I_2} T_8 \frac{I_2}{K_{I_2} + I_2}}_{\text{IL-2 induced proliferation}} \right) \times \underbrace{\frac{1}{1 + \frac{Q}{K_{TQ}}}}_{\text{inhibition by PD-1-PD-L1}} - \underbrace{d_{T8} T_8}_{\text{death}} \tag{2.3.5}$$

$$\frac{\partial C}{\partial t} + \nabla \cdot (\mathbf{u} C) - \delta_C \nabla^2 C = \underbrace{\lambda_C C (1 - \frac{C}{C_M})}_{\text{proliferation}} - \underbrace{(\eta_1 T_1 C + \eta_8 T_8 C)}_{\text{killing by T cells}} - \underbrace{d_C C}_{\text{death}} \tag{2.3.6}$$

$$\frac{\partial G}{\partial t} - \delta_G \nabla^2 G = \lambda_G + \underbrace{G(t)}_{\text{injection}} - \underbrace{d_G G}_{\text{degradation}} \tag{2.3.7}$$

$$\frac{\partial I_{12}}{\partial t} - \delta_{I_{12}} \nabla^2 I_{12} = \underbrace{\lambda_{I_{12} D} D}_{\text{production by DCs}} - \underbrace{d_{I_{12}} I_{12}}_{\text{degradation}} \tag{2.3.8}$$

$$\frac{\partial I_2}{\partial t} - \delta_{I_2} \nabla^2 I_2 = \underbrace{\lambda_{I_2 T_1} T_1}_{\text{production by} T_1} - \underbrace{d_{I_2} I_2}_{\text{degradation}} \tag{2.3.9}$$

$$\frac{\partial P}{\partial t} - \nabla \cdot (\mathbf{u}P) - \delta_T \nabla^2 P = \frac{P}{T_1 + T_8}(\lambda_{T_1 I_{12}} T_{10} + \lambda_{T_8 I_2} T_{80}) \frac{I_{12}}{K_{I_{12}} + I_{12}}$$
$$+ (\lambda_{T_1 I_2} T_1 + \lambda_{T_8 I_2} T_8) \frac{I_2}{K_{I_2} + I_2} \times \frac{1}{1 + \frac{Q}{K_{TQ}}} \tag{2.3.10}$$
$$- \frac{P}{T_1 + T_8}(d_{T_1} T_1 + d_{T_8} T_8) - \underbrace{\mu_{PA} P A}_{\text{depletion by anti-PD-1}}$$

$$L = \rho_L (T_1 + T_8 + \epsilon_C C) \tag{2.3.11}$$

$$\frac{\partial Q}{\partial t} - \nabla \cdot (\mathbf{u}Q) - \delta_T \nabla^2 Q = \alpha_{PL} P L - d_Q Q \tag{2.3.12}$$

$$\frac{\partial A}{\partial t} - \delta_A \nabla^2 A = \underbrace{A(t)}_{\text{injection}} - \underbrace{\mu_{PA} P A}_{\text{depletion through blocking PD-1}} - \underbrace{d_A A}_{\text{degradation}} \tag{2.3.13}$$

Using the model (2.3.1)-(2.3.13) Lai and Friedman (2017) investigated the following cases: a) No drugs are applied b) Different dosage levels for the monotherapy treatments c) Potential synergy of the combination treatment. These led to the following conclusions: a) Verified that the assumptions of the steady state arguments used for parameter estimation agree with the simulations. b) Increased dosage of anti-PD-1 leads to tumor size reduction while a combination therapy was shown to only reduce the growth of the tumor. Tumor radius is sensitive to the respective dosage levels of GVAX and anti-PD-1 drugs. c) Optimum synergy is proposed based on a developed synergy map between the GVAX and anti-PD-1 drug.

Overall, their model examines the synergy of the two drugs, suggesting that the immune checkpoint inhibitor and tumor vaccine work better to reduce the tumor volume in combination than individually. Their results are verified through a comparison with data collected from mice experiments. An optimal combination level of each drug is found, which lies within the bounds of the maximum tolerated dose allowed in clinical trials.

The model (2.3.1)-(2.3.13) in Lai and Friedman (2017) is a complex system of partial differential equations which forbids a comprehensive mathematical exploration

and an insightful biological interpretation of the model. Our main objective is to simplify their model into a tractable system of ordinary differential equations to help gain a better mathematical and biological understanding of its rich dynamics. Additionally, although we appreciate the need for a combination of treatments as addressed by Lai and Friedman (2017), we wish to solely examine the effects of a single treatment. We hope an in-depth understanding of the immune checkpoint inhibitor therapy will enhance our appreciation and comprehension of the combined treatment. We consider the case when only one treatment, anti-PD-1, is applied. Our model depicts the tumor-immune interactions following the activation process of T cells by interleukins.

We compare the treatment in the case when continuous drug and periodic injections are applied. In Lai and Friedman (2017) paper most of the main dependent variables in the model go to steady state. We take advantage of these steady state values in our simplification, reducing the system to three nonlinear ordinary differential equations. The effectiveness of intermittent versus continuous therapy will be examined in detail. Specifically, a study will be conducted into how altering the dosage frequency, while maintaining the same total dosage, impacts the tumor volume. We examine the drug-free system and perform an analysis on the existence and local stability of the model equilibria. Moreover, we illustrate our findings through selective simulation and bifurcation results.

2.4 Model Formulation

The variables of our simplified model, their meanings, and their respective units are listed in Table 2.2.

The essence of our simplified mathematical model is captured by the following dramatically simplified tumor-immune interactions network following activation of T

Table 2.2: Description of variables in the model system (2.4.14)-(2.4.16).

Variable	Meaning	Unit
C	density of tumor cells	g/cm^3
T	density of activated T cells	g/cm^3
P	free PD-1 concentration	g/cm^3
A	anti-PD-1 concentration	g/cm^3
Q	PD-1-PD-L1 concentration	g/cm^3

cells shown in Figure 2.2.

Our model of tumor-immune interaction with immune checkpoint inhibitor anti-PD-1 treatment is a vastly simplified and slightly modified version of the model presented in Lai and Friedman (2017). Our model consists of three nonlinear ordinary differential equations of the following form:

$$\frac{dC}{dt} = \underbrace{\lambda_C C\left(1-\frac{C}{C_K}\right)}_{\text{net growth}} - \underbrace{\eta C T,}_{\text{killed by T cells}} \tag{2.4.14}$$

$$\frac{dT}{dt} = \left(\underbrace{\lambda_{TI_{12}} T_N \frac{I_{12}}{K_{I_{12}}+I_{12}}}_{\text{activation by IL-12}} + \underbrace{\lambda_{TI_2} T \frac{I_2}{K_{I_2}+I_2}}_{\text{stimulation by IL-2}}\right) \cdot \underbrace{F_1(Q)}_{\text{inhibition by PD-1-PD-L1}} - \underbrace{d_T T,}_{\text{death}} \tag{2.4.15}$$

$$\frac{dA}{dt} = \underbrace{A(t)}_{\text{effective level of anti-PD-1}} - \underbrace{\mu_{PA} P A}_{\text{depletion through blocking PD-1}} - \underbrace{d_A A,}_{\text{natural degradation}} \tag{2.4.16}$$

where P is defined as:

$$P = (\rho_P - \gamma A)T. \tag{2.4.17}$$

The function for suppression of T cell activation and proliferation by the PD-1-PD-L1 complex is given by:

$$F_1(Q) = \frac{1}{1+\frac{Q}{K_{TQ}}}.$$

As in Lai and Friedman (2017), we assume the dissociation ($d_Q Q$) and association

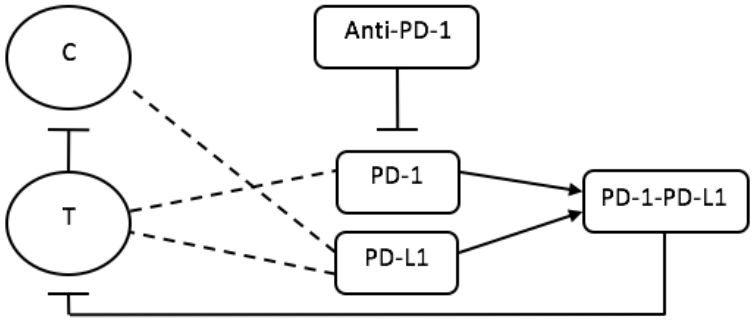

Figure 2.2: The tumor-immune interactions following activation of T cells. Sharp arrows indicate proliferation/activation. Blocked arrows indicate killing/blocking. Dashed lines indicate proteins on the tumor or T cells. Tumor cells express PD-L1. Activated T cells express PD-1 and PD-L1. Activated T cells kill tumor cells. When PD-1 and PD-L1 bind together, the complex PD-1-PD-L1 is formed, which inhibits the function of activated T cells. Anti-PD-1 binds to PD-1, inhibiting the formation of the PD-1-PD-L1 complex.

($\alpha_{PL}PL$) of the complex PD-1-PD-L1 are fast so that we can apply the usual quasi-steady-state argument to obtain $\alpha_{PL}PL = d_Q Q$. Thus,

$$Q = \sigma PL, \text{ with } \sigma = \alpha_{PL}/d_Q.$$

As in Lai and Friedman (2017), we assume the level of free PD-L1 can be represented by

$$L = \rho_L(T + \epsilon_C C),$$

since PD-L1 is expressed on both T cells and tumor cells, and upregulated on tumor cells, indicated by $\epsilon_C > 1$. Thus

$$Q = \kappa P(T + \epsilon_C C), \text{ with } \kappa = \sigma\rho_L.$$

The parameters, their meanings, and estimates of their values are given in Table C.1. A more detailed discussion of the parameter estimates is given in Appendix C.

The cytokines IL-2 and IL-12 were estimated from their steady-state values. In our model, we consider the process after the T cell population has been activated. Our hope is to focus primarily on the interactions between the T cells, cancer cells, and PD-1-PD-L1 complexes. As a result, we base the values of IL-2 and IL-12 densities off the control case simulated in Figure 2 of Lai and Friedman (2017). The simulation shows the IL-2 and IL-12 densities are not very dynamic, as they both move within a tight range. Since the densities tend to a steady-state in Lai and Friedman's simulations, we assume a steady-state in our model and take IL-2 $= 2.37 \cdot 10^{-11}$ g/cm^3 and IL-12 $= 1.5 \cdot 10^{-11}$ g/cm^3.

Eq (2.4.14) models the tumor cell population, where logistic growth is used to denote the net growth of the tumor cells in the presence of an anti-PD-1 immune checkpoint inhibitor (Kirschner and Panetta, 1998). Through interactions between tumor cells and activated T cells, the loss of tumor cells occurs at rate η. We assume that the PD-1/PD-L1 interaction reduces the number of activated effective T cells with negligible inhibition on the immune cytotoxicity. Eq (2.4.15) captures the rate of change of the activated (effective) T cell population. IL-12 and IL-2 play a major role in activation and differentiation of the population of T cells, shaping the immune response. The first source term accounts for the activation of naive T cells (T_N) by IL-12. The other source term represents the proliferation of activated T cells, as stimulated by IL-2. Michaelis-Menten forms are used to capture the saturation in the immune response (Kirschner and Panetta, 1998). Larger values of PD-1-PD-L1 concentration inhibit the activation and proliferation of T cells, reducing the source terms by a factor of $\frac{1}{1+Q/K_{TQ}}$. Natural death of T cells occurs at rate d_T. The anti-PD-1 treatment is modeled by Eq (2.4.16), where $A(t) = \gamma_A$ corresponds to an intravenous, continuous injection. Intradermal injections are also considered with varying dosage frequencies, as discussed in Section 2.7. PD-1 binds to anti-PD-1

at a rate of μ_{PA}. We assume there is no dissociation of PD-1 with anti-PD-1 once bound due to the very quick nature of the association and dissociation. The rates of association and dissociation are relatively small values and lead to an assumption that the variables can be approximated by their levels at quasi-steady state. Anti-PD-1 naturally decays at rate d_A. Finally, Eq (2.4.17) describes the density of the free PD-1. Newly activated T cells have a fixed amount of PD-1 per T cell, ρ_P. As anti-PD-1 is injected and the drug binds to PD-1, PD-1 is depleted at a rate of γA.

2.5 Treatment Free Model Dynamics

It is easy to see that the functions contained in the full system (2.4.14)-(2.4.16) are differentiable, which ensures its solutions with positive initial values exist and are unique by a direct application of standard differential equation theory. Observe that the full system (2.4.14)-(2.4.16) consists of three highly nonlinear differential equations that prevent us from conducting a comprehensive mathematical analysis. In order to appreciate the full model complexity and to gain an in-depth understanding of the natural tumor-immune interaction via the lens of a mathematical model, we examine the case when no anti-PD-1 treatment is applied ($A = 0$) in the full system (2.4.14)-(2.4.16). In this case, Eq (2.4.17) becomes $P = \rho_P T$ and

$$Q = \beta T(T + \epsilon_C C), \beta = \kappa \rho_P.$$

The reduced system takes the form:

$$\begin{aligned} \frac{dC}{dt} &= \lambda_C C\left(1 - \frac{C}{C_K}\right) - \eta CT, \\ \frac{dT}{dt} &= (M + NT)F(C,T) - d_T T, \end{aligned} \tag{2.5.18}$$

where we use the assumptions on the complex-forming process to define $F(C,T)$:

$$F(C,T) = \frac{1}{1 + \frac{\beta T(T+\epsilon_C C)}{K_{TQ}}}.$$

M and N are two positive parameters defined as:

$$M = \lambda_{TI_{12}} T_N \frac{I_{12}}{K_{I_{12}} + I_{12}},$$
$$N = \lambda_{TI_2} \frac{I_2}{K_{I_2} + I_2}.$$

We seek to examine the local and global stability for our system. In doing so, we first need to establish positivity and boundedness of the solutions with positive initial values.

Proposition 2.5.1 *Solutions of (2.5.18) that start positive remain positive and bounded.*

Proof.

We first seek to show the proof of positivity, examining T first using proof by contradiction. We assume $T(t_0) \geq 0$. If $T(t) < 0$ for some $t > 0$, we would require $\frac{dT}{dt} \leq 0$ when $T = 0$. However, we have $\frac{dT}{dt}|_{T=0} = M > 0$ since all parameters are positive, which leads to a contradiction. Thus $T(t) > 0, \forall t > 0$.

In examining the positivity of C, we assume $C(t), T(t)$ exist on $[0, t_1]$. By a standard separation of variables,

$$\frac{dC}{dt} = \lambda_C C \left(1 - \frac{C}{C_K}\right) - \eta C T$$

becomes

$$\frac{dC}{C} = \left(\lambda_C \left(1 - \frac{C}{C_K}\right) - \eta T\right) dt.$$

We can then conclude

$$C(t_1) = C(0) \exp\left[\int_0^{t_1} \left(\lambda_C \left(1 - \frac{C(s)}{C_K}\right) - \eta T(s)\right) ds\right] > 0,$$

since $C(0) > 0$.

Since solutions remain nonnegative, we now seek to prove boundedness. We start with boundedness of C using a comparison argument:

$$\begin{aligned}\frac{dC}{dt} &= \lambda_C C\left(1-\frac{C}{C_K}\right) - \eta CT \\ &\leq \lambda_C C\left(1-\frac{C}{C_K}\right),\end{aligned}$$

which implies that

$$C(t) \leq \max\{C(0), C_K\}.$$

In addition, we see that

$$\limsup_{t\to\infty} C(t) \leq C_K.$$

Therefore C is eventually bounded above by $C_K + a$ for any positive constant a.

We then look to prove that T is bounded. First, let $G(C,T) = (M+NT)F(C,T)$. Then

$$G(C,T) \leq G(0,T) = \frac{M+NT}{1+\beta' T^2} \leq \alpha$$

where $\beta' = \beta/K_{TQ}$ and $\alpha = \max\{G(0,T)\} = \frac{\sqrt{\beta'(\beta' M^2+N^2)}}{\beta' N} - \frac{M}{N}$. Now

$$\frac{dT}{dt} = (M+NT)F(C,T) - d_T T \leq \alpha - d_T T.$$

By a standard comparison argument,

$$\limsup_{t\to\infty} T(t) \leq \frac{\alpha}{d_T}.$$

Then $T \leq \max\{T_0, \frac{\alpha}{d_T}\}$, and T is bounded. □

The reduced system (2.5.18) may contain two types of equilibria: the tumor-free equilibria $E_0^* = (0, T_0^*)$ and tumorous equilibria $E_1^* = (C^*, T^*)$, $C^* > 0$, $T^* > 0$. Before examining stability, we must establish the existence and uniqueness of the tumor-free equilibrium $E_0^* = (0, T_0^*)$.

Proposition 2.5.2 *The system* (2.5.18) *has a unique tumor-free equilibrium* $E_0^* = (0, T_0^*)$. T_0^* *is a strictly increasing function of parameter* M.

Proof. When $C^* = 0$,

$$\frac{dT}{dt} = 0 \Rightarrow \frac{M + NT^*}{1 + \beta' T^{*2}} - d_T T^* = 0, \text{ where } \beta' = \frac{\beta}{K_{TQ}}.$$

The T^* values corresponding to $C^* = 0$ are the roots of the equation:

$$p(T) = \beta' d_T T^3 + (d_T - N)T - M = 0.$$

Assume that $d_T \geq N$. Then $p'(T) > 0$ if $T > 0$. Since $p(0) = -M < 0$ and $\lim_{T\to\infty} p(T) = +\infty$, we see that $p(T) = 0$ has a unique positive root which is a strictly increasing function of M.

If $d_T < N$, with $M = 0$, then $p(T) = 0$ has three real roots:

$$T_1^* = -\sqrt{\frac{N - d_T}{\beta' d_T}},\ T_2^* = 0,\ T_3^* = \sqrt{\frac{N - d_T}{\beta' d_T}}.$$

However, when $M > 0$, the entire curve is shifted down, as shown in Figure 2.3.

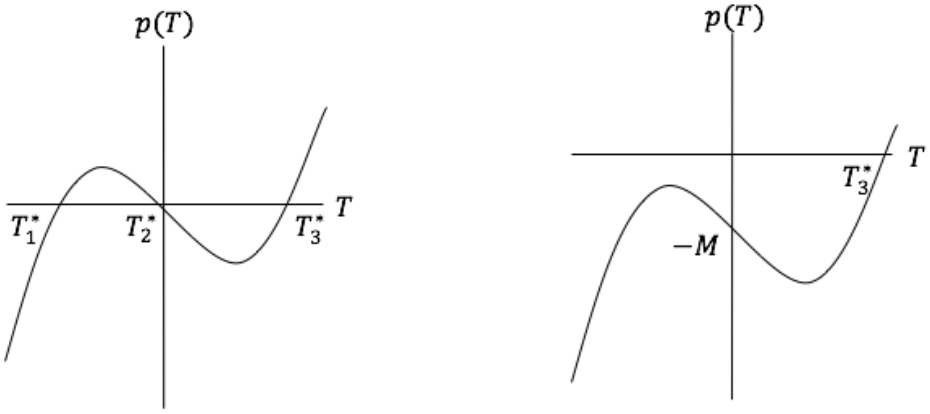

Figure 2.3: $p(T)$ when $d_T < N$, with $M = 0$ and $M > 0$ respectively.

There is only one real positive root T_3^*, and T_3^* increases strictly as M increases.

□

We now establish the existence and uniqueness of the tumorous equilibrium $E_1^* = (C^*, T^*)$, $C^* > 0$, $T^* > 0$.

Proposition 2.5.3 *The system (2.5.18) has a unique tumorous equilibrium* $E_1^* = (C^*, T^*)$, $C^* > 0$, $T^* > 0$ *if* $\epsilon_C C_K \frac{\eta}{\lambda_C} < 1$, $\frac{N}{d_T} < 1$, *and* $f\left(\frac{\lambda_C}{\eta}\right) < 0$.

Proof. It is easy to see that

$$\lambda_C \left(1 - \frac{C^*}{C_K}\right) = \eta T^*, \tag{2.5.19}$$

$$M + NT^* = d_T T^* (1 + \beta' T^* (T^* + \epsilon_C C^*)). \tag{2.5.20}$$

These together yield

$$f(T^*) \equiv \beta' \left(\epsilon_C C_K \frac{\eta}{\lambda_C} - 1\right) (T^*)^3 - \beta' \epsilon_C C_K (T^*)^2 + \left(\frac{N}{d_T} - 1\right) T^* + \frac{M}{d_T} = 0. \tag{2.5.21}$$

The number of positive roots of Eq (2.5.21) can be determined by the Descartes' rule of signs. For example, if $\epsilon_C C_K \frac{\eta}{\lambda_C} < 1$ and $\frac{N}{d_T} < 1$, then the polynomial $f(T^*)$ in Eq (2.5.21) has only one change of signs in coefficients and hence has a single positive root; while if $\epsilon_C C_K \frac{\eta}{\lambda_C} > 1$ and $\frac{N}{d_T} < 1$, then the polynomial $f(T^*)$ in Eq (2.5.21) has two changes of signs in coefficients and hence may have two positive roots or none.

We also need to ensure the positivity of C^*. We have $f(0) = \frac{M}{d_T} > 0$ and $f'(T^*) < 0$. Now by Eq (2.5.19), $C^* > 0$ if and only if $\frac{\lambda_C}{\eta} > T^*$. Thus, we require $0 < T^* < \frac{\lambda_C}{\eta}$. By the Intermediate Value Theorem, $f(\frac{\lambda_C}{\eta}) < 0$ ensures the intersection of $f(T^*) = 0$ occurs for $0 < T^* < \frac{\lambda_C}{\eta}$. Thus, there exists a unique positive equilibrium $E_1^* = (C^*, T^*)$ with $C^* > 0$ when $f(\frac{\lambda_C}{\eta}) < 0$. □

We are now able to perform a stability analysis with our reduced system. The Jacobian for the system (2.5.18) is given by:

$$\begin{pmatrix} \lambda_C \left(1 - \frac{C}{C_K}\right) - \lambda_C \frac{C}{C_K} - \eta T & -\eta C \\ (M + NT) \frac{\partial}{\partial C} F(C,T) & NF(C,T) + (M + NT) \frac{\partial}{\partial T} F(C,T) - d_T \end{pmatrix}.$$

We first examine the stability of the tumor-free equilibrium $E_0^* = (0, T_0^*)$.

Proposition 2.5.4 *Assume that $d_T > N$. Then for system (2.5.18) the following statements are true:*

(a) If $\lambda_C < \eta T_0^*$, then E_0^* is locally asymptotically stable.

(b) If $\lambda_C > \eta T_0^*$, then E_0^* is a saddle point.

Proof. For part (a) and the first part of (b), the Jacobian matrix for the tumor-free equilibrium $E_0^* = (0, T_0^*)$ is :

$$\begin{pmatrix} \lambda_C - \eta T_0^* & 0 \\ (M + NT_0^*)\frac{\partial}{\partial C}F(0, T_0^*) & NF(0, T_0^*) + (M + NT_0^*)\frac{\partial}{\partial T}F(0, T_0^*) - d_T \end{pmatrix}.$$

Since we know $F(C, T) \leq 1$ and $F(C, T)$ is a decreasing function of C and T, $\frac{\partial}{\partial T}F(C, T), \frac{\partial}{\partial C}F(C, T) < 0$, and the eigenvalues are:

$$\lambda_1 = \lambda_C - \eta T_0^* < 0 \text{ (by condition in part (a))}$$
$$\lambda_2 = NF(0, T_0^*) + (M + NT_0^*)\frac{\partial}{\partial T}F(0, T_0^*) - d_T < 0$$

Thus, we have local asymptotic stability for E_0^*. Similarly, if $\lambda_C > \eta T_0^*$, then E_0^* is a saddle point. □

We can biologically interpret several of the conditions for the local stability. We have that $\lambda_C < \eta T_0^*$ implies that during the onset of tumor initiation, resident T cells can kill the cancer cells faster than the cancer cells can multiply. Thus, it is unsurprising to find that this condition is necessary for the local stability of the tumor-free equilibrium. The condition $d_T > N$ can be interpreted as the death rate of the T cells being greater than the stimulation rate of T cells by IL-2.

We next examine the stability of the tumorous equilibrium $E_1^* = (C^*, T^*)$.

Proposition 2.5.5 *Assume that* $\epsilon_C C_K \frac{\eta}{\lambda_C} < 1$, $\frac{N}{d_T} < 1$, *and* $f\left(\frac{\lambda_C}{\eta}\right) < 0$, *then the tumorous steady state* E_1^* *of system* (2.5.18) *is unique and is locally asymptotically stable.*

Proof. The Jacobian matrix for the tumorous equilibrium E_1^* is:

$$\begin{pmatrix} -\lambda_C \frac{C^*}{C_K} & -\eta C^* \\ (M+NT^*)\frac{\partial}{\partial C}F(C^*,T^*) & NF(C^*,T^*) + (M+NT^*)\frac{\partial}{\partial T}F(C^*,T^*) - d_T \end{pmatrix}.$$

Assume that $d_T > N$. Then the trace for the tumorous equilibrium is

$$\tau = \underbrace{-\lambda_C \frac{C^*}{C_K}}_{<0} + \underbrace{NF(C^*,T^*) - d_T}_{<0} + \underbrace{(M+NT^*)\frac{\partial}{\partial T}F(C^*,T^*)}_{<0}.$$

Therefore, $\tau < 0$. The determinant is given by:

$$\begin{aligned}\Delta = \left(-\lambda_C \frac{C^*}{C_K}\right)\left(NF(C^*,T^*) + (M+NT^*)\frac{\partial}{\partial T}F(C^*,T^*) - d_T\right) \\ - (-\eta C^*)\left((M+NT^*)\frac{\partial}{\partial C}F(C^*,T^*)\right).\end{aligned}$$

We can rearrange the terms in Δ:

$$\Delta = \underbrace{-\lambda_C \frac{C^*}{C_K}}_{<0}\underbrace{(NF(C^*,T^*) - d_T)}_{<0} + \underbrace{(M+NT^*)}_{>0}\Gamma C^*$$

where

$$\Gamma = -\lambda_C \frac{1}{C_K}\frac{\partial}{\partial T}F(C^*,T^*) + \eta \frac{\partial}{\partial C}F(C^*,T^*).$$

Recall $Q = \beta T(T + \epsilon_C C)$ and $F_1(Q) = \frac{1}{1+Q/K_{TQ}}$. We have $\frac{\partial}{\partial T}F(C,T) = \frac{dF_1(Q)}{dQ}\frac{\partial Q}{\partial T}$ with $\frac{dF_1(Q)}{dQ} < 0$. Likewise, $\frac{\partial}{\partial C}F(C,T) = \frac{dF_1(Q)}{dQ}\frac{\partial Q}{\partial C}$. Hence

$$\Gamma = \frac{dF_1(Q)}{dQ}\left(-\frac{\lambda_C}{C_K}\frac{\partial Q}{\partial T} + \eta \frac{\partial Q}{\partial C}\right).$$

Observe that $\frac{\partial Q}{\partial T} > 0$ and $\frac{\partial Q}{\partial C} > 0$. We see that $\Gamma > 0$ if and only if

$$\eta \frac{\partial Q}{\partial C} < \frac{\lambda_C}{C_K}\frac{\partial Q}{\partial T},$$

which is equivalent to

$$\eta\epsilon_C T < \frac{\lambda_C}{C_K}(2T + \epsilon_C C).$$

Clearly this is true if $\eta\epsilon_C < 2\frac{\lambda_C}{C_K}$ or $\frac{1}{\lambda_C}\eta\epsilon_C C_K < 2$. The first condition of Proposition 2.5.3 ensures this is true. Therefore, $\Delta > 0$. Together with Proposition 2.5.3, we have the following local stability result for the tumorous equilibrium E_1^*. □

We now establish global asymptotic stability of the tumorous steady state E_1^* of system (2.5.18). To this end, we need to identify conditions that can rule out the existence of nontrivial positive periodic solutions from system (2.5.18).

Proposition 2.5.6 *The system* (2.5.18) *has no nontrivial positive periodic solutions provided that* $d_T > N$.

Proof. We employ the Dulac criterion to show there are no nontrivial positive periodic orbits. Let $h(C,T) = 1/C$. We have:

$$\begin{aligned}
\Omega &= \frac{\partial}{\partial C}\left\{\frac{1}{C}\left[\lambda_C C\left(1-\frac{C}{C_K}\right)-\eta CT\right]\right\} + \frac{\partial}{\partial T}\left\{\frac{1}{C}\left[(M+NT)\,F(C,T)-d_T T\right]\right\} \\
&= \frac{\partial}{\partial C}\left(\lambda_C - \frac{\lambda_C C}{C_K} - \eta T\right) + \frac{\partial}{\partial T}\left\{\frac{1}{C}\left[(M+NT)F(C,T)-d_T T\right]\right\} \\
&= -\frac{\lambda_C}{C_K} + \frac{1}{C}\left[(M+NT)\frac{\partial}{\partial T}F(C,T) + NF(C,T) - d_T\right] < 0.
\end{aligned}$$

since $\frac{\partial}{\partial T}F(C,T) < 0$ and $d_T > N$.

Thus, the Dulac criterion ensures there will be no nontrivial positive periodic solutions for system (2.5.18).

□

We are ready to state the following global stability results for system (2.5.18).

Theorem 1 *Assume that* $d_T > N$. *Then the following are true:*

(i) If $\lambda_C < \eta T_0^*$ and no tumorous equilibrium exists, then the tumor-free equilibrium E_0^* of system (2.5.18) *is globally asymptotically stable.*

(ii) If $\epsilon_C C_K \frac{\eta}{\lambda_C} < 1$ and $f\left(\frac{\lambda_C}{\eta}\right) < 0$, then the tumorous steady state E_1^* of system (2.5.18) *is globally asymptotically stable.*

Proof. Recall solutions of system (2.5.18) with respect to positive initial values are positive and bounded. By Poincare-Bendixson Theorem, bounded positive solution must tend to a nonnegative equilibrium, a nontrivial positive periodic solution, a homoclinic cycle, or a heteroclinic cycle. In case of (i), the system (2.5.18) admits no positive steady states, nontrivial positive periodic solutions, homoclinic cycles, or heteroclinic cycles. This implies that all positive solutions of system (2.5.18) tend to the tumor-free equilibrium E_0^*.

In case of (ii), the system (2.5.18) admits a unique positive steady state E_1^*, which is locally asymptotically stable. This eliminates the existence of heteroclinic cycles since system (2.5.18) admits only two equilibria. It is easy to see that if E_0^* is locally asymptotically stable, then there can not be any homoclinic cycles originating from E_0^*. Observe that the T axis is invariant. If there is any homoclinic cycle originating from E_0^*, then the cycle will contain at least one branch of its stable manifold, which is unbounded, a contradiction to the fact that positive solutions of the system (2.5.18) are bounded. Together, these arguments exclude the possibility of the existence of any homoclinic cycle originating from E_0^*. By Poincare-Bendixson Theorem, the tumorous steady state E_1^* of system (2.5.18) attracts all its positive solutions. □

2.6 Sensitivity Analysis

By the method outlined in (Marino *et al.*, 2008), we performed a sensitivity analysis using partial rank correlation coefficients (PRCC) via Latin hypercube sampling

(LHS) to identify the main drivers of the tumor burden. We used LHS to produce 1000 sets of randomly determined parameters, which were then used to compute the PRCC and corresponding p-values. Parameters were tested within the ranges given in Table C.1. For parameters without ranges, sampling was completed within a range from 1/10 to twice the values in Table C.1. The sensitivity analyses with respect to the tumor cell density C and the activated T cell density T at day 200 are shown in Figure 2.4 and Figure 2.5 respectively.

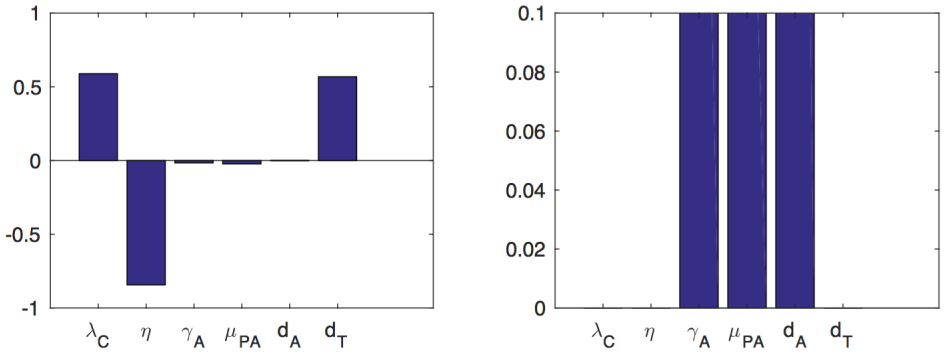

Figure 2.4: PRCC values (left) and p-values (right) for density of tumor cells $C(t)$ at time $t = 200$ days.

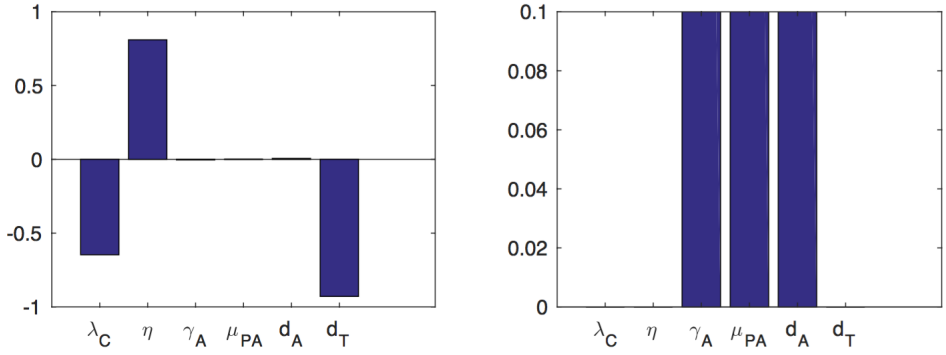

Figure 2.5: PRCC values (left) and p-values (right) for activated T cell density $T(t)$ at time $t = 200$ days.

The density of tumor cells is most sensitive to changes in the tumor cell growth

rate (λ_C), kill rate of tumor cells by T cells (η), and death rate of T cells (d_T) (p-value $< .01$ for each). We notice that C, the tumor cell density, is highly positively correlated with the tumor cell growth rate (λ_C) and the death rate of T cells (d_T), and negatively correlated with the kill rate of tumor cells by T cells (η).

The sensitivity analysis conducted with respect to T, the activated T cell density, reveals the tumor cell growth rate (λ_C), death rate of T cells (d_T), and kill rate of tumor cells by T cells (η) are the main parameters influencing T (p-value $< .01$ for each). As could be expected, the activated T cell density is negatively correlated with the growth rate of the tumor cells (λ_C) and death rate of T cells (d_T). The kill rate of the tumor cells by the T cells (η) captures the most highly positively correlated parameter.

In making biological sense of the results, we note that the interaction between immune cells (T cells) and tumor cells can either result in the death of tumor cells or the inactivation of the immune cells. Our model solely represents the former case. Thus, the density of tumor cells and activated T cells are sensitive to d_T, the death rate of T cells, which causes the T cells to decline. As the activated T cells decline, there are less reactions, and thereby less deaths of tumor cells. The kill rate of tumor cells by T cells (η) increasing or decreasing reflects a stronger or weaker immune response. As η increases, the tumor-immune interactions result in more killing of tumor cells. When the tumor cells are decreased, less PD-L1 is in the system to bind to PD-1. Thus, less PD-1-PD-L1 complexes are formed to inhibit the activation of T cells. Therefore, η is positively correlated with the activated T cell density and negatively correlated with the density of tumor cells. Finally, the production parameter for the tumor cells, λ_C, is positively correlated with the density of tumor cells. As the number of tumor cells, and thereby the amount of PD-L1, increases, more T cells are being inactivated as a result of the increased PD-1/PD-L1 bindings.

Therefore, λ_C is negatively correlated with the activated T cell density.

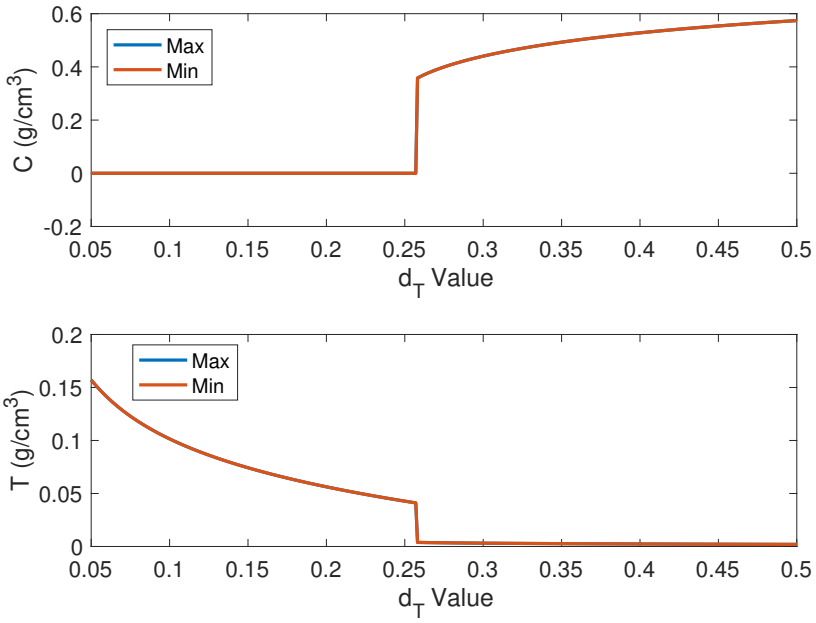

Figure 2.6: Bifurcation diagram corresponding to continuous treatment for parameter d_T, the death rate of T cells. Maximum/minimum tumor/T cell density in blue and red, respectively. To tend towards a tumor-free steady state, the diagram suggests a maximum threshold of $d_T \approx N$ (since $N = 0.25$), after which the tumorous steady state is stable. It also suggests $d_T < N$ is not necessary for the stability of the tumor-free equilibrium.

The bifurcation plot of d_T, as shown in Figure 2.6, suggests the existence of a critical value for the maximum death rate of T cells d_T, namely $d_T \approx N$, since $N = 0.25$. When $d_T < N$, this causes an increase in the number of activated T cells, resulting in the killing of more tumor cells. However, when $d_T > N$, the tumor cells dramatically increase towards the carrying capacity. The plot suggests our mathematical results can be improved upon to find sharper conditions, as $d_T > N$ is not required for the tumor-free equilibrium E_0^* to be stable. We can now discern

that Proposition (2.5.4) and (2.5.5) provide sufficient, but not necessary conditions for the stability of the tumor-free and tumorous equilibria. Further exploration of the bifurcation plots for different parameters illustrate the approach of the same steady state.

2.7 Numerical Simulations

All simulations of the mathematical model were performed by MATLAB using the `ode23tb` solver and the parameter estimates given in Table C.1 and the initial conditions (in units of g/cm^3) $C(0) = 0.3968$, $T(0) = 6 \cdot 10^{-3}$, and $A(0) = 0$ (Lai and Friedman, 2017). We examine the cases when no drug, a continuous drug, and injections of varying periodicity are applied.

We first explore the control case when no drug is applied (Figure 2.7). We keep the death of the T cells small enough so that the results closely resemble the behavior seen for those with a normally functioning immune system. The simulation is run for a duration of 150 days to determine the behavior of certain cell densities/concentrations. We observe that the number of activated T cells increases up to a certain level, and later stabilizes, approaching a steady state. The density of tumor cells decreases significantly until reaching a disease free equilibrium. Since the death rate of T cells is small, tumor is controlled to a great extent. Consequently, people with a strong immune system have a chance to eradicate tumor. However, for those with a weakened immune system, tumors are significantly less responsive to treatment.

We next consider intermittent anti-PD-1 therapy compared to continuous treatment. We seek to determine how the densities of tumor and activated T cells are affected by varying dosage frequencies and maintaining the dosage level. The time period between injections is varied from 3 days to 150 days. Simulations are run for 365 days to reflect a clinically realistic treatment period. Figure 2.8 suggests a

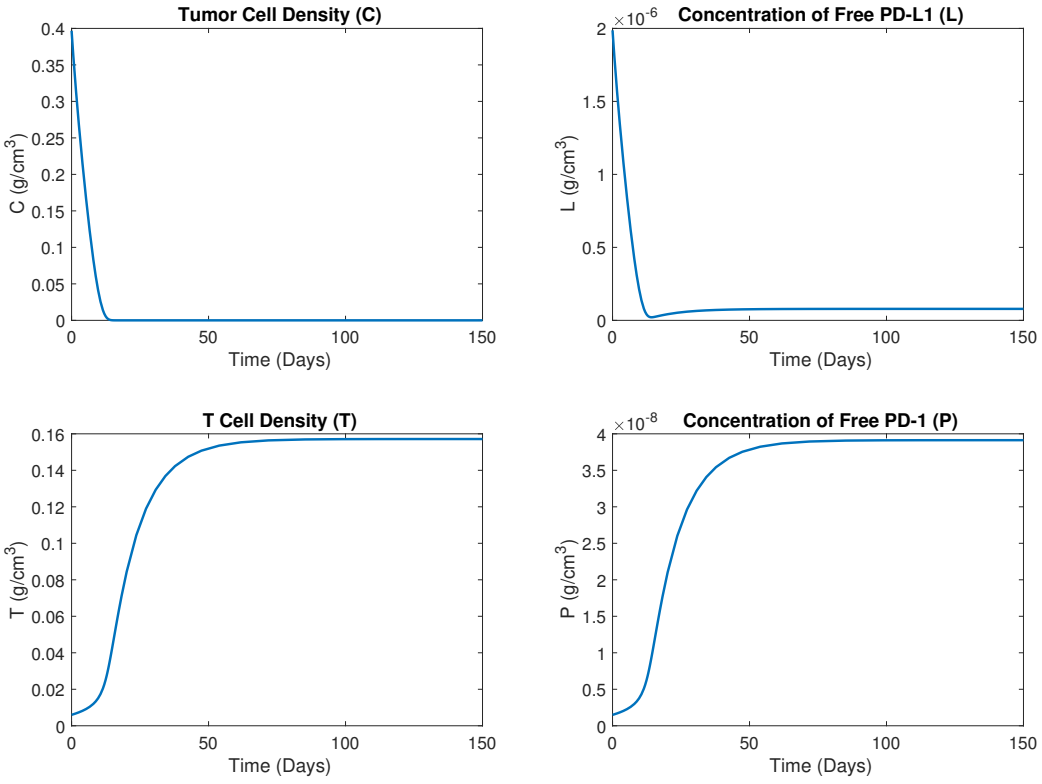

Figure 2.7: Densities/concentrations of tumor cells, activated T cells, free PD-1, and free PD-L1 without treatment. Simulations are run for 150 days with $d_T = 0.05$.

periodicity in the immune response, resulting from the treatment acting as a forced oscillator. Each time the anti-PD-1 is administered, the level of activated T cells increases due to less PD-1-PD-L1 complexes being formed and thereby less inhibition of T cell activation. As a result, the tumor cells sharply decrease. Following the decline, the tumor cells logistically grow, returning to their previous level. A continuous therapy offers the best control for the tumor cells.

Figure 2.9 suggests that when treatments are less frequent (every 60, 90, 150 days), the tumor cells periodically approach the same density as when no drug is applied before decreasing with the next treatment. The more frequent treatments (every 3, 10,

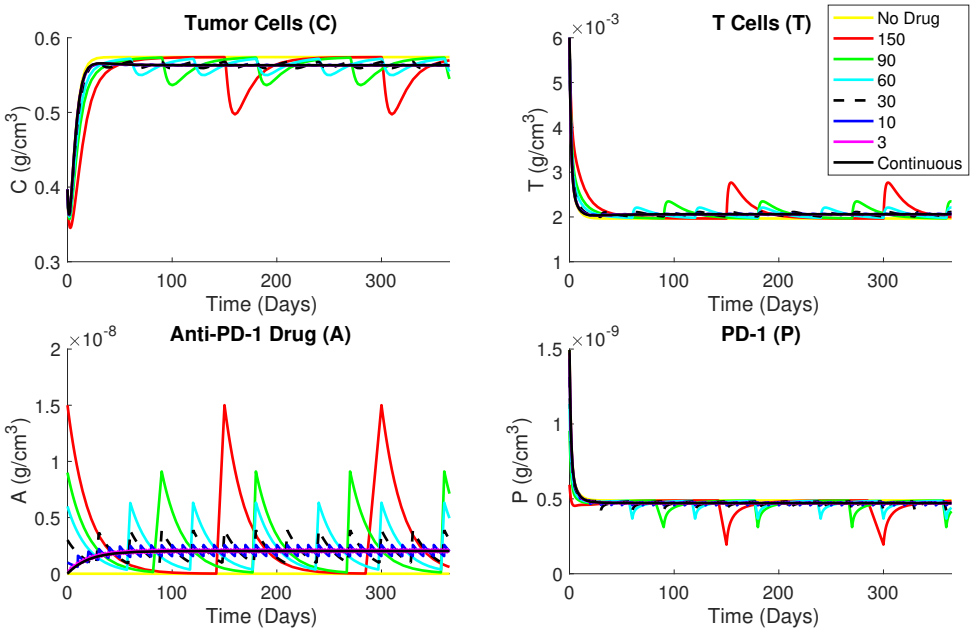

Figure 2.8: Densities/concentrations of tumor cells, activated T cells, free PD-1, and anti-PD-1 following varying dosage frequencies (every 3, 10, 30, 60, 90, 150 days, and the continuous case). Simulations run for 365 days. The spikes in the T cell density correspond to injections of anti-PD-1, as the drugs allow for an increased activation of T cells. The tumor cells are most effectively contained for the continuous case. Drops in the PD-1 concentration correspond to injections of anti-PD-1 drugs, as more free PD-1 binds to the drug. As the dosage of the drug wears off, we notice an increase in the level of PD-1.

30 days) periodically approach a lower density, closer to that of the continuous drug. Thus, the simulations suggest that more frequent treatments produce more effective results. As the tumor-immune reactions and PD-1-PD-L1 complex formations are fast, the drug is entirely eliminated from the system before the next treatment begins. When the time between treatments is smaller, the drug remains continuously in the system and is thus more effective.

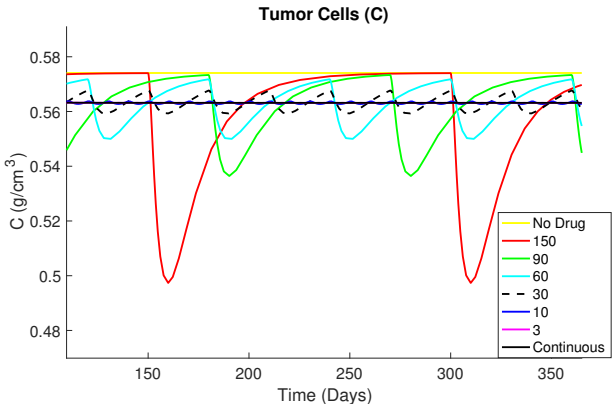

Figure 2.9: Zoomed in density of tumor cells following varying dosage frequencies (every 3, 10, 30, 60, 90, 150 days, and the continuous case). One period is shown.

An interesting area we wish to explore with our model is the behavior of the tumor-immune system when the treatment is abruptly ended (switch on/off treatment). We have chosen a period of 180 days (approximately half of a year) to apply the treatment, after which the treatment will be terminated, as shown in Figure 2.10. Once the treatment has ended, the density of the tumor cells and activated T cells eventually approach the same steady state as if no drug had ever been applied. Similar results were found when the time interval before treatment termination was increased.

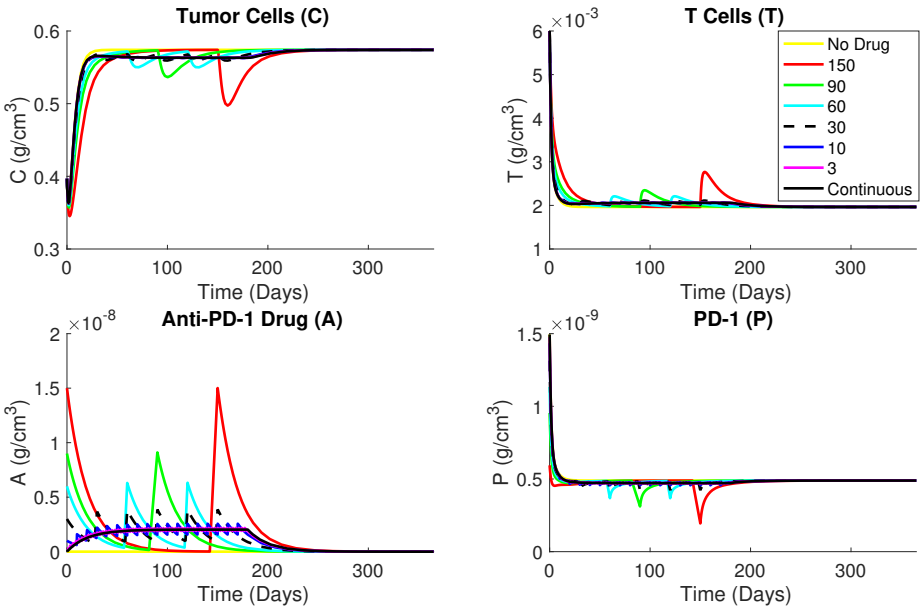

Figure 2.10: Anti-PD-1 and PD-1 concentrations with the following varying dosage frequencies (every 3, 10, 30, 60, 90, 150 days, and the continuous case). Treatments are shut off after 180 days. Simulations run for 365 days.

2.8 Discussion

Tumor immunotherapy is one of the current focuses in oncology. One common form of immunotherapy employs the use of immune checkpoint inhibitors, such as anti-PD-1, in a variety of tumors, including melanoma, and lung cancer. A growing number of clinical trials using drugs with this mode of action seek to improve survival rates and quality of life. Current trials suggest that the use of a single agent such as anti-PD-1 produces a low tumor-immune response. Combinations of anti-PD-1 with other types of treatments are the recommended protocol to produce the most effective results (Hamanishi *et al.*, 2016).

The primary purpose of this work is to gain insight into the tumor-immune response while highlighting immune checkpoint therapy. Due to lack of data, many

of the parameter values are difficult to estimate. Therefore, we developed a simplified model in an effort to explore interesting mathematical results. In particular, we assume that association and dissociation of PD-1/PD-L1 are fast enough to be at a steady state at the scale of tumor growth. Despite this simplification, our simulations reflect expected dynamics. Although we cannot currently test the predictive capability of our model because of sparse data, we can use the results to predict general behaviors of the tumor-immune response to treatment.

Our approach contrasts and complements that of (Lai and Friedman, 2017). Their model is a system of 13 partial differential equations with 48 parameters. Their goal was to explore the synergy of two drugs (anti-PD-1 and GVAX). One of Lai and Friedman's major contributions is a detailed parameterization. Unfortunately, many of these parameters are unexplored in the empirical literature, usually due to overwhelming technical challenges. Because of these uncertainties, we arrived at quite wide ranges for many of the parameters. In some cases, these ranges were not in agreement with Lai and Friedman. For example, since many tumor cells express PD-L1, they set ϵ_C, the expression of PD-L1 in tumor cells versus T cells, to be $0 - 0.01$. However, we concluded that $\epsilon_C = 1 - 100$ based on literature indicating PD-L1 is upregulated in some tumor types (Spranger *et al.*, 2013).

Due to a lack of data, our model cannot be validated, so there is limited predictive capability. However, it provides insight into how the tumor and T cell densities depend on parameter values. Our sensitivity analysis using PRCC via LHS showed λ_C, the tumor cell growth rate, η, the kill rate of tumor cells by T cells, and d_T, the death rate of T cells, were the most sensitive parameters and are thus the main drivers of the tumor burden. Furthermore, the bifurcation analysis for d_T confirmed the findings of the sensitivity analysis. The bifurcation diagram suggests that the stability of the tumor-free and tumorous equilibria changes as d_T varies. These results are biologically

significant. If the lifetime of T cells lasts less than four days, the tumorous equilibrium becomes stable, resulting in a significant disease. Thus, our model suggests that cancers are likely to be more common and significant for patients with weakened immune systems, whether from age, emotional, or physical stress. Our model further suggests that, if caught early enough before the immune system becomes too weak, it is possible to eradicate the tumor with minimal treatment.

The simulations suggest anti-PD-1 is most effective when it is applied continuously. Without a continuous or frequent injection of the drug, the end results are as if no drug was applied. However, even when applied continuously, it is not a sufficient treatment to eradicate the tumor cells. It would be most beneficial to pair anti-PD-1 with another treatment. Previous anti-PD-1 trials reached similar conclusions (Antonios *et al.*, 2016). When combined with a dendritic cell vaccination, the treatment produced a substantial increase in survival. However, when anti-PD-1 alone was used, the benefit was not notable.

Recent clinical trials suggest that combining the immune checkpoint inhibitor with an alternative treatment is the most effective way to treat tumors (Antonios *et al.*, 2016). Anti-PD-1 is not fully effective due to a lack of T cells (Kleponis, Skelton, and Zheng, 2015). Although a single-agent checkpoint inhibitor increases T cell density, our simulations suggest anti-PD-1 alone cannot raise the activated T cells to the level needed to eradicate the tumor cells (Figure 2.8). When combined with a vaccine or therapy that increases the amount of T cells, anti-PD-1 has a more substantial anti-tumor immune response, as it can help more T cells remain active in killing tumor cells (Lai and Friedman, 2017).

Our stability analysis of the drug-free system established requirements for global stability of the tumorous and tumor-free equilibria. Two conditions are required to eliminate the tumor: $\lambda_C < \eta T_0^*$ and $d_T > N$. Biologically, we see that $\lambda_C < \eta T_0^*$

means that when the tumor is initially growing, the T cells can kill the cancer cells faster than the cancer cells multiply. The condition $d_T > N$ can be interpreted as the death rate of the T cells being greater than the stimulation rate of T cells by IL-2. Thus, the mathematical analysis suggests that even patients with weakened immune systems, and thereby shorter lifetimes of T cells, can see tumor elimination for slow-growing tumors. Though the condition $d_T > N$ complements the mathematical analysis, the bifurcation diagram suggests our mathematical results still have room for improvement. This condition proves to be sufficient but not necessary for determining the stability of the tumor-free and tumorous equilibria. Further exploration is required to determine necessary conditions.

Chapter 3

MATHEMATICAL MODELING OF AN IMMUNE CHECKPOINT INHIBITOR AND ITS SYNERGY WITH AN IMMUNOSTIMULANT

3.1 Abstract

Immune checkpoint inhibitors (ICIs) are a novel cancer therapy that may induce tumor regression across multiple types of cancer. There has recently been interest in combining the ICIs with other forms of treatments, as not all patients benefit from monotherapy. We propose a mathematical model consisting of ordinary differential equations to investigate the combination treatments of the ICI avelumab and the immunostimulant NHS-muIL12. We validated the model using the average tumor volume curves provided in Xu et al. (2017). We initially analyzed a simple generic model without the use of any drug, which provided us with mathematical conditions for local stability for both the tumorous and tumor-free equilibrium. This enabled us to adapt these conditions for special cases of the model. Additionally, we conducted systematic mathematical analysis for the case that both drugs are applied continuously. Numerical simulations suggest that the two drugs act synergistically, such that, compared to monotherapy, only about one-third the dose of both drugs is required in combination for tumor control.

3.2 Introduction

Immune checkpoint inhibitors are a family of novel cancer therapies under investigation in multiple clinical trials. The checkpoint protein programmed death-1, mainly expressed on the surface of activated T cells, inhibits immune activation upon binding

to its ligand programmed death-ligand 1 (Alsaab *et al.*, 2017). Induction of PD-L1 on cancer cells and T cells is an important mechanism for tumor immune escape (Juneja *et al.*, 2017). The development of drugs such as avelumab (PD-L1 inhibitor) and nivolumab (PD-1 inhibitor), that inhibit the binding of PD-1 with PD-L1, have shown promising results in treating different types of cancer, including melanoma and bladder cancer (Alsaab *et al.*, 2017). However, as reported in Yan *et al.* (2018), up to $60 - 70\%$ of patients fail to respond to ICI monotherapy. On the other hand, combination treatment may improve efficacy across tumor types and help address issues such as resistance (Zamarin and Postow, 2015). Particularly, recent clinical trials suggest that coupling ICIs with treatments such as radiation, chemotherapy or other forms of immunotherapies, such as dendritic cell (DC) vaccines, improves the efficacy of the treatment (Kang *et al.*, 2016).

Mathematical modeling has proven to be an important tool in cancer research, as it not only provides insights by capturing tumor mechanisms but also helps guide the design of new experiments based on predictions from the model (Blair *et al.*, 2012). Additionally, the incorporation of drug treatments in mathematical models can result in better understanding and improved treatments (Stephanou *et al.*, 2019). In recent years several mathematical models focusing on ICIs in conjunction with other treatments have been developed (Lai and Friedman, 2017; Radunskaya *et al.*, 2018; Serre *et al.*, 2016). Specifically, Lai and Friedman (Lai and Friedman, 2017) formulated a system of partial differential equations to study the efficacy and synergy between anti-PD1 treatment and a GM-CSF secreting cancer vaccine (GVAX), and created a synergy map of the recommended amount of drug dosages that should be administrated to reduce the tumor level as presented in Chapter 2. Radunskaya et al. (Radunskaya *et al.*, 2018) studied the effects of anti-PD-L1 in combination with a dendritic cell (DC) vaccine, tested against mouse data and investigated treatment

schedules and effects of varying dosage amounts. Serre et al. (Serre *et al.*, 2016) constructed a discrete pharmacokinetic model investigating synergism between radiotherapy anti-PD1/PD-L1 antibodies and/or CTLA4 inhibitor and used experimental data for validation.

While these models yield interesting results, we wish to capture the dynamics of applying a combination treatment to a continuous model in a more simplified manner than Lai and Friedman (2017) and Radunskaya *et al.* (2018). In Nikolopoulou *et al.* (2018) we developed a simple tumor-immune response model that incorporated the effects of a single immune checkpoint inhibitor (anti-PD-1) and mathematically analyzed the no drug case. Further global analysis of the mathematical model was presented in Shi *et al.* (2020). Using our work as a basis Nikolopoulou *et al.* (2018) and taking advantage of the data found in Xu *et al.* (2017), we present a modification of the model and examine the effects of combining PD-L1 inhibitor with an immunostimulant. One important difference with the existing model is the use of the anti-PD-L1 antibody, avelumab. Avelumab is a monoclonal antibody that targets PD-L1, thus inhibiting its binding with PD-1 and enabling immune stimulation (Chin *et al.*, 2017). Additionally, we incorporate in the model an additional immunotherapy, NHS-muIL12. NHS-muIL12 is a fusion protein that binds to the DNA targeting the administration of IL-12 to damaged intratumoral regions (Xu *et al.*, 2017).

In this work we initially propose a simple generic mathematical model that represents the dynamics of a tumor-immune response model without treatment. We mathematically analyze special cases of the generic model with the goal of building a biologically and mathematically sound model that will describe the dynamics of a combination treatment based on the experiment in Xu *et al.* (2017). We use the mouse data from Xu *et al.* (2017) to determine appropriate biological, data-driven parameter estimates, and validate the model. Aside from the types of treatments

used in the experiment Xu *et al.* (2017), we also investigate the effects of continuous injection of both drugs (avelumab and NHS-muIL12). Finally, we numerically study the drug in combination to explore possible synergy between the drugs.

3.3 Formulation of the Mathematical Model

In an effort to biologically capture the behavior of a tumor-immune response system that represents the data in Xu *et al.* (2017) in the absence of treatments, we initially propose a simple generic mathematical model that follows a predator-prey structure. Examples of such mathematical models have been noted in several publications (Meng *et al.*, 2018).

The initial model consists of two simple generic differential equations for the tumor cell volume (V) and the number of activated T cells (T) and has the following form:

$$\frac{dV}{dt} = Vg(V) - p(V)T, \tag{3.3.1}$$

$$\frac{dT}{dt} = \delta F(V,T) - d_T T. \tag{3.3.2}$$

We assume all functions appearing in the model are sufficiently smooth. In addition, we make the following more specific assumptions:

(A1): The initial tumor growth rate $g(0)$ is positive and the growth rate $g(V)$ is a non-increasing function of the tumor volume (V), as V approaches the maximum resources in the environment known as the carrying capacity.

(A2): The kill rate of the tumor cells $p(V)$ is an increasing function of the tumor volume V.

(A3): The T cell activation function $F(V,T)$ is a positive and decreasing function of both variables.

Table 3.1: State variables of the model system (3.3.1)-(3.3.2) and (3.3.3)-(3.3.6).

Variable	Meaning	Unit
V	tumor cell volume	mm^3
T	number of activated T cells	mm^3
L	free PD-L1 volume	mm^3
P	free PD-1 volume	mm^3
A_1	anti-PD-L1 concentration	g
A_2	NHS-muIL12 concentration	g
Q	PD-1-PD-L1 volume	mm^3

All the information regarding the variables of the generic model are described by Table 3.1. Equation (3.3.1) describes the tumor cell volume (V), where $g(V)$ denotes the growth rate of the tumor volume. There is a variety of ways that the growth rate can be represented such as the logistic model $g(V) = r(1 - \frac{V}{K})$ with $K \geq 0$, the exponential model $g(V) = r > 0$, the Gompertz model $g(V) = a - b \ln V$, and other forms (Kuang *et al.*, 2015). The term $p(V)$, kill rate of tumor volume by activated T cells, is a function of the tumor volume (V) and can be represented by expressions such as $p(V) = \eta V$ and $p(V) = \frac{\eta V}{K_V + V}$. Equation (3.3.2) describes the activated T cells volume (T), where $F(V, T)$ describes the growth of activated T cells, and $d_T T$ represents the natural death of the T cells. Based on this generic model, we mathematically investigate two special cases of the model. The special cases consist of different tumor growth models, i.e logistic and exponential model. Both logistic and exponential growth models are commonly used to model tumor growth. A lot of work has been done that compares different growth models with the goal of achieving best fits as shown in Saparata and Pillis (2014). Logistic growth describes

tumor growth over a long period of time, since the tumor has a limited amount of resources (carrying capacity), such as oxygen and nutrients to survive. Exponential growth has been widely used to model experimental data for early growth of the tumor (Talkington and Durett, 2015). We analyze these special cases of the generic model in the absence of treatments to gain mathematical and biological insights. These insights help us to build a special case model that best captures the synergistic effects of a combination treatment.

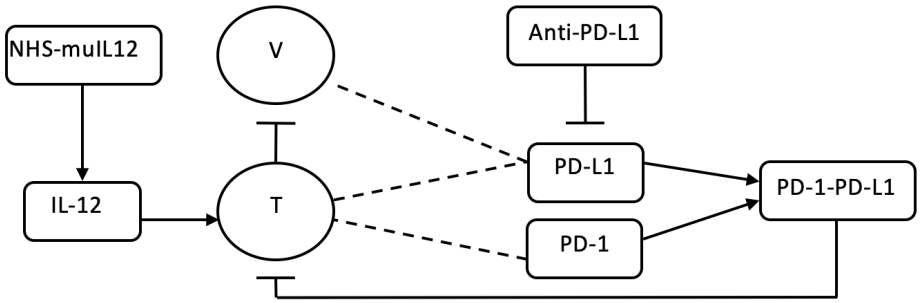

Figure 3.1: Schematic model representation for tumor-immune interactions. Sharp arrows indicate proliferation/activation. Blocked arrows indicate killing/blocking. Dashed lines indicate proteins on the tumour (V) or T cells (T). IL-12 stimulates the proliferation of activated T cells. NHS-muIL12's role is to administrate IL-12 to damaged intratumoral regions. PD-L1 is mainly expressed on tumor cells. Anti-PD-L1 binds to PD-L1 to prevent the formation of the PD-1-PD-L1 complex.

We extend equations (3.3.1)-(3.3.2), using the previous work in Nikolopoulou *et al.*

(2018), to develop a model of treatment response to two immunotherapies. Figure 3.1 represents a schematic network between all the model variables. The model consists of four nonlinear ordinary differential equations, which takes the following generic form:

$$\frac{dV}{dt} = \underbrace{Vg(V)}_{\text{net tumor growth}} - \underbrace{p(V)T}_{\text{killed by T cells}}, \tag{3.3.3}$$

$$\frac{dT}{dt} = \underbrace{\delta F(V,T,A_1,A_2)}_{\text{T cell activation}} - \underbrace{d_T T}_{\text{death}}, \tag{3.3.4}$$

$$\frac{dA_1}{dt} = \underbrace{\gamma_1(t)}_{\text{infusion rate of avelumab}} - \underbrace{d_{A_1}A_1}_{\text{natural degradation}}, \tag{3.3.5}$$

$$\frac{dA_2}{dt} = \underbrace{\gamma_2(t)}_{\text{infusion rate of NHS-muIL12}} - \underbrace{d_{A_2}A_2}_{\text{natural degradation}}. \tag{3.3.6}$$

For the purpose of numerical simulations we choose the following functions:

$$g(V) = r,$$

$$p(V) = \eta V,$$

$$F(V,T,A_1,A_2) = \left(1 + \frac{\lambda_{TI_{12}}T}{\delta}\frac{c_2A_2}{K_{A_2}+c_2A_2}\right)\cdot\frac{1}{1+\frac{Q(V,T,A_1)}{K_{TQ}}}.$$

All state variables of the system are described in Table 3.1. Equations (3.3.3) and (3.3.4) are the same as equations (3.3.1) and (3.3.2), where we choose exponential growth and a mass action term for the T cell tumor killing. For the T cell activation function, F, we assume that NHS-muIL12 drug (A_2) activates T cells in a saturating manner, according to the Michaelis-Menten law. Note that c_2 represents a constant, where $c_2 \in [\frac{1}{75}\cdot 10^{-7}, \frac{1}{75}\cdot 10^{-6}]$ as derived in Appendix D. As the amount of the complex PD-1-PD-L1 (Q) increases, T cell activation is reduced by a factor of $\frac{1}{1+\frac{Q}{K_{TQ}}}$. As above, d_T is the natural death rate for T cells.

The rate of change of avelumab (A_1) is modeled by Equation (3.3.5), where $\gamma_1(t)$ is the prescribed infusion rate of avelumab. We consider the treatment protocol in Xu *et al.* (2017), where avelumab is injected on days $0, 3, 6$. The parameter d_{A_1} denotes the natural decay of A_1. Similarly to A_1, we consider a very simple differential equation for NHS-muIL12 (A_2), which is administered on day 0 as denoted by Equation (3.3.6). The parameter d_{A_2} depicts the natural decay of A_2. Moreover, we consider the case where we administrate both A_1 and A_2 continuously, and study the tumor dynamics for approximately 220 days.

What remains is to derive an expression for the complex PD-1-PD-L1 (Q) in equation (3.3.4). To that end, we start by observing that PD-1 (P) is expressed on the surface of activated T cells (Simon and Labarriere, 2017; Shi *et al.*, 2013). Hence, we take

$$P = \rho_P T, \tag{3.3.7}$$

where, ρ_P is the cell rate of expression of PD-L1 on T cells as in Lai and Friedman (2017) and similar to Chapter 2.

PD-L1 (L) is expressed on the surface of activated T cells and cancer cells (Shi *et al.*, 2013). Thus, the concentration of PD-L1 is proportional to T cells and cancer cells as in Lai and Friedman (2017) and similar to Chapter 2.

$$L_{total} = \rho_L(T + \epsilon_V V),$$

where, ρ_L the cell rate of expression of PD-1 on T cells and ϵ_v depends on the specific type of tumor.

The amount of total PD-L1 consists of the amount of free PD-L1 and the amount of PD-L1 bound to the drug as described below.

$$L_{total} = L_{free} + L_{bound}, \tag{3.3.8}$$

$$L_{free} = L_{total} - L_{bound} = \rho_L(T + \epsilon_V V) - L_{bound}. \tag{3.3.9}$$

We assume the dissociation ($d_Q Q$) and association (α_{PL}) of the complex PD-1-PD-L1 are fast so that we can apply the usual quasi-steady-state argument to the reaction as in Lai and Friedman (2017).

$$P + L \underset{d_Q}{\overset{\alpha_{PL}}{\rightleftharpoons}} Q.$$

We obtain $\alpha_{PL} PL = d_Q Q$, where α_{PL} and d_Q are the association of PL and dissociation rate of Q, respectively . Thus, by equations (3.3.7) and (3.3.9)

$$Q = \sigma P L_{free} = \sigma \rho_p T(\rho_L(T + \epsilon_V V) - L_{bound}), \text{ with } \sigma = \alpha_{PL}/d_Q. \tag{3.3.10}$$

Next, we consider the reaction scheme:

$$L_{free} + A_1 \underset{k_{-1}}{\overset{k_{+1}}{\rightleftharpoons}} L_{bound},$$

where k_{+1} and k_{-1} are the constants for the forward and reverse reactions. The parameter k_{+1} describes the association reaction, and k_{-1} denotes the dissociation of anti-PD-L1 from the receptor. By the law of mass action and assuming the process is at equilibrium we have,

$$\frac{dL_{bound}}{dt} = k_{+1} L_{free} A_1 - k_{-1} L_{bound} = 0,$$
$$L_{bound} = \frac{k_{+1}}{k_{-1}} L_{free} A_1 = \frac{k_{+1}}{k_{-1}} (L_{total} - L_{bound}) A_1.$$

After solving for L_{bound} with algebraic manipulation, we conclude that

$$L_{bound} = \frac{k_{+1} A_1}{k_{+1} A_1 + k_{-1}} (\rho_L(T + \epsilon_V V)).$$

Hence,

$$L_{bound} = \frac{A_1}{A_1 + \frac{k_{-1}}{k_{+1}}} (\rho_L(T + \epsilon_V V)),$$

$$L_{bound} = \frac{c_1 A_1}{c_1 A_1 + K_{A_1}} (\rho_L(T + \epsilon_V V)), \text{ with } K_{A_1} = \frac{k_{-1}}{k_{+1}}. \tag{3.3.11}$$

Note that c_1 represents a constant, where $c_1 \in [\frac{1}{55} \cdot 10^{-7}, \frac{1}{55} \cdot 10^{-6}]$ as derived in Appendix D. By substituting equation (3.3.11) into equation (3.3.12), we have derived the following expression for Q,

$$Q = \sigma \rho_P \rho_L T(T + \epsilon_V V)\left(1 - \frac{c_1 A_1}{c_1 A_1 + K_{A_1}}\right), \text{ with } \sigma = \alpha_{PL}/d_Q. \tag{3.3.12}$$

Finally, using all the above derived equations we seek to gain a better understanding of the system (3.3.3)-(3.3.6).

3.4 Mathematical Analysis for the General Case

We initially consider the case when no drug is applied using the system of equations (3.3.1)-(3.3.2). We wish to determine some necessary conditions for the local stability of the tumorous and tumor-free steady states in the general form.

The general model has the following form:

$$\frac{dV}{dt} = Vg(V) - p(V)T, \tag{3.4.13}$$

$$\frac{dT}{dt} = \delta F(V, T) - d_T T. \tag{3.4.14}$$

To facilitate the mathematical analysis, we make the following more specific assumptions:

1. $g(V)$ is a continuously differentiable function and there exists a $K > 0$ such that $g(V) > 0$ when $V \in (0, K)$ and $g(V) < 0$ for $V > K$.

2. $p(V)$ is a continuously differentiable strictly increasing function such that $p(0) = 0$.

3. $F(V, T)$ is a continuously differentiable strictly decreasing, positive and bounded function.

We begin by studying the positivity and boundedness of solutions of system (3.4.13)-(3.4.14). The following proposition assures us that these desirable properties are held by system (3.4.13)-(3.4.14).

Proposition 3.4.1 *Solutions of system* $(3.4.13)-(3.4.14)$ *that start positive remain positive and bounded.*

Proof. We first show that $T(t)$ can not be zero or negative before V using proof by contradiction. We assume that the starting time is t_0. Hence $T(t_0) > 0$. Then for $T(t) \leq 0$ for some $t > t_0$, there must be a time $t_1 > t_0$ such that $T(t_1) = 0$ and $\frac{dT}{dt}(t_1) \leq 0$. However, $\frac{dT}{dt}(t_1) = \delta F(V, 0) > 0$. Thus, $T(t) > 0$, for $t \geq t_0$.

Next we assume that there is a $t_1 > t_0$ such that $V(t_1) = 0$, and $V(t), T(t)$ are nonegative on $[t_0, t_1]$. By a standard separation of variables,

$$\frac{dV}{dt} = p(V)\left(V\frac{g(V)}{p(V)} - T\right) = p(V)(H(V) - T),$$

where, $H(V) = \frac{Vg(V)}{p(V)}$

$$\frac{dV}{dt} = \frac{Vp(V)}{V}(H(V) - T),$$
$$\frac{dV}{V} = \left(\frac{p(V)}{V}(H(V) - T)\right)dt.$$

We can conclude that,

$$V(t_1) = V(t_0)\exp\left[\int_{t_0}^{t_1}\left(\frac{p(V)}{V}(H(V) - T)\right)dt\right] > 0$$

since $V(t_0) > 0$.

Hence, both $T(t)$ and $V(t)$ are positive when exist. Next, we will prove that they stay bounded.

We start with boundedness of V using comparison argument.

$$\frac{dV}{dt} = Vg(V) - p(V)T$$
$$\leq Vg(V)$$

which implies that

$$V(t) \leq \max\{V(0), K\}.$$

In addition, we see that

$$\limsup_{t\to\infty} V(t) \leq K.$$

Therefore, V is eventually bounded by $K + \alpha$, for any positive constant α.

We then look to prove that T is bounded. Since V is bounded, then $F(V, T)$ is also bounded above by a positive constant, which we assume that it is γ. Hence

$$\begin{aligned}\frac{dT}{dt} &= \delta F(V,T) - d_T T \\ &\leq \delta\gamma - d_T T\end{aligned}$$

which implies that

$$\limsup_{t\to\infty} T(t) \leq \frac{\delta\gamma}{d_T}.$$

Similarly, we see that

$$T(t) \leq \max\left\{T_0, \frac{\delta\gamma}{d_T}\right\}.$$

Hence, T and V are bounded. □

Proposition 3.4.2 *System* (3.4.13) − (3.4.14) *has a unique tumor-free equilibrium* $E_0^* = (0, T_0^*)$, $T_0^* > 0$.

Proof. Observe that $E_0^* = (0, T_0^*)$, $T_0^* > 0$ is an equilibrium of system (3.4.13) − (3.4.14) if and only if $\delta F(0, T_0^*) - d_T T_0^* = 0$. It is easy to see that $\delta F(0, T) - d_T T = 0$ has a unique positive solution since the function $\delta F(0, T) - d_T T$ is positive when $T = 0$, negative when T is very large and is strictly decreasing when $T > 0$. □

Proposition 3.4.3 *System* (3.4.13) − (3.4.14) *has a unique positive tumorous equilibrium* $E^* = (V^*, T^*)$, $V^* > 0, T^* > 0$, *if and only if* $\delta F(V, H(V)) - d_T H(V) = 0$ *has a*

unique positive solution in $(0, K)$*, where* $H(V) = \frac{Vg(V)}{p(V)}$*. In fact,* $E_i = (V_i, T_i)$ *is a positive equilibrium of system* (3.4.13)−(3.4.14) *if and only if* $\delta F(V_i, H(V_i)) - d_T H(V_i) = 0$ *and* $v_i \in (0, K)$*.*

Proof. Setting $\frac{dV}{dt} = 0$ in equation (3.4.13) gives $T = H(V)$, where $H(V) = \frac{Vg(V)}{p(V)}$. Then,

$$\frac{dT}{dt} = 0 \implies \delta F(V, H(V)) - d_T H(V) = 0. \tag{3.4.15}$$

Hence, system (3.4.13)−(3.4.14) has a positive equilibrium $E^* = (V^*, T^*)$, if and only if V^* satisfies equation (3.4.15) and $V^* \in (0, K)$. This implies that the proposition is true. □

The next steps are to perform stability analysis for system (3.4.13)−(3.4.14). The Jacobian for the system written in terms of H to facilitate further analysis is given by:

$$\begin{pmatrix} p'(V)(H(V) - T) + p(V)H'(V) & -p(V) \\ \delta \frac{\partial}{\partial V} F(V, T) & \delta \frac{\partial}{\partial T} F(V, T) - d_T \end{pmatrix}.$$

We examine the stability of both the tumor-free $E_0^* = (0, T_0^*)$ and tumorous equilibrium $E^* = (V^*, T^*)$. Observe that $\lim_{V \to 0^+} H(V) = g(0)/p'(0)$. For convenience, we define

$$H(0) = g(0)/p'(0). \tag{3.4.16}$$

Proposition 3.4.4 *For system* (3.4.13)−(3.4.14)*, the following statements are true.*

(*a*) *If* $T_0^* > H(0)$*, then* E_0^* *is locally asymptotically stable.*

(*b*) *If* $T_0^* < H(0)$*, then* E_0^* *is a saddle point.*

Proof. The Jacobian matrix for the tumor-free equilibrium $E_0^* = (0, T_0^*)$, has the

following form.

$$\begin{pmatrix} p'(0)(H(0)-T_0^*) & 0 \\ \delta\frac{\partial}{\partial V}F(0,T_0^*) & \delta\frac{\partial}{\partial T}F(0,T_0^*)-d_T \end{pmatrix}.$$

We know that $\frac{\partial}{\partial V}F(V,T) < 0$ and $\frac{\partial}{\partial T}F(V,T) < 0$ by assumption, and that the eigenvalues are of the form:

$$\lambda_1 = p'(0)(H(0)-T_0^*) < 0, \text{ if } T_0^* > H(0),$$
$$\lambda_2 = \delta\frac{\partial}{\partial T}F(0,T_0^*) - d_T < 0.$$

Thus, E_0^* is locally asymptotically stable if $T_0^* > H(0)$ and a saddle point if $T_0^* < H(0)$. □

The next proposition deals with the stability of a tumorous equilibrium.

Proposition 3.4.5 *For system* $(3.4.13)-(3.4.14)$*, the following statements are true:*

(a) *If* $H'(V^*) < 0$ *and* $H'(V^*)\left[\delta\frac{\partial}{\partial T}F(V^*,T^*) - d_T\right] + \delta\frac{\partial}{\partial V}F(V^*,T^*) > 0$*, then* $E^* = (V^*,T^*)$ *is stable.*

(b) *If* $H'(V^*) > 0$ *or* $H'(V^*)\left[\delta\frac{\partial}{\partial T}F(V^*,T^*) - d_T\right] + \delta\frac{\partial}{\partial V}F(V^*,T^*) < 0$*, then* $E^* = (V^*,T^*)$ *is a saddle point.*

Proof. The Jacobian matrix for both parts (a) and (b) for the tumorous equilibrium $E^* = (V^*,T^*)$ has the following form.

$$\begin{pmatrix} p(V^*)H'(V^*) & -p(V^*) \\ \delta\frac{\partial}{\partial V}F(V^*,T^*) & \delta\frac{\partial}{\partial T}F(V^*,T^*)-d_T \end{pmatrix}.$$

Then the trace for the tumorous equilibrium is

$$\tau = \underbrace{p(V^*)}_{>0}H'(V^*) + \underbrace{\delta\frac{\partial}{\partial T}F(V^*,T^*)}_{<0} - \underbrace{d_T}_{>0}.$$

It is easy to see that the trace is negative when $H'(V^*) < 0$ by condition in part (a). The determinant is given by

$$\Delta = \underbrace{p(V^*)}_{>0}\left\{\underbrace{H'(V^*)}_{<0}\underbrace{\left[\delta\frac{\partial}{\partial T}F(V^*,T^*) - d_T\right]}_{<0} + \underbrace{\delta\frac{\partial}{\partial V}F(V^*,T^*)}_{<0}\right\}. \tag{3.4.17}$$

The determinant is positive provided

$$H'(V^*)\left[\delta\frac{\partial}{\partial T}F(V^*,T^*) - d_T\right] + \delta\frac{\partial}{\partial V}F(V^*,T^*) > 0.$$

Hence, the tumorous equilibrium $E^* = (V^*, T^*)$ is stable provided the condition in part (a) is true. Similarly, the conclusion of part (b) follows. □

Proposition 3.4.6 *If $H'(V) < 0$ for $V > 0$, then system (3.4.13) − (3.4.14) has no nontrivial positive periodic solutions.*

Proof. We employ the Dulac criterion to show there are no nontrivial positive periodic orbits. Let $b(V) = 1/p(V)$. Let $F_1(V,T) = \frac{Vp(V)}{V}(H(V) - T)$ and $F_2(V,T) = \delta F(V,T) - d_T T$. Then it is easy to see that

$$\Omega = \frac{\partial[b(V)F_1(V,T)]}{\partial V} + \frac{\partial[b(V)F_2(V,T)]}{\partial T} = H'(V) + \frac{1}{p(V)}\frac{\partial[b(V)F_2(V,T)]}{\partial T} < 0.$$

By the Dulac criterion, we see that the system (3.4.13) − (3.4.14) has no nontrivial positive periodic solutions. □

With arguments similar to that of the proof of Theorem 1 in Chapter 2, we can obtain the following global stability result for the tumor free equilibrium in system (3.4.13)-(3.4.14).

Theorem 2 *If $H'(V) < 0$ for $V > 0$ and $\delta F(V, H(V)) - d_T H(V) = 0$ has no positive solution, then the tumor free equilibrium $E_0^* = (0, T_0^*)$ in system (3.4.13) − (3.4.14) is globally attractive with respect to positive solutions.*

3.4.1 Dynamics with Logistic Growth

To perform local stability analysis for the logistic growth case, we use the following set of functions: $g(V) = r(1 - \frac{V}{K_V}), p(V) = \eta V$ and

$$F(V,T) = \frac{1}{1 + \alpha' T(T + \epsilon_V V)},$$

where $\alpha' = \frac{\sigma \rho_p \rho_l}{K_{TQ}}$. We provide a step-by-step derivation of the proofs using results from Section 3.4 in combination to the details provided in Nikolopoulou *et al.* (2018).

The system (3.4.13)-(3.4.14) takes the following form:

$$\frac{dV}{dt} = rV(1 - \frac{V}{K_v}) - \eta VT \tag{3.4.18}$$

$$\frac{dT}{dt} = \delta F(V,T) - d_T T \tag{3.4.19}$$

where we use the assumptions that

$$\begin{aligned} F(V,T) &= \frac{1}{1 + \frac{Q}{K_{TQ}}} = \frac{1}{1 + \frac{\sigma \rho_p \rho_l T(T + \epsilon_V V)}{K_{TQ}}} \\ &= \frac{1}{1 + \alpha' T(T + \epsilon_V V)} \end{aligned}$$

and $\alpha' = \frac{\sigma \rho_p \rho_l}{K_{TQ}}$.

The system has the following equilibria: $E_0^* = (0, T_0^*)$ and $E_1^* = (V^*, T^*)$. We first start by insuring uniqueness and existence of the equilibria. Our steps closely follow the mathematical analysis performed in Chapter 2.

Proposition 3.4.7 *The system (3.4.18)-(3.4.19) has a unique tumor-free equilibrium* $E_0^* = (0, T_0^*)$.

Proof. When $V^* = 0$ then $\frac{\delta}{1 + \alpha' T^2} - d_T T = 0$, where $\alpha' = \frac{\sigma \rho_p \rho_l}{K_{TQ}}$. The T^* values corresponding to $V^* = 0$ are the roots of the following equation:

$$p(T) = d_T \alpha' T^3 + d_T T - \delta = 0$$

Since $p(0) = -\delta$ and $\lim_{T\to\infty} p(T) = \infty$ and $p'(T) = 3d_T\alpha' T^2 + d_T > 0$ implies that there is a single root. Hence, our first equilibrium is of the form $E_0^* = (0, T^*)$. $\square$

Proposition 3.4.8 *The system (3.4.18)-(3.4.19) has a unique tumorous equilibrium* $E_1^* = (V^*, T^*)$, $V^* > 0$, $T^* > 0$ *if* $\frac{\epsilon_V K_V \eta}{r} < 1$ *and* $f\left(\frac{r}{\eta}\right) < 0$.

Proof. It is easy to see that

$$r(1 - \frac{V^*}{K_V}) = \eta T^*$$

$$\delta = d_T T^*(1 + \alpha' T^*(T^* + \epsilon_V V))$$

These together yield to

$$f(T^*) = d_T\alpha'(\frac{\epsilon_V K_V \eta}{r} - 1)T^{*3} - d_T\alpha'\epsilon_V K_V T^{*2} - d_T T^* + \delta = 0$$

Following exactly the same steps as in Proposition 2.5.3, we conclude that the system (3.4.18)-(3.4.19) has a unique tumorous equilibrium $E_1^* = (V^*, T^*)$, $V^* > 0$, $T^* > 0$ provided $\frac{\epsilon_V K_V \eta}{r} < 1$ and $f\left(\frac{r}{\eta}\right) < 0$. $\square$

Proof of the corollary below follows extactly from Proposition 3.4.4.

Corollary 3.4.9 *For the tumour-free equilibrium* $E_0^* = (0, T_0^*)$, *the following statements are true.*

(a) If $r < \eta T_0^*$, *then* E_0^* *is locally asymptotically stable.*

(b) If $r > \eta T_0^*$, *then* E_0^* *is a saddle point.*

Proposition 3.4.10 *Assume that* $\frac{\eta\epsilon_V K_V}{r} < 1$ *and* $f\left(\frac{r}{\eta}\right) < 0$, *then the tumorous steady state* E_1^* *of system (3.4.18)-(3.4.19) is unique and is locally asymptotically stable.*

Proof. The trace for the tumorous equilibrium is then:

$$\tau = -r\frac{V}{K_V} + \delta\frac{\partial}{\partial T}F(V^*, T^*) - d_T < 0$$

The determinant based on equation (3.4.17) is given by:

$$\begin{aligned}
\Delta &= \eta V^*\left\{ -\frac{r}{\eta K_V}\left[\delta\frac{\partial}{\partial T}F(V^*, T^*) - d_T\right] + \delta\frac{\partial}{\partial V}F(V^*, T^*)\right\} \\
\Delta &= r\frac{V^*}{K_V}d_T + V^*\delta\Big(-\frac{r}{K_V}\frac{\partial}{\partial T}F(V^*, T^*) + \eta\frac{\partial}{\partial V}F(V^*, T^*)\Big) \\
\Delta &= r\frac{V^*}{K_V}d_T + (V^*\delta)\Gamma
\end{aligned}$$

where,

$$\Gamma = -\frac{r}{K_V}\frac{\partial}{\partial T}F(V^*, T^*) + \eta\frac{\partial}{\partial V}F(V^*, T^*)$$

The proof that $\Gamma > 0$ follows directly from Proposition 2.5.5. □

As for determining whether or not the system (3.4.18)-(3.4.19) has periodic orbits, Proposition 3.4.6 can be directly applied.

Corollary 3.4.11 *The system (3.4.18)-(3.4.19) has no nontrivial positive periodic solutions.*

The following Theorem that determines the global stability for the system (3.4.18)-(3.4.19) follows exactly as Theorem 1 in Chapter 2.

Theorem 3 *The following are true:*

(i) If $r < \eta T_0^*$ and no tumorous equilibrium exists, then the tumor-free equilibrium E_0^* of the system (3.4.18)-(3.4.19) is globally asymptotically stable.

(ii) If $\frac{\eta\epsilon_V V_K}{r} < 1$ and $f\left(\frac{r}{\eta}\right) < 0$, then the tumorous steady state E_1^* of the system (3.4.18)-(3.4.19) is globally asymptotically stable.

3.4.2 Dynamics with Exponential Growth

The exponential growth case can be regarded as the limiting profile for logistic growth when the carrying capacity is set as infinity. With this in mind, we can apply the conditions found above to the exponential growth model. Since the exponential growth case will be the focus of the treatment study, we present the following specific local stability results for the case with $g(V) = r$, $p(V) = \eta V$ and

$$F(V,T) = \frac{1}{1 + \alpha' T(T + \epsilon_V V)}, \tag{3.4.20}$$

where $\alpha' = \frac{\sigma \rho_p \rho_l}{K_{TQ}}$. We present them as corollaries. Proofs of the corollaries follow directly from Propositions 3.4.4 and 3.4.5.

Corollary 3.4.12 *For the tumour-free equilibrium $E_0^* = (0, T_0^*)$, the following statements are true.*

(a) If $r < \eta T_0^*$, then E_0^* is asymptotically stable.

(b) If $r > \eta T_0^*$, then E_0^* is a saddle point.

The condition $r < \eta T_0^*$ can be biologically interpreted, as the fact that T cells killing rate is faster than the growth rate of cancer cells.

Corollary 3.4.13 *The tumorous equilibrium $E^* = (V^*, T^*)$ is a saddle point.*

Now we wish to explore the dynamics of the model (3.3.3)-(3.3.6), when both drugs are applied continuously as shown in Section 3.6 and the dynamics of an approximation of the system (3.3.3)-(3.3.6) as described below.

3.5 Mathematical Analysis for the Continuous Treatment Case: Limiting System

We consider the differential equation system (3.3.3)-(3.3.6) and examine the case when both anti-PD-L1 treatment and NHS-muIL12 treatment are applied continu-

ously. In this section, we assume that $g(V) = r$, $p(V) = \eta V$ and (3.4.20) holds. We wish to obtain necessary conditions for the local stability of the tumorous and the tumor-free steady states. We apply a quasi-steady state approximation, where we let A_1 and A_2 go to quasi-steady state. In equations (3.3.5)-(3.3.6), we let $\gamma_1(t) = \gamma_1$ and $\gamma_2(t) = \gamma_2$. Using the quasi-steady state argument we obtain:

$$A_1 = \frac{\gamma_1}{d_{A_1}}, A_2 = \frac{\gamma_2}{d_{A_2}} \tag{3.5.21}$$

Substituting (3.5.21) in (3.3.4) we get the following reduced system consisting of a set of positive differential equations:

$$\frac{dV}{dt} = rV - \eta VT, \tag{3.5.22}$$

$$\frac{dT}{dt} = \Big(\delta + \lambda_{TI_{12}} TM\Big) F(V,T) - d_T T, \tag{3.5.23}$$

where,

$$\begin{aligned} M &= \frac{c_2\gamma_2}{d_{A_2}K_{A_2} + c_2\gamma_2}, \\ N &= \frac{c_1\gamma_1}{d_{A_1}K_{A_1} + c_1\gamma_1}, \\ Q &= \sigma\rho_p\rho_l T(T + \epsilon_v V)(1 - N), \\ F(V,T) &= \frac{1}{1 + \alpha' T(T + \epsilon_v V)}, \\ \alpha' &= \frac{\sigma\rho_p\rho_l}{K_{TQ}}(1 - N), \quad \text{with } N < 1. \end{aligned}$$

Due to the fact that the function $\Big(\delta + \lambda_{TI_{12}} TM\Big) F(V,T)$ may not be decreasing with respect to T, we see that system (3.5.22) − (3.5.23) is not a special case of system (3.4.13) − (3.4.14). It is easy to see the solution of the above system (3.5.22) − (3.5.23) with positive initial values is positive. We seek to examine conditions ensuring boundedness of solutions for the system. Due to the assumption of an exponential growth form for V, we see that V can grow exponentially in the absence of T. Hence,

for any constant $M > 0$, we can find a solution with small positive initial values in both V and T that can have values of V exceed M at some later time. Therefore, we are not able to establish boundedness for V. However, the following proposition is true.

Proposition 3.5.1 *The T component of any positive solution of system* (3.5.22) − (3.5.23) *is bounded.*

Proof. System (3.5.22)-(3.5.23) is equivalent to

$$\frac{dV}{dt} = rV - \eta VT \tag{3.5.24}$$

$$\frac{dT}{dt} = \left(\delta + \lambda_{TI_{12}} TM\right) \frac{1}{1 + \alpha' T(T + \epsilon_v V)} - d_T T. \tag{3.5.25}$$

It is easy to see that for positive values of V and T, the function $\left(\delta + \lambda_{TI_{12}} TM\right) \frac{1}{1+\alpha' T(T+\epsilon_v V)} < \gamma$ for some positive constant γ. This implies, that

$$\frac{dT}{dt} < \gamma - d_T T.$$

By comparison argument, we see that $T \leq \max\{T_0, \frac{\gamma}{d_T}\}$ and

$$\limsup_{t\to\infty} T(t) \leq \frac{\gamma}{d_T}.$$

□

Proposition 3.5.2 *System* (3.5.22) − (3.5.23) *always has a tumor-free equilibrium $E_0^* = (0, T_0^*)$ with $T_0^* > 0$. System* (3.5.22) − (3.5.23) *has a unique tumor-free equilibrium $E_0^* = (0, T_0^*)$ with $T_0^* > 0$ if $d_T > \lambda_{TI_{12}} M$. System* (3.5.22) − (3.5.23) *has a tumorous equilibrium $E_1^* = (V_1^*, T_1^*)$ if $-d_T \alpha' (\frac{r}{\eta})^3 - (d_T - \lambda_{TI_{12}} M)(\frac{r}{\eta}) + \delta > 0$.*

Proof. If (V^*, T^*) is an equilibrium of system (3.5.22)-(3.5.23), then we have $V^*(r - \eta T^*) = 0$, which implies that $V^* = 0$ or $T^* = \frac{r}{\eta}$.

If $V^* = 0$ then $\frac{\delta+\lambda_{TI_{12}}T^*M}{1+\alpha'(T^*)^2} - d_T T^* = 0$. Then,

$$\delta + \lambda_{TI_{12}} TM - d_T T(1+\alpha' T^2) = 0$$

$$p(T) = d_T \alpha' T^3 + (d_T - \lambda_{TI_{12}} M)T - \delta = 0$$

Since $p(0) = -\delta$ and $\lim_{T\to\infty} p(T) = \infty$, we see that $p(T) = 0$ has at least one positive solution. Observe that $p'(T) = 3d_T\alpha' T^2 + (d_T - \lambda_{TI_{12}} M) > 0$, if $d_T - \lambda_{TI_{12}} M > 0$. Hence we conclude that if $d_T > \lambda_{TI_{12}} M$, then $p(T) = 0$ has a single positive root. Next, when $T^* = \frac{r}{\eta}$, we see that

$$(\delta + \lambda_{TI_{12}} T^* M)\frac{1}{1+\alpha' T^*(T^* + \epsilon_v V^*)} - d_T T^* = 0,$$

$$\delta + \lambda_{TI_{12}} T^* M - d_T T^*(1 + \alpha' T^*(T^* + \epsilon_v V^*)) = 0,$$

$$d_T \alpha' T^{*3} + d_T \alpha' \epsilon_v V^* T^{*2} + (d_T - \lambda_{TI_{12}} M)T^* - \delta = 0,$$

$$V^* = \frac{-d_T\alpha'(\frac{r}{\eta})^3 - (d_T - \lambda_{TI_{12}} M)(\frac{r}{\eta}) + \delta}{d_T \alpha' \epsilon_v (\frac{r}{\eta})^2}.$$

To ensure the equilibrium is tumorous we need to ensure that $V^* > 0$, which implies

$$-d_T\alpha'\Big(\frac{r}{\eta}\Big)^3 - (d_T - \lambda_{TI_{12}} M)\Big(\frac{r}{\eta}\Big) + \delta > 0.$$

□

Hence, a tumorous equilibrium is of the form

$$E_1^* = (V_1^*, T_1^*) = \left(\frac{-d_T\alpha'(\frac{r}{\eta})^3 - (d_T - \lambda_{TI_{12}} M)(\frac{r}{\eta}) + \delta}{d_T \alpha' \epsilon_v (\frac{r}{\eta})^2}, \frac{r}{\eta}\right).$$

The Jacobian for system (3.5.22) − (3.5.23) is given by:

$$\begin{pmatrix} r - \eta T & -\eta V \\ (\delta + \lambda_{TI_{12}} MT)\frac{\partial}{\partial V}F(V,T) & (\delta + \lambda_{TI_{12}} MT)\frac{\partial}{\partial T}F(V,T) + \lambda_{TI_{12}} MF(V,T) - d_T \end{pmatrix}.$$

Proposition 3.5.3 *For the system (3.5.22)-(3.5.23) the following statements are true:*

1. *If* $T_0^* > \max\{\frac{r}{\eta}, \sqrt{\frac{1}{\alpha'}}\}$, *then* E_0^* *is a stable node.*

2. *If* $\min\{\frac{r}{\eta}, \sqrt{\frac{1}{\alpha'}}\} < T_0^* < \max\{\frac{r}{\eta}, \sqrt{\frac{1}{\alpha'}}\}$, *then* E_0^* *is a saddle.*

3. *If* $T_0^* < \min\{\frac{r}{\eta}, \sqrt{\frac{1}{\alpha'}}\}$, *then* E_0^* *is an unstable node.*

Proof. The Jacobian for the tumor-free equibrium $E_0^* = (0, T_0^*)$ is the following:

$$\begin{pmatrix} r - \eta T_0^* & 0 \\ (\delta + \lambda_{TI_{12}} M T_0^*) \frac{\partial}{\partial V} F(0, T_0^*) & (\delta + \lambda_{TI_{12}} M T_0^*) \frac{\partial}{\partial T} F(0, T_0^*) + \lambda_{TI_{12}} M F(0, T_0^*) - d_T \end{pmatrix}.$$

As $F(V,T)$ is a decreasing function of V and T, $\frac{\partial}{\partial T} F(V,T), \frac{\partial}{\partial V} F(V,T) < 0$, and the eigenvalues are given by:

$$\lambda_1 = r - \eta T_0^* < 0 \text{ if } T_0^* > \frac{r}{\eta},$$
$$\lambda_2 = (\delta + \lambda_{TI_{12}} M T_0^*) \frac{\partial}{\partial T} F(0, T_0^*) + \lambda_{TI_{12}} M F(0, T_0^*) - d_T.$$

The goal is to find some simple condition that ensures $\lambda_2 < 0$. We start by some algebra manipulation/factoring for the λ_2 expression.

$$\lambda_2 = \underbrace{\delta \frac{\partial}{\partial T} F(0, T_0^*)}_{-} - \underbrace{d_T}_{+} + \underbrace{\lambda_{TI_{12}} M}_{+} \underbrace{(T_0^* \frac{\partial}{\partial T} F(0, T_0^*) + F(0, T_0^*))}_{?}.$$

We seek to determine the sign for $\phi = T_0^* \frac{\partial}{\partial T} F(0, T_0^*) + F(0, T_0^*)$ which is equivalent to

$$\phi = \frac{-2\alpha' T_0^{*2}}{(1 + \alpha' T_0^{*2})^2} + \frac{1}{1 + \alpha' T_0^{*2}}$$
$$\phi = \frac{-2\alpha' T_0^{*2} + 1 + \alpha' T_0^{*2}}{(1 + \alpha' T_0^{*2})^2}$$
$$\phi = \frac{-\alpha' T_0^{*2} + 1}{(1 + \alpha' T_0^{*2})^2}$$

Now, $\phi < 0$ if $-\alpha' T_0^{*2} + 1 < 0$, which implies $T_0^* > \sqrt{\frac{1}{\alpha'}}$ and $T_0^* < -\sqrt{\frac{1}{\alpha'}}$ (unrealistic).

□

Next, we examine the local stability for the tumorous-equilibrium $E_1^* = (V_1^*, T_1^*)$.

Proposition 3.5.4 *The tumorous equilibrium $E_1^* = (V_1^*, T_1^*)$ is a saddle point.*

Proof. The Jacobian for the tumorous equilibrium is of the form:

$$\begin{pmatrix} 0 & -\eta V_1^* \\ W(T_1^*)\frac{\partial}{\partial V}F(V_1^*, T_1^*) & W(T_1^*)\frac{\partial}{\partial T}F(V_1^*, T_1^*) + \lambda_{TI_{12}} M F(V_1^*, T_1^*) - d_T \end{pmatrix},$$

where $W(T_1^*) = \delta + \lambda_{TI_{12}} M T_1^*$. Its determinant is given by:

$$\Delta = \eta V_1^* (\delta + \lambda_{TI_{12}} M T_1^*) \frac{\partial}{\partial V} F(V_1^*, T_1^*) < 0.$$

Since $\Delta < 0$ the tumorous equilibrium is a saddle point. □

We again use the Dulac criterion to obtain a condition that rules out the existence of positive periodic solutions for system (3.5.22) − (3.5.23).

Proposition 3.5.5 *System* (3.5.22) − (3.5.23) *has no nontrivial positive periodic solutions when $T < \sqrt{\frac{1}{\alpha'}}$.*

Proof. Let $h(V, T) = \frac{1}{V}$. We can see:

$$\begin{aligned} \Omega &= \frac{\partial}{\partial V}\left\{\frac{1}{V}(rV - \eta VT)\right\} + \frac{\partial}{\partial T}\left\{\frac{1}{V}((\delta + \lambda_{TI_{12}} TM)F(V,T) - d_T T)\right\} \\ &= \frac{\partial}{\partial V}(r - \eta T) + \frac{(\delta + \lambda_{TI_{12}} MT)}{V}\frac{\partial}{\partial T}F(V,T) + \frac{\lambda_{TI_{12}} M}{V}F(V,T) - \frac{d_T}{V} \\ &= \frac{(\delta + \lambda_{TI_{12}} MT)}{V}\frac{\partial}{\partial T}F(V,T) + \frac{\lambda_{TI_{12}} M}{V}F(V,T) - \frac{d_T}{V} \\ &= \underbrace{\frac{\delta}{V}\frac{\partial}{\partial T}F(V,T)}_{-} + \underbrace{\frac{\lambda_{TI_{12}} M}{V}}_{+}\underbrace{\left(T\frac{\partial}{\partial T}F(V,T) + F(V,T)\right)}_{?} - \underbrace{\frac{d_T}{V}}_{+}. \end{aligned}$$

We need to determine when $\phi_1 = T\frac{\partial}{\partial T}F(V,T) + F(V,T) < 0$.

$$\phi_1 = = T\frac{\partial}{\partial T}F(V,T) + F(V,T)$$
$$\phi_1 = = \frac{-2\alpha' T^2 - \alpha'\epsilon_v VT + 1 + \alpha' T(T+\epsilon_v V)}{(1+\alpha' T(T+\epsilon_v V))^2}$$
$$\phi_1 = = \frac{-\alpha' T^2 + 1}{(1+\alpha' T(T+\epsilon_v V))^2}$$

Hence, $\phi_1 < 0$ if $T < \sqrt{\frac{1}{\alpha'}}$. Thus, the Dulac criterion ensures there will be no nontrivial positive periodic solution as long as $T < \sqrt{\frac{1}{\alpha'}}$. □

3.6 Mathematical Analysis for the Continuous Treatment Case: Full System

The full system consists of four nonlinear equations where γ_1 and γ_2 represent the continuous injection of NHS-muIL12 and Avelumab respectively.

$$\frac{dV}{dt} = rV - \eta VT, \tag{3.6.26}$$
$$\frac{dT}{dt} = \left(\delta + \lambda_{TI_{12}} T\frac{c_2 A_2}{K_{A_2} + c_2 A_2}\right) \cdot \frac{1}{1+\frac{Q(V,T,A_1)}{K_{TQ}}} - d_T T, \tag{3.6.27}$$
$$\frac{dA_1}{dt} = \gamma_1 - d_{A_1} A_1, \tag{3.6.28}$$
$$\frac{dA_2}{dt} = \gamma_2 - d_{A_2} A_2. \tag{3.6.29}$$

where,

$$F(V,T,A_1) = \frac{1}{1+\frac{Q(V,T,A_1)}{K_{TQ}}}$$
$$= \frac{1}{1+\alpha' T(T+\epsilon_v V)(1-\frac{c_1 A_1}{c_1 A_1 + K_{A_1}})}$$

with,

$$\alpha' = \frac{\sigma \rho_p \rho_l}{K_{TQ}}.$$

It is easy to see that the solution of the above system $(3.6.26) - (3.6.29)$ with positive initial values is positive. We use a similar argument as when performing mathematical

analysis for the limiting system (3.5.22)-(3.5.23), and conclude that boundedness for V can not be established. However, the following proposition is true.

Proposition 3.6.1 *The T, A_1 and A_2 components of the solutions of the equations (3.6.26) − (3.6.29) are bounded.*

Proof. It is easy to see that solutions for both A_1 and A_2 are bounded. Additionally, for positive values of V and T and A_1 the function $\left(\delta + \lambda_{TI_{12}} T \frac{c_2 A_2}{K_{A_2} + c_2 A_2}\right) F(V, T, A_1) < \gamma$ for some positive constant γ. This implies that

$$\frac{dT}{dt} < \gamma - d_T T.$$

By comparison argument, we see that $T \leq \max\{T_0, \frac{\gamma}{d_T}\}$ and

$$\limsup_{t \to \infty} T(t) \leq \frac{\gamma}{d_T}.$$

□

Proposition 3.6.2 *System (3.6.26) − (3.6.29) has at least a tumor-free equilibrium $E_0^* = (0, T_0^*, \frac{\gamma_1}{d_{A_1}}, \frac{\gamma_2}{d_{A_2}})$ with $T_0^* > 0$. System (3.6.26) − (3.6.29) has a unique tumor-free equilibrium $E_0^* = (0, T_0^*, \frac{\gamma_1}{d_{A_1}}, \frac{\gamma_2}{d_{A_2}})$ with $T_0^* > 0$ if $(d_T - \lambda_{TI_{12}} \frac{c_2 \gamma_2}{d_{A_2} K_{A_2} + c_2 \gamma_2}) > 0$.*

Proof. We set $\frac{dV}{dt} = 0$, which implies that $V^* = 0$ and $T^* = \frac{r}{\eta}$. We set $\frac{dA_1}{dt} = 0$ and $\frac{dA_2}{dt} = 0$ and get $A_1^* = \frac{\gamma_1}{d_{A_1}}$ and $A_2^* = \frac{\gamma_2}{d_{A_2}}$ respectively.

If $V^* = 0$, $A_1^* = \frac{\gamma_1}{d_{A_1}}$ and $A_2^* = \frac{\gamma_2}{d_{A_2}}$ then

$$\left(\delta + \lambda_{TI_{12}} T^* \frac{c_2 \gamma_2}{d_{A_2} K_{A_2} + c_2 \gamma_2}\right) \cdot \frac{1}{1 + \alpha' T^{*2} (1 - \frac{c_1 \gamma_1}{c_1 \gamma_1 + d_{A_1} K_{A_1}})} - d_T T^* = 0. \quad (3.6.30)$$

Let $p(T^*) = d_T \alpha' (1 - \frac{c_1 \gamma_1}{c_1 \gamma_1 + d_{A_1} K_{A_1}}) T^{*3} + (d_T - \lambda_{TI_{12}} \frac{c_2 \gamma_2}{d_{A_2} K_{A_2} + c_2 \gamma_2}) T^* - \delta$. We see that $p(T^*) = 0$ if and only if equation (3.6.30) holds. Since $p(0) = -\delta$ and $\lim_{T \to \infty} p(T) = \infty$, we see that $p(T) = 0$ has at least one positive solution. Observe that $1 -$

$\frac{c_1\gamma_1}{c_1\gamma_1+d_{A_1}K_{A_1}} > 0$ and $p'(T^*) = 3d_T\alpha' T^{*2}(1 - \frac{c_1\gamma_1}{c_1\gamma_1+d_{A_1}K_{A_1}}) + (d_T - \lambda_{TI_{12}}\frac{c_2\gamma_2}{d_{A_2}K_{A_2}+c_2\gamma_2})$. We see that $p'(T^*) > 0$, provided $(d_T - \lambda_{TI_{12}}\frac{c_2\gamma_2}{d_{A_2}K_{A_2}+c_2\gamma_2}) > 0$, in which case, $p(T)$ has a single positive root. □

In the following, we let

$$\Delta(T, A_2) = \delta + \lambda_{TI_{12}} T \frac{c_2 A_2}{K_{A_2} + c_2 A_2}.$$

The following proposition presents a simple necessary and sufficient condition for system (3.6.26) − (3.6.29) to have a unique tumorous equilibrium.

Proposition 3.6.3 *Let $D = \Delta(r/\eta, \gamma_2/d_{A_2})$. System (3.6.26) − (3.6.29) has a unique tumorous equilibrium $E^* = (V^*, T^*, A_1^*, A_2^*)$ if and only if*

$$\frac{D\eta}{rd_T} > 1 + Q(0, \frac{r}{\eta}, \frac{\gamma_1}{d_{A_1}}).$$

Proof. Observe that if the system (3.6.26) − (3.6.29) has a tumorous equilibrium $E^* = (V^*, T^*, A_1^*, A_2^*)$, then $T^* = \frac{r}{\eta}$, $A_1^* = \frac{\gamma_1}{d_{A_1}}$ and $A_2^* = \frac{\gamma_2}{d_{A_2}}$. Straightforward computation from equation (3.6.27) yields

$$\frac{D\eta}{rd_T} = 1 + Q(V^*, \frac{r}{\eta}, \frac{\gamma_1}{d_{A_1}}) \equiv G(V^*).$$

Observe that $G(V^*)$ is a strictly increasing function for $V^* \geq 0$. This implies that if

$$\frac{D\eta}{rd_T} > 1 + Q(0, \frac{r}{\eta}, \frac{\gamma_1}{d_{A_1}}),$$

then

$$G(V^*) > 1 + Q(0, \frac{r}{\eta}, \frac{\gamma_1}{d_{A_1}}) = G(0),$$

which implies that $V^* > 0$. Since $G(V^*)$ is strictly monotone, we see that in such case, the solution V^* of $G(V^*) = \frac{D\eta}{rd_T}$ is unique. □

The Jacobian for the system (3.6.26)-(3.6.29) is given by:

$$\begin{pmatrix} r-\eta T & -\eta V & 0 & 0 \\ a_{21} & a_{22} & a_{23} & a_{24} \\ 0 & 0 & -d_{A_1} & 0 \\ 0 & 0 & 0 & -d_{A_2} \end{pmatrix}$$

where

$$\begin{aligned} a_{21} &= \Delta(T, A_2)\frac{\partial F(V,T,A_1)}{\partial V}, \\ a_{22} &= \left(\lambda_{TI_{12}}\frac{c_2 A_2}{K_{A_2}+c_2 A_2}\right)F(V,T,A_1) + \Delta(T,A_2)\frac{\partial F(V,T,A_1)}{\partial T} - d_T, \\ a_{23} &= \Delta(T, A_2)\frac{\partial F(V,T,A_1)}{\partial A_1}, \\ a_{24} &= F(V,T,A_1)\lambda_{TI_{12}} T\frac{c_2 K_{A_2}}{(K_{A_2}+c_2 A_2)^2}. \end{aligned}$$

Proposition 3.6.4 *The system* (3.6.26)−(3.6.29) *has a stable tumor-free equilibrium provided that* $T_0^* > \frac{r}{\eta}$ *and* $F(0, T_0^*, \frac{\gamma_1}{d_{A1}}) < 0$.

Proof. The Jacobian for the tumor-free equilibrium $E_0^* = (0, T_0^*, \frac{\gamma_1}{d_{A_1}}, \frac{\gamma_2}{d_{A_2}})$ is given by:

$$\begin{pmatrix} r-\eta T_0^* & 0 & 0 & 0 \\ a_{21} & a_{22} & a_{23} & a_{24} \\ 0 & 0 & -d_{A_1} & 0 \\ 0 & 0 & 0 & -d_{A_2} \end{pmatrix}$$

where

$$a_{21} = \Delta(T_0^*, \frac{\gamma_1}{d_{A_1}})\frac{\partial F(0, T_0^*, \frac{\gamma_1}{d_{A_1}})}{\partial V},$$

$$a_{22} = \left(\lambda_{TI_{12}}\frac{c_2\gamma_2}{d_{A_2}K_{A_2} + c_2\gamma_2}\right)F(0, T_0^*, \frac{\gamma_1}{d_{A_1}}) + \Delta(T_0^*, \frac{\gamma_1}{d_{A_1}})\frac{\partial F(0, T_0^*, \frac{\gamma_1}{d_{A_1}})}{\partial T} - d_T,$$

$$a_{23} = \Delta(T_0^*, \frac{\gamma_1}{d_{A_1}})\frac{\partial F(0, T_0^*, \frac{\gamma_1}{d_{A_1}})}{\partial A_1},$$

$$a_{24} = F(0, T_0^*, \frac{\gamma_1}{d_{A_1}})\lambda_{TI_{12}}T_0^*\frac{c_2K_{A_2}}{(K_{A_2} + \frac{c_2\gamma_2}{d_{A_2}})^2}.$$

As $F(V, T, A_1)$ is a decreasing function of V, T and A_1, $\frac{\partial}{\partial T}F(V, T, A_1)$, $\frac{\partial}{\partial V}F(V, T, A_1)$, $\frac{\partial}{\partial A_1}F(V, T, A_1) < 0$, and the eigenvalues are given by:

$$\lambda_1 = r - \eta T_0^* < 0 \text{ if } T_0^* > \frac{r}{\eta},$$

$$\lambda_2 = \alpha_{22},$$

$$\lambda_3 = -d_{A1} < 0,$$

$$\lambda_3 = -d_{A2} < 0.$$

Regarding the sign of a_{22}, a_{22} can be either positive or negative.

$$a_{22} = \underbrace{\left(\lambda_{T_{I_{12}}}\frac{c_2\gamma_2}{d_{A_2}K_{A_2} + c_2\gamma_2}\right)}_{+}\underbrace{F(0, T_0^*, \frac{\gamma_1}{d_{A_1}})}_{?} + \underbrace{\Delta(T_0^*, \frac{\gamma_1}{d_{A_1}})}_{+}\underbrace{\frac{\partial F(0, T_0^*, \frac{\gamma_1}{d_{A_1}})}{\partial T}}_{-} - \underbrace{d_T}_{+}.$$

If $F(0, T_0^*, \frac{\gamma_1}{d_{A1}}) < 0$, then $a_{22} < 0$, which implies that E_0^* is stable. □

3.7 Method for Parameter Estimation

We estimate the parameters in the model based on (i) Literature review, (ii) Stepwise process by increasing model complexity with the application of a parameter estimation algorithm. All parameters values estimated by these ways are depicted on Table D.1.

We first start with an extensive literature review to seek to estimate parameters for the model (3.3.3)-(3.3.6), as depicted in Appendix D. For the remaining parameters, we numerically simulate the model using the MATLAB built-in function fmincon, which utilizes an interior point algorithm to minimize an objective error function within a range (Byrd *et al.*, 2000). This way we are able to find the set of parameters that best fit the data in Xu *et al.* (2017).

We calculate the error using the following formula:

$$\hat{\theta} = \underset{\{\theta \ \ feasible\}}{\arg\min} \sum_{i=1}^{N} (y^{model}(t_i;\theta) - y_i^{observed})^2. \tag{3.7.31}$$

where N is the total number of data points, y^{model} is the solution of the tumor volume generated from the model under parameters θ and evaluated at the corresponding data time points, and $y^{observed}$ represents the tumor volume data points in Xu *et al.* (2017). We perform all simulations in MATLAB 2019a using the ODE system (3.3.3)-(3.3.6) and the following initial conditions: $V(0) = 100$, $T(0) = 0.03$, $A_1(0) = 0$ and $A_2(0) = 0$. The choice for the tumor volume initial condition is based on the mice initial tumor size $\approx 100mm^3$ (Xu *et al.*, 2017).

3.8 Data Fitting

We extract the data from Xu et al. (Xu *et al.*, 2017) through the use of the application WebPlotDigitizer. In this experiment BALB/c mice were injected with EMT-6 breast cancer cells orthotopically into the mammary fat pad. Once the volume of the tumor reached approximately 100 mm^3, the mice were randomly allocated into treatment groups consisting of eight mice each (Xu *et al.*, 2017). EMT-6 mice were treated both with monotherapy and combination treatments. The two types of treatments used were avelumab and NHS-muIL12. We consider the average tumor

volume curves for each of the following cases: (i) Isotype control (200 μg), (ii) NHS-muIL12 (2 μg), (iii) NHS-muIL12 (10 μg), (iv) Avelumab (200 μg), (v) Avelumab (200 μg) + NHS-muIL12 (2 μg), (vi) Avelumab (200μg) + NHS-muIL12 (10μg).

We initially seek to determine which parameters are the main drivers of the tumor dynamics in each scenario. Two important parameters that affect the overall behavior of the system are the growth rate (r) and the kill rate of the tumor cells by the T cells (η). Using fmincon as described in Section 3.7 and trying a range of reasonable initial guesses, we fit the model to the no drug case data using the optimum guess and get the following estimates: $r = 0.2114$, $\eta = 1$. Note that all other parameters expressed in the no drug case are determined by literature review as shown on the parameter estimation table with $\gamma_1 = \gamma_2 = 0$. As depicted by Figure 3.2 a) below, the model accurately describes tumor growth in the absence of treatment.

We inherit these parameter estimates and sequentially fit the remaining parameters for the submodels using a similar approach as in Wares *et al.* (2015). For each submodel we determine the most sensitive parameters that affect the behavior of the system and fit those to data. This process eventually led to the fit of a higher in complexity model (Wares *et al.*, 2015).

The first submodel captures the dynamics corresponding to treatment A_2 (NHS-muIL12). The drug A_2 was administrated subcutaneously on day 0 and dosages of 2 μg and 10 μg were explored (Xu *et al.*, 2017). We fit the parameter K_{A2} to NHS-muIL12 (2 μg) data and obtain the estimate $K_{A_2} = 7 \cdot 10^{-14}$, which differs from the estimate value in literature as shown in Section D. Using the estimate for the parameter K_{A2}, we fit for treatment NHS-muIL12 (10 μg). As observed on Figure 3.2 b) and c), the fit for case b) captures the behavior of the data qualitatively better than for case c).

We use a similar process for the A_1 (avelumab) data set. The drug A_1 was injected

intravenously on days 0, 3 and 6 at a dosage level of 200 μg. Although based on our literature review $K_{A_1} = 1.8 \cdot 10^{-11}$ in Section D, the model gives better fits when $K_{A_1} = 10^{-13}$ as depicted in Figure 3.2 d).

Now that we established appropriate parameter estimates for each case, we wish to examine whether the parameter estimates result into good predictions for the combination cases. We observe that the model predictions for the combination case avelumab (200 μg) and NHS-muIL12 (2 μg) as shown on Figure 3.2 e), are not satisfactory, implying that the model does not capture the eradication of the tumor as observed by the mice data. However, once the dosage of NHS-muIL12 increases to 10 μg, while maintaining the same dosage level for avelumab, the prediction tends to resemble closer the experimental data as observed in Figure 3.3.

3.9 Asymptotic Behavior

We perform all simulations in MATLAB using the parameter estimates found during the data fitting process, whose values are listed in the table in Appendix D. There are two asymptotic system behavior outcomes, namely tumor control and tumor escape. To distinguish between these two behaviors we define a threshold, V_T, such that if the solution computed at the last time point is greater than V_T, we define the outcome as “tumor escape", otherwise as “tumor control." We set $V_T = V(0) = 100$, and use initial conditions $V(0) = 100, T(0) = 0.03, A_1(0) = 0$ and $A_2(0) = 0$.

We consider the case when both drugs, i.e. NHS-muIL12 and avelumab, are applied continuously and run simulations for a long period of time ($\approx$ 220 days) using both the full system (3.3.3)-(3.3.6) and the limiting system (3.5.22)-(3.5.23). We define the continuous dosages for avelumab and NHS-muIL12 as γ_1 and γ_2, respectively, and determine appropriate ranges from the data of Xu et al.(Xu *et al.*, 2017). Specifically, since avelumab is administered on days $0, 3, 6$ over a time in-

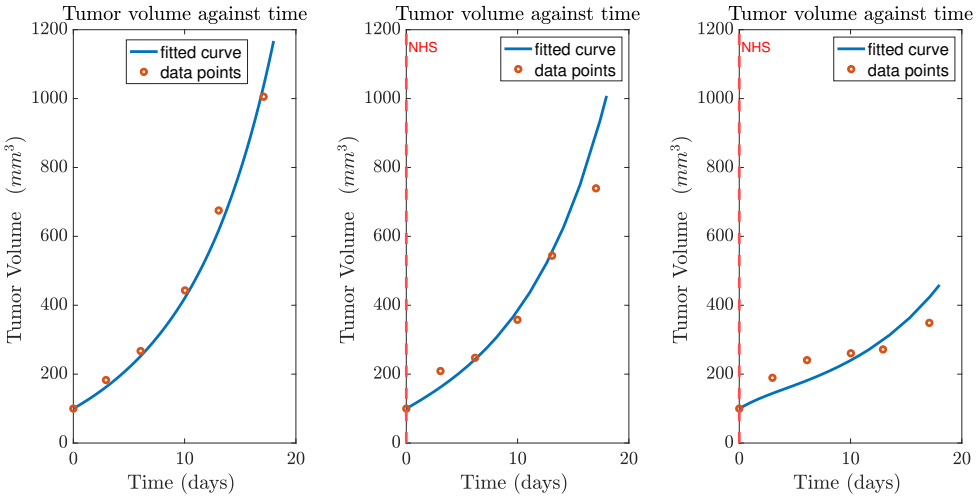

(a) No drug (b) NHS-muIL12 ($2\mu g$) (c) NHS-muIL12 ($10\mu g$)

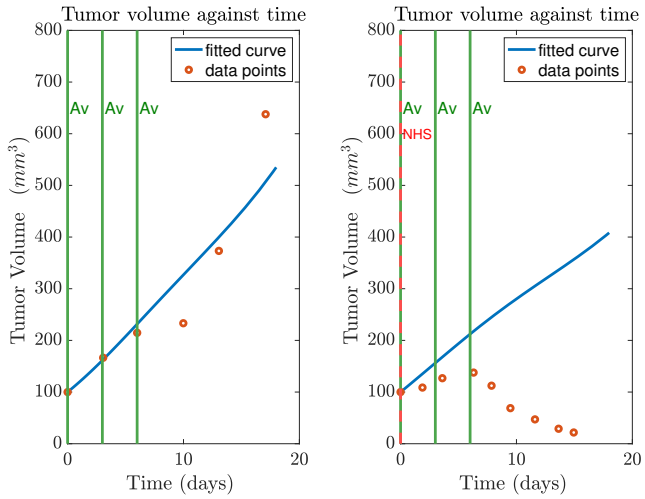

(d) Avelumab ($200\mu g$) (e) Av $200\mu g$+ NHS $2\mu g$

Figure 3.2: Tumor volume data and simulations using model (3.3.3)-(3.3.6) for each single-agent and combination therapy case. Case (a) administration of no drug. Case (b), (c) treatment with NHS-muIL12 $2\mu g$ and $10\mu g$ respectively on day 0. Case (d) administration of avelumab $200\mu g$ on days 0, 3 and 6. Case (e) treatment with both avelumab ($200\mu g$) on days 0, 3, 6 and NHS-muIL12 ($2\mu g$) on day 0.

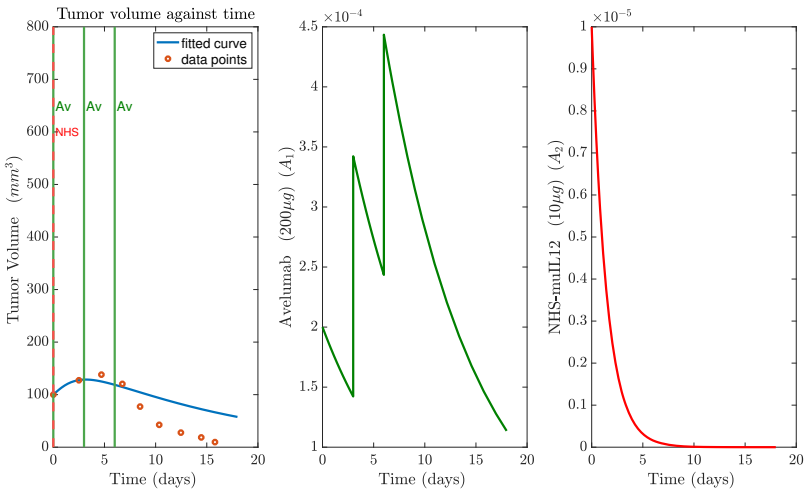

Figure 3.3: First graph depicts the model simulation for the combination treatment case of avelumab ($200\mu g$) and NHS-muIL12 ($10\mu g$). The remaining two graphs correspond to each of the drugs administrated with respect to time.

terval of 18 days and the dosage amount injected is $200\mu g$, γ_1 results to $\gamma_1 \approx (3 * 200 * 10^{-6})/18 = 0.55 * 10^{-4} \frac{\text{g}}{\text{day}}$. Using a similar argument, γ_2 ranges between $\gamma_2 \approx 0.11 * 10^{-6} - 0.33 * 10^{-6} \frac{\text{g}}{\text{day}}$.

Based on this information, we create a surface plot (see Figure 3.4) where three regions are noted, namely, “tumor control",“tumor escape" and “intermediate". We are interested in seeing how the dynamics of the full system (3.3.3)-(3.3.6) compares to the dynamics of the limiting system (3.5.22)-(3.5.23). The intermediate region shown in Figure 3.4 underlines the difference between the dynamics of the two systems. Specifically, we select a point (red circle) within this region to demonstrate this behavior. Depending on which system is used the point lies either in the tumor escape or in the tumor control region. Overall the behavior of the two systems is qualitatively comparable. Hyperbolic curves separate the three regions. To achieve smoother hyperbolic curves, we create a logarithmically spaced vector in MATLAB. We notice that there

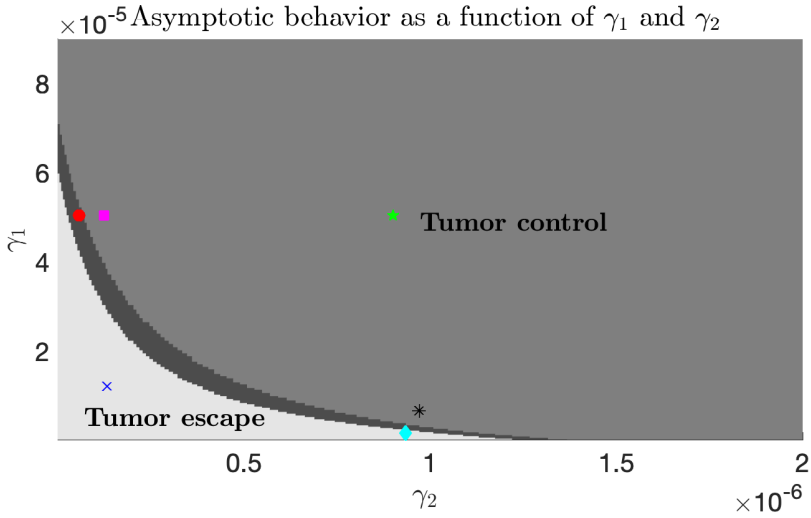

Figure 3.4: Surface plot depicting the asymptotic behavior of systems (3.3.3)-(3.3.6) and (3.5.22)-(3.5.23) for combinations of γ_1 (avelumab) and γ_2 (NHS-muIL12) drugs, where both are applied continuously. Based on a threshold, three regions, namely, 'tumor control','tumor escape' and 'intermediate' are identified, which are separated by hyperbolic curves. The hyperbolic curve closer to the origin corresponds to the system (3.5.22)-(3.5.23) and the other one to (3.3.3)-(3.3.6). Six representative points indicated by different markers and colors, are chosen and shown on the plot. Their respective tumor volume behavior is plotted in Figure 3.5 employing the same marker and color notation. Note that the red point falls in the intermediate region, where the behavior is dependent on the system being used.

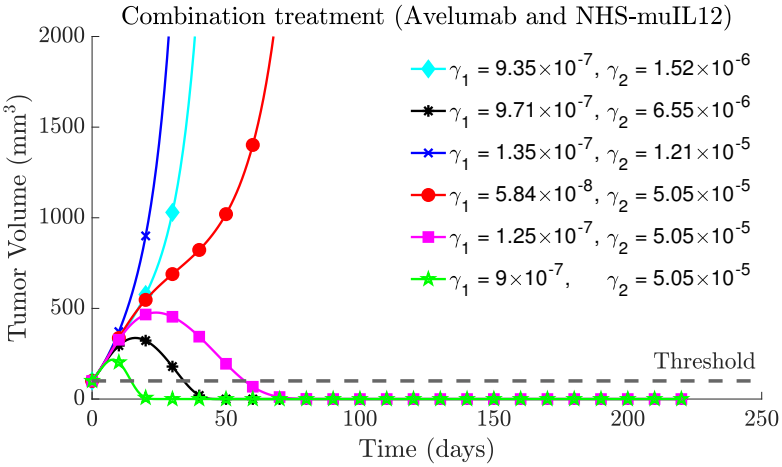

(a) Full system

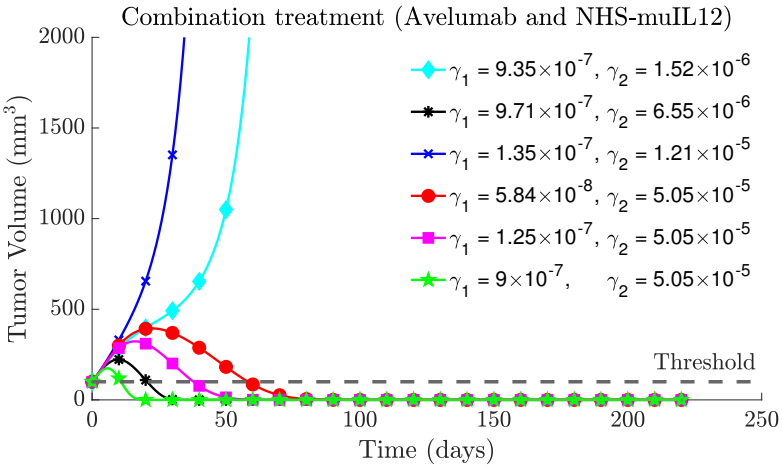

(b) Limiting System

Figure 3.5: A subset of tumor volume behaviors of both the full system (3.3.3)-(3.3.6) and the limiting system (3.5.22)-(3.5.23) for continuous dosage with γ_1 (avelumab) and γ_2 (NHS-muIL12) respectively. The threshold chosen is shown on the plot with a dashed line. We observe that the qualitative tumor volume behaviors between the systems are comparable with the exception of the red point, which lies in the intermediate region as shown in Figure 3.4.

is synergism between the two drugs (avelumab and NHS-muIL12), meaning that the total effect of the drugs in combination is greater than the sum of administrating the drugs individually. Particularly, we would require about one third of the amount of both drugs in combination to control the tumor in comparison to monotherapy.

3.10 Discussion

The last few years have seen a rapid increase in clinical trials investigating immune checkpoint inhibitors anti-PD-1/PD-L1 for a variety of types of cancer. Although these agents have increased survival rates, not all patients respond to monotherapy treatment (Yan *et al.*, 2018). This has led to the examination of combination treatments that have complimentary effects (Warnes and Postow, 2018). Particularly, since 2018 there are approximately $2,250$ active trials from which $1,760$ are exploring the pairing of anti-PD-1/PD-L1 agents with other forms of treatments (Tang *et al.*, 2018).

Xu *et al.* (2017) concluded that combining anti-PD-L1 with NHS-muIL12 enhanced antitumor effectiveness in comparison to single agent treatment. Based on the data presented in their paper, we developed a simple biologically meaningful system of ordinary differential equations that models the tumor volume behavior. This work allowed us to complement and improve our previous work (Nikolopoulou *et al.*, 2018), where we only considered single agent treatments.

We performed mathematical analysis to a simple generic model (3.3.1)-(3.3.2) that allowed us to understand the behavior of the system. We established conditions, which we adapted to determine the dynamics for the exponential growth model. Moreover, we mathematically analyzed the continuous case of administrating both drugs (avelumab and NHS-muIL12) using the limiting system (3.5.22)-(3.5.23) in Section 3.5 and the full system (3.3.3)-(3.3.6) in Section 3.6. The mathematical analysis does

not allow direct comparison of the dynamics of the systems, as it produces more technical results than biological insight. However, the mathematical analysis assists to the verification of the numerical predictions of the model.

Some of the parameters included in the model (3.3.3)-(3.3.6) proved to be challenging to calculate based on limited literature resources. However, the use of data in Xu *et al.* (2017) allowed us to estimate biologically sensible ranges for those parameters based on submodel fitting. We were able to fit well the submodels of the full model to the monotherapy cases. Using these fit parameter values, model predictions indicate that we do not describe dual therapy at lower doses of NHS-muIL12 well. However, the model does make qualitatively good predictions at higher NHS-muIL12 doses. Given the reasonable predictions at higher NHS-muIL12 doses, we exploited the model to make predictions regarding treatment regimens not considered in the experiments of Xu *et al.* (2017). Specifically, we investigated the effects of administrating different combinations of avelumab and NHS-muIL12 continuously for both the full system (3.3.3)-(3.3.6) and the limiting system (3.5.22)-(3.5.23). We found that the dynamics of the systems are not equivalent, as system (3.5.22)-(3.5.23) is an approximation of (3.3.3)-(3.3.6). However, simulations suggested that the qualitative behavior of the two systems is comparable. Finally, we found that the drugs act synergistically and that approximately one third of the amount of both drugs could potentially eliminate the tumor.

Chapter 4

PARAMETER ESTIMATION IN A MATHEMATICAL MODEL OF ONCOLYTIC VIRUS THERAPY

4.1 Introduction

Oncolytic virus therapy (OV) is an emerging field of cancer immunotherapy (Russell and Peng, 2018). It has shown great promise when used in combination with other treatments (Rosewell and Suzuki, 2018). Oncolytic viruses are standard viruses that can infect healthy and cancer cells (Chiocca *et al.*, 2014). Upon injection of the virus, the virus does not have the ability to replicate inside healthy cells. Consequently, healthy cells remain unharmed. Once cancer cells get infected, the rapid replication process of the virus results to the bursting of the tumor cells. This process, known as lysis leads to the consequent infection of other tumor cells (Chiocca *et al.*, 2014). However, the power of the immune system to eliminate the viruses makes the lysing ineffective. As a result, OV as a monotherapy has not shown satisfactory results in tumor eradication (Rosewell and Suzuki, 2018). Recent technological advancements have led to the development of genetically engineered viruses in the form of vectors, which deliver therapeutic molecules to the tumor site. This enhances the ability of the immune system to recognize tumors as foreign (Melcher *et al.*, 2011).

Several mathematical modeling efforts have investigated the coupling of OV with other treatments, such as dendritic cell vaccine (DC) (Wares *et al.*, 2015; Gevertz and Wares, 2018), MEK inhibitors (Bagheri *et al.*, 2011) and immune checkpoint inhibitors (Friedman and Lai, 2018; Storey, Lawler and Jackson, 2020). The work in this chapter is based on a model originally published in Wares *et al.* (2015), and

simplified in Gevertz and Wares (2018).

4.2 Motivation

The minimal model by Gevertz and Wares (2018) in combination with the data in Huang *et al.* (2010), is used in an ongoing analysis performed by Gevertz *et al.*, which demonstrates that the optimal protocol identified for an individual mouse is sensitive to the fitting methodology utilized. That is of particular importance, especially since clinical care of cancer nowadays is moving towards personalized therapeutic design instead of the traditional one-size-fits-all approach that relies on population-level statistics (Deisboeck, 2009; Agur, Elishmereni and Kheifetz, 2014; Lorenzo *et al.*, 2016). Therefore, if one is not careful, there is a risk that an individualized optimal prediction could change at the whim of the fitting methodology. This led to the motivation of this chapter: *Can an explanation be found for this sensitivity to fitting methodology?*

To answer this question, the practical identifiability method is employed on the submodel in Gevertz and Wares (2018) using the average mice data in Huang *et al.* (2010). In the following sections relevant background of both models (Wares *et al.*, 2015; Gevertz and Wares, 2018) will be presented to the reader before the results of the practical identifiability investigation are put forward.

4.3 Mathematical Model Proposed by Wares *et al.* (2015)

The authors propose a system of six differential equations, which consists of the volume of uninfected tumor cells U, infected tumor cells I, virions V, T-cells T,

antigen-presenting cells A, injected dendritic cells D, and takes the following form:

$$\frac{dU}{dt} = rU - \frac{\beta UV}{N} - (k_0 + c_k I)\frac{UT}{N} \tag{4.3.1}$$

$$\frac{dI}{dt} = \frac{\beta UV}{N} - \delta_I I - (k_0 + c_k I)\frac{IT}{N} \tag{4.3.2}$$

$$\frac{dV}{dt} = u_V(t) + \alpha\delta_I I - \delta_V V \tag{4.3.3}$$

$$\frac{dT}{dt} = c_T I + \chi_A A + \chi_D D - \delta_T T \tag{4.3.4}$$

$$\frac{dA}{dt} = c_A I - \delta_A A \tag{4.3.5}$$

$$\frac{dD}{dt} = u_D(t) - \delta_D D \tag{4.3.6}$$

where,

$$N = U + I + T$$

Using the average tumor volume of melanoma mice data from Huang *et al.* (2010) the authors investigate the pairing of immuno-enhanced OV with DC injections. In regards to immuno-enhanced OV they consider adenovirus that expresses 4-1 BBL and IL-12 both in combination and seperately. 4-1BBL is the ligand of 4-1BB, which is a costimulatory member of the tumor necrosis factor receptor superfamily (Wen, Bukczynski and Watts, 2002). IL-12 is a cytokine which role is to activate naive T-cells (Colombo and Trinchieri, 2002). The model is fitted in a hierarchical fashion. Specifically, a very simple model is first proposed and fitted, which provides the basis for continuation of the higher in complexity model construction process. Each time a submodel is fitted, estimated parameters are inherited to the next step until the final most advanced model is formulated. Using this fitting methodology, the authors obtain increasingly accurate fits for simpler models.

Upon model parameter estimation, the goal of Wares *et al.* (2015) was to find the optimal treatment strategy based on the experiment in Huang *et al.* (2010). An

important observation in Huang *et al.* (2010) was that the combination treatment resulted in the decrease of the tumor size but not tumor eradication. It was hypothesized that the increase of DC injections could cause tumor elimination. Wares *et al.* (2015) indeed determined that higher dosages of DC could eradicate the tumor. Additionally, Huang *et al.* (2010) proposed a combination treatment strategy that was more effective than monotherapy. They considered a total of 6 injections, 3 of each treatment, while maintaining the dose and determined that the alternating with OV first was the most effective. Their proposed strategy was OV-DC-OV-DC-OV-DC. Wares *et al.* (2015) further investigated the most effective order of administrating OV and DC. Their results indicated that tumor elimination was observed for the OV-OV-OV-DC-DC-DC strategy. Moreover, the optimal treatment strategy also depends on the dose of each drug. The authors also explored the effects of changing the number of doses and the time between injections. They found that higher number of doses result in tumor reduction, while underlining the importance of induced toxicity effects based on the dosage level. Furthermore, dose administration in short time steps and early in the therapy was proven to be the most effective strategy. Finally, the authors noted the dependency of the treatment efficacy on the temporal drug administration.

However, analysis of the findings in Wares *et al.* (2015) raised questions in regards to the predictive ability of the model. Particularly, it was shown that a minimal change in the dosage could have effects on the protocol, indicating the existence of a bifurcation point. Based on that observation, Barish *et al.* (2017) employed the Virtual Expansion of Populations for Analyzing Robustness of Therapies (VEPART) to determine the robustness of the original optimal strategy predicted by Wares *et al.* (2015). The authors' investigation validated the fragility of the originally predicted model.

4.4 Mathematical Model Proposed by Gevertz and Wares (2018)

Using the modeling approach in Wares *et al.* (2015), the authors reduce the dimensionality of the model and propose a system of five differential equations instead of six. They eliminate the equation representing the antigen-presenting cells A in system (4.3.1)-(4.3.6). As a result, the minimal model proposed takes the following form:

$$\frac{dU}{dt} = rU - \frac{\beta UV}{N} - (k_0 + c_k I)\frac{UT}{N} \tag{4.4.7}$$

$$\frac{dI}{dt} = \frac{\beta UV}{N} - \delta_I I - (k_0 + c_k I)\frac{IT}{N} \tag{4.4.8}$$

$$\frac{dV}{dt} = u_V(t) + \alpha\delta_I I - \delta_V V \tag{4.4.9}$$

$$\frac{dT}{dt} = c_T I + \chi_D D - \delta_T T \tag{4.4.10}$$

$$\frac{dD}{dt} = u_D(t) - \delta_D D \tag{4.4.11}$$

where,

$$N = U + I + T$$

The authors conclude that the simplification made to the system describes the experimental data in Huang *et al.* (2010) as well as the six equation model presented in equations (4.3.1)-(4.3.6) by Wares *et al.* (2015). As a result, in this work we consider the minimal model proposed by Gevertz and Wares (2018).

4.5 Problem Statement

Before addressing the question of identifiability, the general form of a mathematical model expressed by the following equations is defined similar to Raue *et al.*

(2009):

$$\frac{dx}{dt} = F(x, u, t, p)$$
$$y = g(x, t, p)$$
$$z_n = y(t_n) + \epsilon_n, \ \ \forall \ \ n = 1, ...N$$

Here x represents the vector of state variables of the model, u the input vector, i.e treatment, t depicts time and p the parameter vector of our model and F is expressed by rate equations and represents the interactions between the state variables. The variable y represents the vector of output variables and g is the map from the internal state to the measurement z_n. The noise ϵ_n is assumed to be additive Gaussian with zero mean and known variance σ^2.

4.6 Oncolytic Virus Therapy Model

For the purpose of this project the case of OV as a monotherapy is first considered. A simplified version of the model (4.4.7) -(4.4.11) provided in Gevertz and Wares (2018) is utilized in combination with the data provided in Huang *et al.* (2010). Figure 4.1 represents a schematic network between the variables in Gevertz and Wares (2018) and Table 4.1 contains all the state variables of the model system (4.6.12)-(4.6.14).

The following sets of differential equation describe the oncolytic virus therapy

Table 4.1: State variables of the model system (4.6.12)-(4.6.14).

Variable	Meaning	Unit
U	volume of uninfected tumor cells	mm^3
I	volume of infected tumor cells	mm^3
V	number of virons	mm^3
N	total volume of tumor cells	mm^3

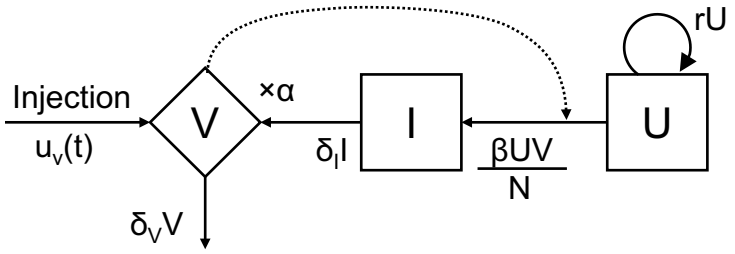

Figure 4.1: Schematic representation of the model (4.6.12)-(4.6.14) (Gevertz and Wares, 2018). Once oncolytic virus is injected into the system, uninfected tumor cells U become infected tumor cells I. Through the virus replication process, infected tumor cells can not bear the viral load resulting in the lysing of the infected cells and release of virons.

submodel presented in Gevertz and Wares (2018).

$$\frac{dU}{dt} = \underbrace{rU}_{\text{uninfected tumor growth}} - \underbrace{\frac{\beta UV}{N}}_{\text{infection process of uninfected cells}} \tag{4.6.12}$$

$$\frac{dI}{dt} = \underbrace{\frac{\beta UV}{N}}_{\text{infection process of uninfected cells}} - \underbrace{\delta_I I}_{\text{viral release from lysed infected cells}} \tag{4.6.13}$$

$$\frac{dV}{dt} = \underbrace{u_v(t)}_{\text{infusion rate}} + \underbrace{\alpha\delta_I I}_{\text{viral release from lysed infected cells}} - \underbrace{\delta_V V}_{\text{viral decay}} \tag{4.6.14}$$

$$\tag{4.6.15}$$

where,

$$N = U + I$$

Equation (4.6.12) describes the number of uninfected tumor cells U, where rU denotes the exponential growth of uninfected tumor cells. The uninfected tumor cells U become infected tumor cells I by the virions V at a density-dependent rate $\frac{\beta}{N}$. Infected cells lyse at rate δ_I releasing α new virions and clearing free virions at a rate δ_V. The term $u_v(t)$ represents the injection of 10^{10} virions on days 0, 2 and 4, as per the protocol in Huang *et al.* (2010) and $\delta_V V$ denotes the viral decay. In terms of the general model in Section 4.5, here $x = (U, I, V)$, $F(x, u, t, p)$ represents the right hand side of the model (4.6.12)-(4.6.14), where u are the injections $u_v(t)$ and p the parameters in Table 4.2. The variable $y = U + I$ represents the tumor volume, and z_n is the noisy tumor volume data.

The initial steps are to reproduce the plots in the original full model in Wares *et al.* (2015), using the data in Huang *et al.* (2010), the parameters in Table 4.2 and initial conditions, $U(0) = 55.68, I(0) = 0$ and $V(0) = 10$. The behavior of the system as depicted by Figure 4.2 matches the simulation in Wares *et al.* (2015). To obtain the fit shown in Figure 4.2, Wares *et al.* (2015) followed a hierarchical fitting approach. They first started by fitting the net tumor growth parameter r and the initial condition $U(0)$ to the control data using a simple exponential growth model ($\frac{dU}{dt} = rU$). Upon inheriting the parameter r, they continued by fitting the infection rate parameter β and initial condition $U(0)$ to the OV data (which is different than the $U(0)$ fit to the control data), while maintaining all other parameters constant throughout the fitting process. The constant parameters include the infected lysis δ_I, the viral production α, and the viral decay δ_V. These were acquired from extensive literature research, and their values are listed in Table 4.2.

Motivated by the work in Wares *et al.* (2015), this dissertation follows a different optimization approach, which differs from the hierarchical fitting method. Hierarchical fitting is often advantageous, as it assists in reducing the dimensionality of the parameter space throughout the optimization process. However, error at lower levels accumulates and gets inherited and amplified at higher levels. Therefore, one can not be certain that the optimum parameter set obtained is indeed the optimum one. As a result, the optimization method introduced below fits all the parameters simultaneously. Using "everything-at-once methods" results to more robust outcomes although it is computationally intensive and demands numerical optimization in high dimension. Before describing the method in full detail, first some background is introduced.

Table 4.2: Parameter values of the model system (4.6.12)-(4.6.14).

Variable	Meaning	Ad	Units
r	Net tumor growth	0.3198	day^{-1}
β	Infection rate	1.0085 ($\times 10^{-3}$)	day^{-1}
δ_I	Infected lysis rate	1	day^{-1}
α	Viral production	3 ($\times 10^{3}$)	-
δ_V	Viral decay rate	2.3	day^{-1}

4.7 Maximum Likelihood

To estimate parameter values for a model, the maximum likelihood estimation method is often employed and the derivation is outlined in Sivia and Skilling (2006); Bishop (2006); Lee (2012). Let p be the parameter vector in our differential equation

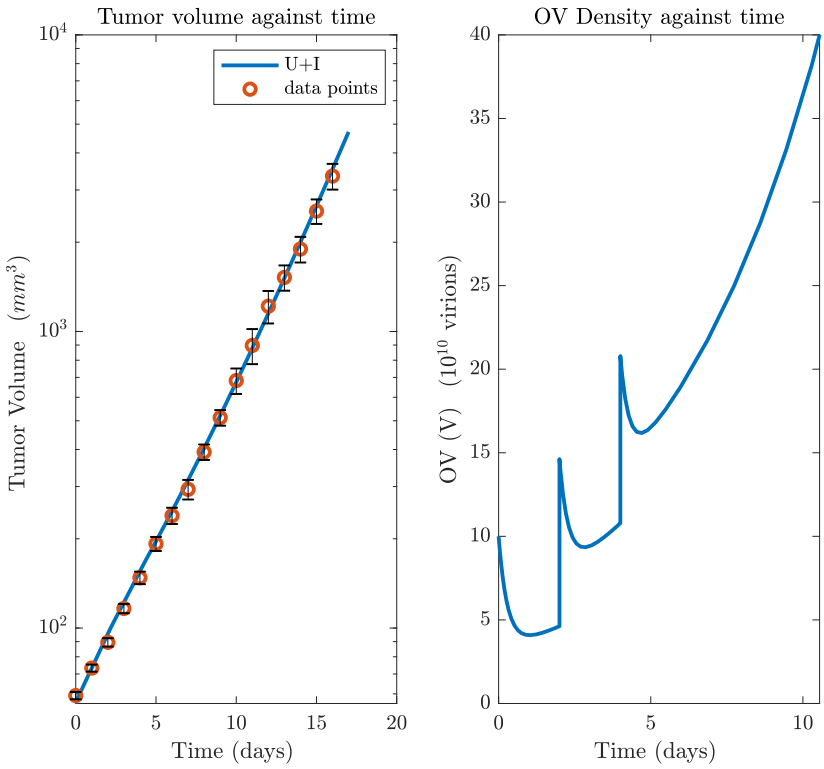

Figure 4.2: Graph depicts the reproduced model simulation for the oncolytic virus monotherapy (OV) using the parameters in Table 4.2. OV therapy was injected (10^{10} virions) on days 0, 2 and 4. Note the logarithmic scale of the vertical axis for the left plot.

system and z_n for $n = 1, ...N$ the measured data that is assumed for this problem to follow a normal distribution with mean $y(x, t_n, p)$ and known variance σ^2.

The probability density of each data point is:

$$f(z_n|y(t_n, p), \sigma_n^2) = \frac{1}{\sqrt{2\pi\sigma_n^2}} \exp\left(-\frac{(z_n - y(t_n, p))^2}{2\sigma_n^2}\right) \tag{4.7.16}$$

The likelihood function which represents the likeliness of the measured data z_n, given

a model with parameters p is defined by $L(p; z_1, ...z_N)$.

$$\begin{aligned} L(p; z_1, ...z_N) &= \prod_{n=1}^{N} f(z_n|y(t_n, p), \sigma_n^2) \\ &= \prod_{n=1}^{N} \frac{1}{\sqrt{2\pi\sigma_n^2}} \exp\left(-\frac{(z_n - y(t_n, p))^2}{2\sigma_n^2}\right) \end{aligned} \tag{4.7.17}$$

To find the values of the parameters that gives the best fit the likelihood function is maximized. In other words:

$$p^* = \arg\max_p L(p; z_1, ...z_N)$$

However, for computational simplicity, either the log likelihood function is maximized, or the negative log likelihood function minimized. Here the latter is considered:

$$\begin{aligned} -LL(p; z_1, ...z_N) &= -\log\left(\prod_{n=1}^{N} f(z_n|y(t_n, p), \sigma_n^2)\right) \\ &= -\prod_{n=1}^{N} \log\left(\frac{1}{\sqrt{2\pi\sigma_n^2}} \exp\left\{-\frac{(z_n - y(t_n, p))^2}{2\sigma_n^2}\right\}\right) \\ &= \sum_{n=1}^{N} \frac{1}{2}\log(2\pi\sigma_n^2) + \frac{1}{2}\sum_{n=1}^{N}\left(\frac{z_n - y(t_n, p)}{\sigma_n}\right)^2 \\ &= \sum_{n=1}^{N} \frac{1}{2}\log(2\pi) + \sum_{n=1}^{N} \frac{1}{2}\log\sigma_n^2 + \frac{1}{2}\sum_{n=1}^{N}\left(\frac{z_n - y(t_n, p)}{\sigma_n}\right)^2 \\ &= \frac{N}{2}\log(2\pi) + \sum_{n=1}^{N} \frac{1}{2}\log\sigma_n^2 + \frac{1}{2}\sum_{n=1}^{N}\left(\frac{z_n - y(t_n, p)}{\sigma_n}\right)^2 \end{aligned} \tag{4.7.18}$$

This mimization is equivalent to:

$$\min_p(-2LL(p; z_1, ...z_N)) = \min_p\left(\sum_{n=1}^{N}\left(\frac{z_n - y(t_n, p)}{\sigma_n}\right)^2\right) \tag{4.7.19}$$

The first two terms do not influence the overall result as they are independent of the parameters, hence they can be ignored. As a result the third term is minimized, which is defined as the objective function in this case, where $y(t, p) = U(t) + I(t)$.

Note that for the data set in Huang *et al.* (2010) apart from the average tumor volume and time, it is essential to use the standard deviation σ_n at each time point, since the variation of the data points needs to be accounted for.

4.8 Parameter Fitting Method

The parameter fitting method introduced is used to fit all the parameters in the model (4.6.12)-(4.6.14): r, the net tumor growth, β, the infection rate, δ_I the infected lysis, α the viral production, δ_V the viral decay and $U(0)$, the initial condition for uninfected tumor cells. All simulations of the system (4.6.12)-(4.6.14) were carried out with MATLAB 2019a. Since the system (4.6.12)-(4.6.14) contains stiff ordinary differential equations, `ode15s` solver is preferred. Compared to other ode solvers, `ode15s` solver has proven to be efficient for these type of problems as it allows for a big number of iterations to be executed. To obtain the optimum parameters given the data set, the following approach is followed, which is also graphically demonstrated in Figure 4.3:

1. Quasi Monte Carlo sampling method with Sobol sequences to find the neighborhood where best-fit parameter set occur.

2. Perturb the best-fit parameter set to find the final optimum parameters utilizing a simplified version of the simulated annealing method.

These methods are described in more detail in the following subsections.

4.8.1 Quasi Monte Carlo Method with Sobol Sequences

The quasi Monte Carlo method is widely used as a method of numerical integration and optimization (Kucherenko, 2015). For the purpose of this project the optimization aspect of the method is explored. Quasi Monte Carlo uses quasi-random sequences,

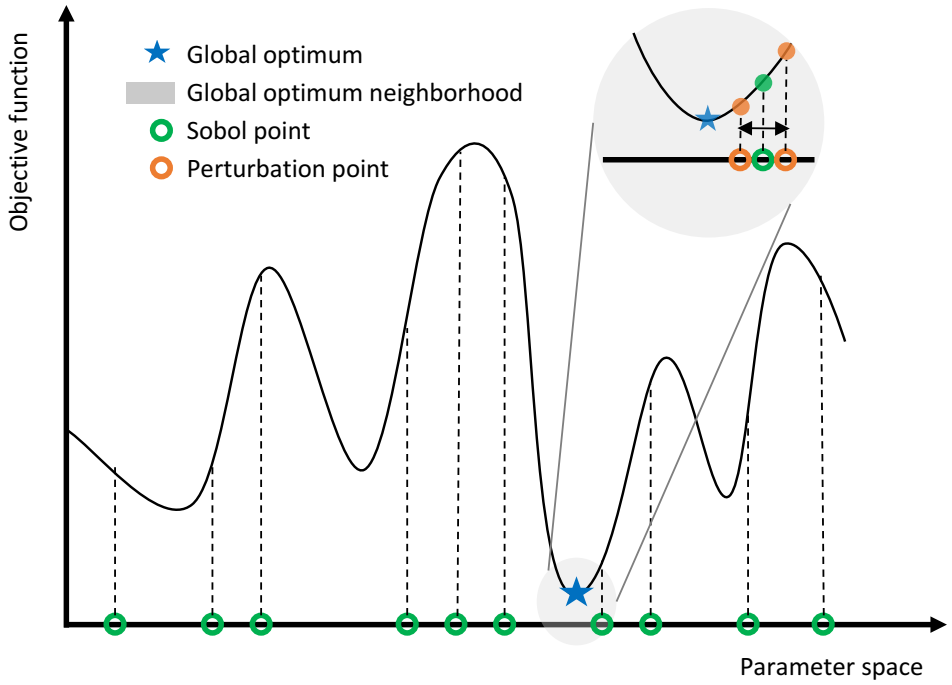

Figure 4.3: 1D Graphic illustration of the quasi Monte Carlo sampling method with Sobol sequences in combination with a simplified version of simulated annealing. The green points represent the sobol points which are quasirandomly spaced across the parameter space. Using the quasi Monte Carlo sampling method, the neighborhood where the best-fit parameter set occurs is depicted by the grey circle. The best-fit parameter set is then randomly perturbed until the global optimum parameter set is identified.

including the Halton sequence, the Sobol sequence, or the Faure sequence. The Sobol Low Discrepancy Sequence (LDS) achieves uniformity across the parameter space and is preferred, since it efficiently samples space in shorter computational time than other methods (Kucherenko, 2015). Regarding optimization, it allows to locate the neighborhood where the global minimum occurs. The quasi Monte Carlo method with Sobol sequences is described by Algorithm 1, lines $1-5$. Specifically, the Sobol sequence depends on the dimension of the parameter set p, as shown by line 1 in Algorithm 1.

4.8.2 Perturbation Method and Simulated Annealing

Once the parameter set from the quasi Monte Carlo method is obtained, a simplified version of the simulated annealing method is used to attain the global minimum. The first step is to randomly perturb the parameters found by the quasi Monte Carlo method. However, since the model parameters in (4.6.12) - (4.6.14) are of different order of magnitude, careful selection of the perturbation scales should be carried out to ensure a proportional change in the parameter set. Hence, the following perturbation method for each parameter is used:

1. Compute the order of magnitude of the parameter denoted by OM.
2. Compute the perturbation magnitude denoted by PM = OM + perturbation scale. The choice of the perturbation scale for this problem is -1.
3. Pick a random number n_r within the perturbation interval $[-10^{PM}, 10^{PM}]$.
4. Add n_r to the current parameter value.

When the optimal parameter set found through the Sobol method is perturbed, the objective function in equation (4.7.19) is evaluated at the new parameter set

and compared to the objective function value from the optimal quasi Monte Carlo parameter set. If the value of the objective function for the new parameter set is smaller, the new parameter set is accepted. If it is larger, the new parameter set is rejected. The process continues by perturbing and comparing the new parameter set to the last accepted parameter set and comparing it to the last parameter set. The algorithm is repeated until the convergence criterion is met. The convergence criterion is based upon the relative change within the last 5 accepted values of the objective function values and the relative threshold is set to 10^{-4}. In the case of slow convergence, the simulation runs for a set number of iterations (1 million). This process is described by Algorithm 1, lines $6 - 19$.

Let p be the parameter space and $LL(p)$ the objective function evaluated at the parameter set p as depicted by Equation 4.7.19. The goal is to minimize the objective function $LL(p)$ with respect to the parameter space $p = \{r, \beta, \delta_I, \alpha, \delta_V\}$ and initial condition $U(0)$.

Once the optimum parameter set is obtained through the quasi Monte Carlo and the version of simulated annealing method described above, the identifiability of the model (4.6.12) - (4.6.14) is investigated using the profile likelihood approach which is described below.

4.9 Identifiability

The need for mathematical models motivated by data is of paramount importance in the field of mathematical biology. An essential task is to construct meaningful mathematical models that describe biological mechanisms and to estimate parameters given experimental data. However, estimating unique parameters for a model is often challenging due to the uncertainty in the experimental data, which are inevitably noisy, and also due to the lack of experimental data. Confidence in the

Algorithm 1

$sample = sobolset(dim(p), N)$

for i = 1:N **do**

  $x_{sample(i)} = p_{min} + (p_{max} - p_{min}) * sample(i)$

  $LL_{sob(i)} = LL(x_{sample(i)})$

end for

$i_{opt} = \text{argmin}_i \, LL_{sobol}$

$p_{opt} = x_{sample(i_{opt})}$

$LL_{opt} = LL(p_{opt})$

$OM = \log(p_{opt})$

$PM = OM - 1$

while convergence criteria not met **do**

  $n_r =$ random pick $n_r \in [10^{-\text{PM}}, 10^{\text{PM}}]$

  $LL_{pert} = P_{opt} + n_r$

  $LL_{pert} = LL(P_{pert})$

  if $LL_{pert} < LL_{opt}$ **then**

    $p_{opt} = p_{pert}$

    $LL_{opt} = LL_{pert}$

  end if

end while

parameter estimation process is required in order to trust predictions made by a model. Particularly, it is noted that multiple values of parameters could potentially give good fits of the model to the data. Hence, when trying to estimate parameters for a model given a data set, we are interested in answering the following question: *"Can we uniquely estimate parameters for a model given a data set?"* This question characterizes identifiability (Eisenberg and Harsh, 2017). Identifiability is divided in two main categories; *structural* and *practical* identifiability (Eisenberg and Harsh, 2017). Structural identifiability poses the question of *"whether unique parameter values for a model can be estimated given noiseless data"* (Wu *et al.*, 2008; Eisenberg *et al.*, 2013). On the other hand, practical identifiability answers the question of *"whether unique parameter values can be estimated given the available noisy data"* (Jacquez and Greif, 1985; McLean and McAuley, 2012). Over recent years, several data-driven approaches have been carried out with the goal of investigating both structural and practical identifiability of the models in different areas such as cancer treatment. Such efforts include Eisenberg and Harsh (2017) and Wu *et al.* (2019) to name a few. Eisenberg and Harsh (2017) use a two-compartment model for chemotherapy to investigate parameter identifiability. The authors explore parameter identifiability to answer biological questions and demonstrate the usefulness of practically identifiable combinations. An application of parameter identifiability was carried out by Wu *et al.* (2019) for prostate cancer models under androgen suppression therapy.

4.10 Practical Identifiability: Profile Likelihood Method

To address practical identifiability, the profile likelihood approach (Murphy and Van Der Vaart, 2000; Venzon and Moolgavkar, 1988) is followed. The goal is to find confidence intervals for the estimated parameters p^*. Here, a step by step implementation of the profile likelihood method is introduced.

Let p be the parameter vector that contains all parameters of the model, and let θ be one parameter of interest contained in the vector p. Using the likelihood function defined in Equation 4.7.19, the profile likelihood $PL(\theta)$ for the parameter θ is denoted as follows:

$$PL_k(\theta) = \min_{p\in\{p|p_k=\theta\}}(-2LL(p; z_1, ...z_N)) = \min_{p\in\{p|p_k=\theta\}}\left(\sum_{n=1}^{N}\left(\frac{z_n - y(t_n, p)}{\sigma_n}\right)^2\right) \tag{4.10.20}$$

Step-by-step Profile Likelihood Method process:

1. Determine a range for values of the parameter θ.

2. Fix $\theta = \theta^*$ at a value in the range.

3. For the fixed value in step 2 fit the parameters p_k^* and obtain the best-fit values by minimizing the objective function defined in equation (4.10.20) using the quasi Monte Carlo method and the simplified version of simulated annealing described earlier.

4. Evaluate the objective function at those optimum values for the fixed value of θ^*.

5. Repeat the process described in steps 2-4 for a discrete set of values in the range of the parameter θ. This yields the profile likelihood function for the parameter θ.

The above process is followed to find profile likelihood curves for multiple parameters of interest. A confidence interval for the parameter of interest can be determined using the profile likelihood method. This is accomplished with the use of a threshold. The confidence interval for a parameter θ at a level of significance α is of the form

$$PL(\theta) - 2LL(p_k^*) \leq \Delta_\alpha,$$

where $\Delta_\alpha = \chi^2(\alpha, df)$ denotes the threshold and is represented by a χ^2 distribution with df the number of model parameters (e.g. if $df = 1$ all model parameters except for one are fixed) and level of significance α (e.g $\alpha = 0.95$ for 95% confidence interval) (Raue *et al.*, 2009; Kreutz *et al.*, 2013; Eisenberg and Harsh, 2017; Wu *et al.*, 2019). The intersection points between the threshold and the profile likelihood curve at given parameter values result to the bounds of the 95% confidence interval (Raue *et al.*, 2009). A parameter is said to be practically identifiable if the shape of the profile likelihood plot is locally convex with a finite confidence interval as shown in Figure 4.4 a) (Eisenberg and Harsh, 2017). Otherwise, a parameter is practically unidentifiable as shown in Figure 4.4 b).

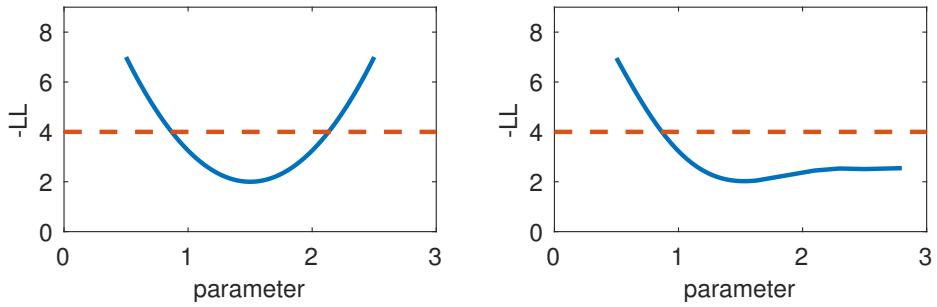

(a) Identifiable (b) Practically Unidentifiable

Figure 4.4: Example of an identifiable and practically unidentifiable parameter as shown in Eisenberg (2018).

4.11 Identifiability of Oncolytic Virus Model

Several rounds of increasing the number of fixed parameters is investigated until practical identifiability is reached for all parameters.

4.12 Full Parameter Fitting

The submodel (4.6.12) - (4.6.14) presented in Gevertz and Wares (2018) consists of a total of five parameters ($df = 5$) which are listed in Table 4.2. Once the optimum parameters are obtained as shown in Table 4.3 using the method in Section 4.8, practical identifiability for all five parameters and initial condition $U(0)$ is explored as described in Section 4.10.

The likelihood profiles for each of the five parameters and initial condition are obtained using equation (4.10.20) and the approach described in Section 4.10. Figure 4.5 illustrates practical unidentifiability for all parameters except for the net tumor growth r and the initial condition $U(0)$. The profile curves for r and $U(0)$ exceed the threshold implying practical identifiability. Reasonable confidence bounds obtained are in line with the biological ranges for these parameters. The rest of the plots appear to be flat, showing signs of practical unidentifiability for the infection rate parameter β, the infected lysis parameter δ_I, the viral production parameter α, and the viral decay parameter δ_V.

Table 4.3: Optimal scaled parameter values obtained for the model system (4.6.12) - (4.6.14), with non-scaled values shown in parentheses.

Variable	Meaning	Value	Units	Reference
r	Net tumor growth	0.264	day^{-1}	fitted
β	Infection rate	0.8655 ($\times 10^{-3}$)	day^{-1}	fitted
δ_I	Infected lysis rate	1.432	day^{-1}	fitted
α	Viral production	0.0587 ($\times 10^{3}$)	-	fitted
δ_V	Viral decay rate	1.3354	day^{-1}	fitted
$U(0)$	Initial condition	58.779	mm^3	fitted

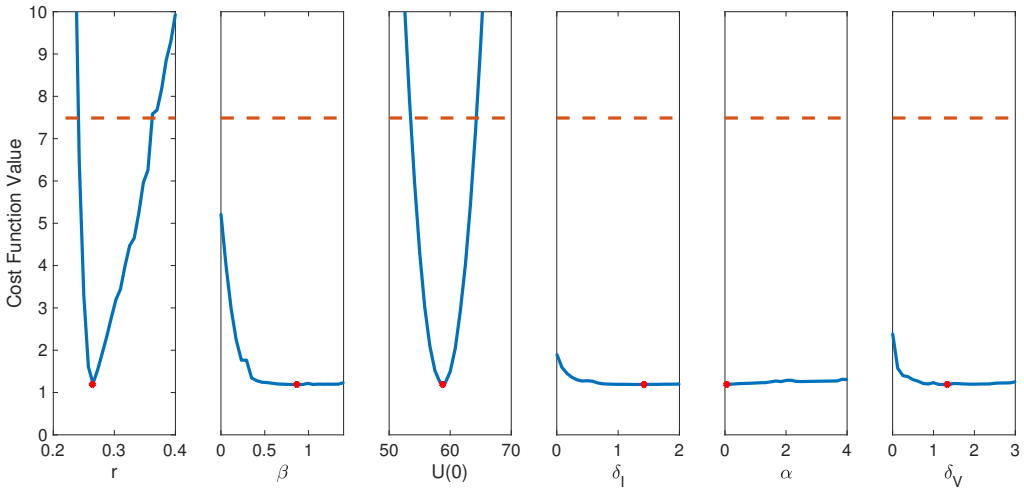

Figure 4.5: Profile likelihood plots for parameters r, β, U(0), $\delta_I, \alpha, \delta_V$. The dotted line depicts the threshold and the intersection points between the threshold and profile likelihood curve are the 95% confidence interval bounds using $df = 5$. The red points are the parameter estimates shown in Table 4.3.

4.13 Partial Parameter Fitting

The results in Section 4.12 indicate that the model is unidentifiable when simultaneous fitting of the parameters is performed. Particularly, only two parameters are identifiable, the net tumor growth rate r and the initial condition $U(0)$.

4.13.1 Partial Parameter Fitting : α and δ_I Fixed

When observing the model (4.6.12) -(4.6.14), it is noted that both parameters δ_I, the infected lysis, and α, the viral production, involved in equation (4.6.14) are in the form of a product indicating dependency between the two parameters. Additionally, it is suspected that $I = 0$ is a fixed point of the system, as a result, the effect of

equation (4.6.13) is insignificant once infected tumor cells die out. To determine whether these two parameters alone are responsible for the unidentifiability of the model, both parameters α and δ_I are fixed as a next step, while fitting the remaining parameters. The optimum and fixed values are listed in Table 4.4.

Table 4.4: Optimal scaled parameter values obtained for the model system (4.6.12) - (4.6.14) for the partial parameter fitting method: α and δ_I fixed, with non-scaled values shown in parentheses.

Variable	Meaning	Value	Units	Reference
r	Net tumor growth	0.2673	day^{-1}	fitted
β	Infection rate	2.451 ($\times 10^{-3}$)	day^{-1}	fitted
δ_I	Infected lysis rate	1	day^{-1}	fixed
α	Viral production	3 ($\times 10^{3}$)	-	fixed
δ_V	Viral decay rate	7.566	day^{-1}	fitted
$U(0)$	Initial condition	58.052	mm^3	fitted

Figure 4.6 indicates that only two parameters, namely r, the net tumor growth and $U(0)$, the initial condition are identifiable. The identifiability results did not improve, in fact are the same as Section 4.12, where only r and $U(0)$ were proven to be practically identifiable. This indicates that an additional parameter is required to be fixed.

4.13.2 Partial Parameter Fitting: α, δ_I and δ_V Fixed

Since the results in Section 4.13.1 did not improve the identifiability results, here the viral decay parameter δ_V is also fixed. For the analysis, the following parameters

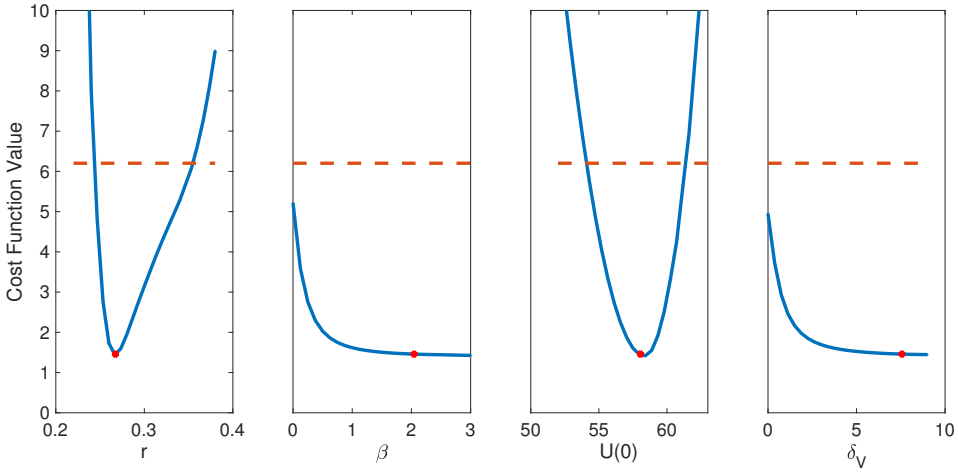

Figure 4.6: Profile likelihood plots for parameters r, β, U(0) and δ_V, while fixing the remaining parameters δ_I, α. The dotted line depicts the threshold and the intersection points between the threshold and profile likelihood curve are the 95% confidence interval bounds using $df = 3$. The red points are the parameter estimates shown in Table 4.4.

are varied: r, the net tumor growth, β, the infection rate and $U(0)$, the initial condition for uninfected tumor cells. The optimum and fixed values are listed in Table 4.5.

Figure 4.7 depicts that all parameters are now practically identifiable. Particularly, the net tumor growth rate, r, the infection rate, β and the initial condition $U(0)$ are identifiable. It is important to note that the profile for parameter β, the infection rate, shows wide 95% confidence interval bounds, which suggests high uncertainty. This could potentially be resolved with the incorporation of additional data regarding infected cells or free viral load.

Table 4.5: Optimal scaled parameter values obtained for the model system (4.6.12) - (4.6.14) for the partial parameter fitting method: α, δ_I and δ_V fixed, with non-scaled values shown in parentheses.

Variable	Meaning	Value	Units	Reference
r	Net tumor growth	0.2672	day^{-1}	fitted
β	Infection rate	0.6620 ($\times 10^{-3}$)	day^{-1}	fitted
δ_I	Infected lysis rate	1	day^{-1}	fixed
α	Viral production	3 ($\times 10^3$)	-	fixed
δ_V	Viral decay rate	2.3	day^{-1}	fixed
$U(0)$	Initial condition	57.439	mm^3	fitted

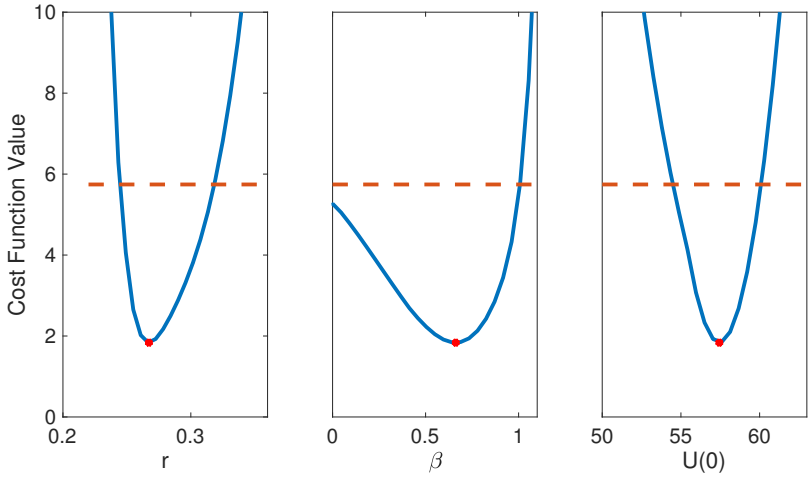

Figure 4.7: Profile likelihood plots for parameters r, β and U(0), while fixing the remaining parameters δ_I, α and δ_V. The dotted line depicts the threshold and the intersection points between the threshold and profile likelihood curve are the 95% confidence interval bounds with $df = 2$. The red points are the parameter estimates shown in Table 4.5.

4.14 Discussion

Mathematical models provide the tools to uncover underlying mechanisms and answer important biological questions. Experimental data are used to validate mathematical models with the goal of making reliable predictions. However, imperfect and incomplete data make it extremely difficult to reveal insights of the model. One of the main challenges is the uncertainty contained in parameters, which leads to unidentifiability issues. One of the main purposes of this work is to determine how reliable the model is in making predictions. To have confidence in the optimal prediction, it is important to ensure that there are no multiple parameter sets that equally-well describe the data. As a result practical identifiability is investigated.

A submodel of Gevertz and Wares (2018) that describes oncolytic virus therapy is used, which contains a total of 5 parameters and one initial condition. Although the original publication followed a hierarchical fitting approach to obtain the optimum parameter set, this method has some disadvantages (Wares *et al.*, 2015). One of the main disadvantages is the accumulation of error that occurs in every step. As a result, a different fitting approach is considered here, where all parameters are fit simultaneously. The optimization method considered uses a quasi Monte Carlo sampling method with Sobol sequences in combination with a simplified version of the simulated annealing method. Once the optimum parameter set is obtained, profile likelihood curves are produced for each of the parameters.

Initially, all five parameters of the model including an initial condition are fit, and the profile likelihood curves are produced. The profile curves suggest that only two parameters, namely the net tumor growth rate, r, and the initial condition, $U(0)$, are practically identifiable. Given the structure of the model, it is observed that a product between two parameters occurs, which suggests strong dependency between

parameters α, the viral production term, and δ_I, the infected cell lysis rate. Upon fixing the two correlated parameters, profile curves are produced, which indicate that the same set of parameters remains identifiable, the net tumor growth, r, and the initial condition, $U(0)$. As a next step, an additional parameter is fixed, δ_V, the viral decay rate. This results in the fit parameters r, β and $U(0)$ being practically identifiable.

Based on the results in the case when all six parameters are fitted, it is speculated that certain parameter combinations lead to diminished I, the infected tumor cells. Some of these parameters include δ_I, the infected lysis rate, α, the viral production term, and δ_V, the viral decay rate. In turn, because the effects of δ_I and α are mediated by terms of the form $\delta_I \cdot \alpha$, as shown in equation 4.6.13, the effects are also diminished. Since these parameters are no longer reflected in the equations, as the effect of I gets eliminated, consequently these parameters are unidentifiable.

However, since relatively good experimental measurements on certain parameters exist, it is reasonable to fix those parameters. Particularly, there is a sense of how many viruses it takes to lyse open a cell, so α, the viral production can be approximated well (Chen *et al.*, 2001). From experimental literature, the decay rate of the virus, δ_V, is considered a known rate (Li *et al.*, 2008; Wang *et al*, 2006). Similarly, the duration from infection to lysis, δ_I, can be approximated well as measured in Bajzer *et al.* (2008); Friedman *et al.* (2006); Ganly, Mautner and Balmain (2000); Jogler *et al.* (2006). When fixing these three known parameters, it was found that the model is identifiable, meaning the accuracy of the model's predictions can be trusted.

The next step for this project is to investigate the practical identifiability of the full model, which examines the effects of a combination treatment, where an immunostimulatory oncolytic virus therapy and dendritic cell injections are employed, as described in equations (4.4.7)-(4.4.11). The results of this analysis are expected

to be more interesting as the oncolytic virus model analyzed has dynamics largely dictated by an exponential growth term (as treatment effects are transient). As a result, the dynamics of uninfected tumor cells U have qualitatively the same behavior regardless of the choice of treatment-related parameters. However, the use of a combination treatment in the full model perturbs the dynamics away from a pure exponential growth and may allow for reliability testing of the model. At this point, a suggestion for improving the practical identifiability in the case when all parameters are fit is to obtain experimental measurements for both infected tumor cells I and number of virons V.

Chapter 5

CONCLUSION

5.1 Summary of Findings for Chapter 2

One purpose of this dissertation was to develop a simple enough but still capturing all the underlying biological mechanisms model that describes immune checkpoint inhibitor therapy. This work was inspired by Lai and Friedman (2017), who developed a system of partial differential equations model to examine the synergy between an immune checkpoint inhibitor and GVAX vaccine. Although their work was insightful, it did not allow for any type of mathematical analysis due the complicated nature of partial differential equations. As a result, the model proposed in Chapter 2 is a system of differential equations that considers only the monotherapy case, specifically the anti-PD-1 immune checkpoint inhibitor.

Even though experimental data was not available for model validation, it allowed to determine model parameters that influence the dynamics of the model. The tumor cell growth rate, λ_C, the killing rate of tumor cells by immune cells, η, and the death rate of T cells d_T proved to be the most influential. Additionally, by conducting a bifurcation analysis for d_T, it suggested that tumor eradication is achievable if caught early. Furthermore, the model investigated and compared intermittent versus continuous treatment injection and concluded that continuous injection is preferable. In the case of intermittent treatment more frequent injections proved to have more effective results. Tumor elimination though can only be achieved with combination. Finally, mathematical analysis of the model when no drug is applied established conditions for global stability of the tumorous and tumor-free equilibria.

5.2 Summary of Findings for Chapter 3

The goal of the third chapter was to further enhance the work in Chapter 2 and further investigate suggested observations. Specifically, the anti-PD-1 model only considered the monotherapy case and suggested a combination type of treatment as a more efficient method. In this work, data from Xu *et al.* (2017) were extracted and used to investigate the pairing of immune checkpoint inhibitor anti-PD-L1 with an immunostimmulant NHS-muIL12. One of the main differences with the previous work is the use of anti-PD-L1 therapy compared to anti-PD-1 therapy.

One of the highlights of this work was the development of a simple generic model consisting of a system of differential equations in the case when no drugs were administrated. This allowed the determination of conditions required for the local stability of the tumorous and tumor-free steady state. Given the generic form of the conditions, both the logistic and exponential tumor growth dynamics we explored. Moreover, the model was extended to incorporate two immunotherapies (anti-PD-L1 and NHS-muIL12). For the purpose of the mathematical analysis, continuous injection was considered to ease the mathematical computations for the full system. Additionally, a quasi-state approximation was used to reduce the dimensions of the model resulting to the limiting system, for which mathematical analysis was also conducted. One of the downsides of the mathematical analysis was the technical nature of the results, which did not allow for biological insights. Yet, it supported in verifying the numerical predictions of the model.

The experimental data from Xu *et al.* (2017) proved crucial for model validation and parameter estimation. Due to limited literature resources, a few of the parameters were estimated though submodel fitting. For each submodel the most sensitive parameters were identified and fit against Xu *et al.* (2017). Once inherited, they

were used to predict the combination therapies. Simulations showed that only in the case when higher dosage of NHS-muIL12 was administrated the qualitative behavior matched those of the data in Xu *et al.* (2017). Furthermore, a continuous administration of both drugs was investigated, which was not presented in Xu *et al.* (2017). The treatment regimen was considered for both the full model and limiting system and suggested similar qualitative behavior. Lastly, a synergistic effect was observed for the combination of avelumab and NHS-muIL12 and suggested that tumor eradication could potentially be achieved when administrating about one-third of the amount of both drugs compared to monotherapy.

5.3 Summary of Findings for Chapter 4

The final purpose of this dissertation was to address the challenges faced when using mathematical models to make predictions. Parameter uncertainty is an important factor that causes unidentifiability issues. The goal in Chapter 4 was to determine the reliability of a model to make predictions. For this purpose, the minimal oncolytic virus therapy model from Gevertz and Wares (2018) was utilized. In the original publication by Wares *et al.* (2015) a hierarchical fitting approach was used to obtain the optimum parameter set. However, accumulation of error in every step is one of the main disadvantages of this method. Therefore, an alternative optimization approach was considered, which instead fits all parameters simultaneously.

As a first step, all parameters of the model were fit using a quasi Monte Carlo method paired with a simplified version of simulated annealing and profile likelihood curves were produced. The profile likelihood curves suggested that only two parameters are practically identifiable, namely the net tumor growth r and the initial condition $U(0)$. Based on the structure of the proposed model, there was a strong indication of dependency between certain parameters. These parameters include the

infected lysis rate δ_I, the viral production α, and the viral decay rate δ_V. As a result, these parameters were fixed with values supported by experimental measurements reported in the literature. In this case, profile likelihood curves suggested that the remaining parameters (r, β, $U(0)$) were practically identifiable, which can potentially lead to more accurate predictions.

5.4 Future Work

As the field of mathematical modeling of immune checkpoint inhibitors therapy is relatively new, a lot of work still needs to be done to develop reliable models that can guide experimental work. Additionally, one of the main challenges in mathematical modeling is obtaining unique and reliable parameters to make accurate predictions. The goal of this dissertation is to gain insights into the dynamics of different treatments with the use of reduced complexity models. Below I list thoughts and ideas that could be implemented in the future building upon the developed models within this dissertation.

Although anti-PD-1 is one of the most effective single agent treatments, immune checkpoint inhibitors develop much higher signs of resistance in comparison to other treatments. Studies have shown that some of the main reasons for T-cells resistance are tumor immunogenicity and different immunosuppressive pathways (Donnell *et al.*, 2016). Based on these facts, future work for Chapter 2 includes the incorporation of two competing tumor species: anti-PD-1 sensitive and anti-PD-1 insensitive to gain more biological insight of the model. Such a model promises to help determine the most effective frequency and dose of treatment, corresponding to patient-specific initial conditions, to delay the onset of treatment resistance.

In regards to Chapter 3, further investigation can be done in improving the structure of the model presented and determining whether a model that yields a good fit

to the monotherapy cases and both doses of NHS-muIL12 can be found. Such investigations include the examination of modifying or altering any terms in the model after following careful consideration of the biological process. Few model suggestions could be the incorporation of time delay and/or terms that account for resistance to the avelumab drug. One can also follow an alternative modeling approach, where the stoichiometric component of the biological process is considered. Such a modeling approach can allow the study of drug uptake during the biological process. Additionally, for simplicity parameters based on the average tumor volume of the eight mice were determined. However, observing the individual tumor volume curves for each mouse reveals that the administration of treatments impacts each mouse in a different way. Hence, a more personalized approach could be considered by determining patient-specific parameters for each mouse. An example of such an approach that considers patient-specific parameters for GBM patients is noted in Han *et al.* (2019). Furthermore, it would be interesting to explore how to potentially adapt the model to investigate the combination of different immune checkpoint inhibitors with other forms of treatment, such as chemotherapy.

Chapter 4 investigates the practical identifiability of a submodel provided in Gevertz and Wares (2018), which considers a monotherapy case. However, the goal is to explore the practical identifiability of the full model provided in Gevertz and Wares (2018), which explores the pairing between an immunostimulatory oncolytic virus therapy and dendritic cell injections. In this case, the dynamics of the model should not be overwhelmed by an exponential response present in the monotherapy case, and it is anticipated to infer new things about the reliability of the model's predictions.

REFERENCES

Agata, Y., A. Kawasaki, H. Nishimura, Y. Ishida, T. Tsubata, H. Yagita, and T. Honjo, "Expression of the PD-1 antigen on the surface of stimulated mouse T and B lymphocytes." International Immunology **8**, 5, 765–772 (1996).

Agur, Z., M. Elishmereni, and Y. Kheifetz, "Personalizing oncology treatments by predicting drug efficacy, side-effects, and improved therapy: mathematics, statistics, and their integration," WIREs Systems Biology and Medicine **6**, 239–253 (2014).

Alsaab, H. O., S. Sau, R. Alzhrani, K. Tatiparti, K. Bhise, S. K. Kashaw, and A. K. Iyer, "PD-1 and PD-L1 checkpoint signaling inhibition for cancer immunotherapy: mechanism, combinations, and clinical outcome." Frontiers in Pharmacology **8** (2017).

Antonios, J. P., H. Soto, R. G. Everson, J. Orpilla, D. Moughon, N. Shin, S. Sedighim et al., "PD-1 blockade enhances the vaccination-induced immune response in glioma." JCI Insight **1**, 10 (2016).

Azoury, S. C., D. M. Straughan, and Vivek Shukla."Immune Checkpoint Inhibitors for Cancer Therapy: Clinical Efficacy and Safety ", Current Cancer Drug Targets **15**, 6 (2015).

Bailey A., Y. Mao, J. Zeng, V. Holla, A. Johnson, L. Brusco, K. Chen, J. Mendelsohn, M. J. Routbort, G. B. Mills GB, et al., "Implementation of biomarker-driven cancer therapy: existing tools and remaining gaps.", Discovery Medicine **17**, 101–111 (2014).

Bagheri, N., M. Shiina, D. A. Lauffenburger and W. M. Korn, "A dynamical systems model for combinatorial cancer therapy enhances oncolytic adenovirus efficacy by MEK-inhibition", PLoS Computational Biology **7** (2011).

Bajzer, Z., T. Carr, K. Josic, S. J. Russell, and D. Dingli, "Modeling of cancer virotherapy with recombinant measles viruses. " Journal of Theoretical Biology **252**, 1, 109–122 (2008).

Barish, S., M. Ochs, E. Sontag, and J. Gevertz, "Evaluating optimal therapy robustness by virtual expansion of a sample population, with a case study in cancer immunotherapy," Proceedings of the National Academy of Sciences **114**, 31, E6277–E6286 (2017).

Bishop, C. M., "Pattern Recognition and Machine Learning.", Springer (2006).

Blair, R. H., D. L. Trichler and D. P. Gaille, "Mathematical and statistical modeling in cancer systems biology.", Frontiers in Physiology **3** (2012).

Brahmer, J. R., C. G. Drake, I. Wollner, J. D. Powderly, J. Picus, W. H. Sharfman, E. Stankevich et al., "Phase I Study of Single-Agent Anti-Programmed Death-1 (MDX-1106) in Refractory Solid Tumors: Safety, Clinical Activity, Pharmacodynamics, and Immunologic Correlates." Journal of Clinical Oncology **28**, 19, 3167–3175 (2010).

Burova, E., A. Hermann, J. Waite, T. Potocky, V. Lai, S. Hong, M. Liu et al., "Characterization of the anti-PD-1 antibody REGN2810 and its antitumor activity in human PD-1 knock-in mice." Molecular Cancer Therapeutics **16**, 5, 861–870 (2017).

Burton, C., and E. Bartee, "Syncytia Formation in Oncolytic Virotherapy. " Molecular Therapy Oncolytics **15**, 131–139 (2019).

Byrd, R. H., J. C. Gilbert and J. Nocedal, "A trust region method based on interior point techniques for nonlinear programming." Mathematical Programming **89**, 149–185 (2000).

Chen Y., T. DeWeese, J. Dilley, Y. Zhang, Y. Li, N. Ramesh, J. Lee, R. Pennathur-Das, J. Radzyminski, J. Wypych, D. Brignetti, S. Scott, J. Stephens, D. B. Karpf, D. R. Henderson and D. C. Yu, "CV706, a prostate cancer-specific adenovirus variant, in combination with radiotherapy produces synergistic antitumor efficacy without increasing toxicity," Cancer Research **61**, 5453–5460 (2001).

Cheng, X., V. Veverka, A. Radhakrishnan, L. C. Waters, F. W. Muskett, S. H. Morgan, J. Huo et al., "Structure and Interactions of the Human Programmed Cell Death 1 Receptor." The Journal of Biological Chemistry **288**, 17, 11771–11785 (2013).

Chin, K., V. K. Chand, D. S. A. Nuyten, "Avelumab: clinical trial innovation and collaboration to advance anti-PD-L1 immunotherapy.", Annals of Oncology : Official Journal of the European Society for Medical Oncology **28**, 1658–1666 (2017).

Chiocca, E. A., "Oncolytic viruses," Nature Reviews Cancer **2**, 12, 938–950 (2002).

Chiocca, E. A. and S. D. Rabkin, "Oncolytic viruses and their application to cancer immunotherapy." Cancer Immunology Research **2**, 4, 295–300 (2014).

Colombo, M. and G. Trinchieri, "Interleukin-12 in anti-tumor immunity and immunotherapy," Cytokine and Growth Factor Reviews **13**, 2, 155–168 (2002).

Creasey, A. A., H. S. Smith, A. J. Hackett, K. Fukuyama, W. L. Epstein, and S. H. Madin, "Biological properties of human melanoma cells in culture." In Vitro **15**, 5, 342–350 (1979).

Csatary, L. K., G. Gosztonyi, J. Szeberenyi,et al., "MTH-68/H Oncolytic Viral Treatment in Human High-Grade Gliomas", Journal of Neuro-Oncology **67**, (1-2), 83–93 (2004).

Darvin, P., S. M. Toor, V. N. Sasidharan, "Immune checkpoint inhibitors: recent progress and potential biomarkers. " Experimental and Molecular Medicine **50**, 12, 1–11 (2018).

De Boer, R. J., P. Hogeweg, H. F. Dullens, R. A. De Weger, and W. Den Otter, "Macrophage T lymphocyte interactions in the anti-tumor immune response: a mathematical model." The Journal of Immunology **134**, 4, 2748–2758 (1985).

De Pillis, L. G., and A. Radunskaya, "A Mathematical Tumor Model with Immune Resistance and Drug Therapy: An Optimal Control Approach." Journal of Theoretical Medicine **3**, 2, 79–100 (2001).

De Pillis, L. G., A. E. Radunskaya, and C. L. Wiseman, "A Validated Mathematical Model of Cell-Mediated Immune Response to Tumor Growth." Cancer Research **65**, 17 7950–7958 (2005).

De Pillis, L. G., A. Gallegos, and A. Radunskaya, "A model of dendritic cell therapy for melanoma.", Frontiers in Oncology **3**, 17 7950–7958 (2013).

Del Monte, U., "Does the cell number 10(9) still really fit one gram of tumor tissue?", Cell Cycle **8**, 3, 505–506 (2009).

Dingli, D, M. D. Cascino, K. Josic, S. J. Russell, and Z. Bajzer, "Mathematical modeling of cancer radiovirotherapy.", Mathematical Biosciences **199**, 1, 55–78 (2006).

Dingli, D., C. Offord, R. Myers, K. W. Peng, T. W. Carr., K. Josic, S. J. Russell and Z. Bajzer,"Dynamics of multiple myeloma tumor therapy with a recombinant measles virus.", Cancer Gene Therapy **16**, 12, 873–882 (2009).

Deisboeck, T. S., "Personalizing medicine: a systems biology perspective," Molecular Systems Biology **5**, 249 (2009).

Disis, M. L.,"Mechanism of action of immunotherapy." Seminars in Oncology **41**, 5, 3–13 (2014).

Dumbrava, E. I., F. Meric-Bernstam,"Personalized cancer therapy-leveraging a knowledge base for clinical decision-making.", Cold Spring Harbor Molecular Case Study **4**, 2 (2018.)

O'Donnell, J. S., M. J. Smyth, and M. W. L. Teng, "Acquired resistance to anti-PD1 therapy: checkmate to checkpoint blockade?" Genome Medicine, **8**, 111 (2016).

Eftieme, R. J., Dushoff, B. W. Bridle, J. L. Bramson and D. J. D. Earn,"Multistability and multi-instability phenomena in a mathematical model of tumor-immune interactions.", Bulletin of Mathematical Biology **73**, 12, 1–30 (2011).

Ehrhardt, S. L. J. Appel, C. L. Meinert, "Trends in National Institutes of Health Funding for Clinical Trials Registered in ClinicalTrials.gov." Jama **314**, 23, 2566–2567 (2015).

Eikenberry, S., C. Thalhauser, and Y. Kuang, "Tumor-Immune Interaction, Surgical Treatment, and Cancer Recurrence in a Mathematical Model of Melanoma." PLoS Computational Biology **5**, 4 (2009).

Eisenberg, M. C., S. L. Robertson and J. H. Tien, "Identifiability and estimation of multiple transmission pathways in cholera and waterborne disease", Journal of Theoretical Biology **324**, 84–102 (2013).

Eisenberg, M. C., and E. J. Harsh, “A confidence building exercise in data and identifiability: Modeling cancer chemotherapy as a case study.” Journal of Theoretical Biology **431**, 63–78 (2017).

Eisenberg, M, “Introduction to structural and practical identifiability.” (2018).

Friedman, A., and W. Hao, “The Role of Exosomes in Pancreatic Cancer Microenvironment.” Bulletin of Mathematical Biology **80**, 5, 1111-1133 (2018).

Friedman, A. and X. Lai, “Combination therapy for cancer with oncolytic virus and checkpoint inhibitor: A mathematical model.” PloS One **13**, 2, (2018).

Friedman, A., J. P. Tian, G. Fulci, E. A. Chiocca and J. Wang, “Glioma virotherapy: Effects of innate immune suppression and increased viral replication capacity”, Cancer Research **66**, 2314–2319 (2006).

Ganly, I., V. Mautner and A. Balmain, “Productive replication of human adenoviruses in mouse epidermal cells”, Journal of Virology **74**, 6, 2895–2899 (2000).

Garber, K., “China approves world’s first oncolytic virus therapy for cancer treatment” , Journal of National Cancer Institute, **98**, 298–300 (2006).

Gevertz, J. L. and J. R. Wares,“Developing a Minimally Structured Mathematical Model of Cancer Treatment with Oncolytic Viruses and Dendritic Cell Injections.”, Computational and Mathematical Models in Medicine (2018).

Grossman, Z., and G. Berke, “Tumor escape from immune elimination.” The Journal of Theoretical Biology **83**, 2, 267–296 (1980).

Halle, S., K. A. Keyser, F. R. Stahl, A. Busche, A. Marquardt, X. Zheng, M. Galla, V. Heissmeyer, K. Heller, J. Boelter, K. Wagner, Y. Bischoff, R. Martens, A. Braun, K. Werth, A. Uvarovskii, H. Kempf, M. Meyer-Hermann, R. Arens, M. Kremer, G. Sutter, M. Messerle, and Reinhold FÃűrster, “In vivo killing capacity of cytotoxic T Cells is limited and involves dynamic interactions and T Cell cooperativity.”, Immunity **44** (2016).

Hamanishi, J., M. Mandai, N. Matsumura, K. Abiko, T. Baba, and I. Konishi, “PD-1/PD-L1 blockade in cancer treatment: perspectives and issues.” International Journal of Clinical Oncology **21**, 3, 462–473 (2016).

Han, L., S. Eikenberry, C. He, L. Johnson, M. C. Preul, E. J. Kostelich and Y. Kuang, “Patient-specific parameter estimates of glioblastoma multiforme growth dynamics from a model with explicit birth and death rates.”, Mathematical Biosciences and Engineering, **16**, 5307–5323 (2019).

He, J., Y. Hu, M. Hu, and B. Li, “Development of PD-1/PD-L1 Pathway in Tumor Immune Microenviroment and Treatment for Non-Small Cell Lung Cancer.” Scientific Reports **5** (2015).

Hews, S., S. Eikenberry, J. D. Naggy and Y. Kuang, "Rich dynamics of a hepatitis B viral infection model with logistic hepatocyte growth", Journal of Mathematical Biology **60**, 573–590 (2009).

Huang, J. H., S. N. Zhang, K. J. Choi, J. H. Kim, M. G. Lee, M. Lee, H. Kim and C. O. Yun, "Therapeutic and tumor-specific immunity induced by combination of dendritic cells and oncolytic adenovirus expressing IL-12 and 4-1BBL.", Molecular Therapy : the Journal of the American Society of Gene Therapy **18**, 264–274 (2010).

Ishida, Y., Y. Agata, K. Shibahara, and T. Honjo,"Induced expression of PD-1, a novel member of the immunoglobulin gene superfamily, upon programmed cell death.", EMBO Journal **11**, 3887–95 (1992).

Jacquez, J.A. and P. Greif, "Numerical parameter identifiability and estimability: integrating identifiability, estimability, and optimal sampling design." Mathematical Biosciences **77**, 1, 201–227 (1985).

Jogler, C., D. Hoffmann, D. Theegarten, T. Grunwald, K. Uberla and O. Wildner, "Replication properties of human adenovirus in vivo and in cultures of primary cells from different animal species", Journal of Virology **80**, 3549–3558 (2006).

Juneja, V. R., K. A. McGuire, R. T. Manguso, M. W. LaFleur, N. Collins, W. N. Haining, Gordon J. Freeman, and Arlene H. Sharpe, "PD-L1 on tumor cells is sufficient for immune evasion in immunogenic tumors and inhibits CD8 T cell cytotoxicity.", The Journal of experimental medicine, **214**, 4, 895–904 (2017).

Komarova, N. L. and D. Wodarz, "ODE models for oncolytic virus dynamics." Journal of Theoretical Biology **263**, 4, 530–543 (2010).

Kang, J., S. Demaria and S. Formenti , "Current clinical trials testing the combination of immunotherapy with radiotherapy.", Journal for Immunotherapy of Cancer **4** (2016).

Karev, G.P., A. S., Novozhilov, and E. V. Koonin, "Mathematical modeling of tumor therapy with oncolytic viruses: effects of parametric heterogeneity on cell dynamics." Biology Direct **1**, 30 (2006).

Kaufman, H.L., Atkins, M.B., Subedi, P. et al., "The promise of Immuno-oncology: implications for defining the value of cancer treatment." Journal of Immunotherapy of Cancer **7**, 129 (2019).

Kelly, E. and S. J. Russell,"History of oncolytic viruses: genesis to genetic engineering," Molecular Therapy **15**, 4, 651– 659 (2007).

Kim, P. H., J. H. Sohn, J. W. Choi, Y. Jung, S. W. Kim, S. Haam, and C. O. Yun, "Active targeting and safety profile of PEG-modified adenovirus conjugated with herceptin." Biomaterials **32**, 9, 2314–2326 (2011).

Kirschner, D., and J. C. Panetta, "Modeling immunotherapy of the tumor-immune interaction." Journal of Mathematical Biology **37**, 3, 235–252 (1998).

Kleponis, J., R. Skelton, and L. Zheng, "Fueling the engine and releasing the break: combinational therapy of cancer vaccines and immune checkpoint inhibitors." Cancer Biology & Medicine **12**, 3, 201–208 (2015).

Kreutz, C., A. Raue, D. Kaschek, et al., "Profile likelihood in systems biology", FEBS Journal **280**, 2564–2571 (2013).

Kuang, Y., J. D. Nagy and S. E. Eikenberry, "Introduction to Mathematical Oncology", 1st edition, Chapman and Hall/CRC, (2015).

Kucherenko, S., D. Albrecht, and A. Saltelli, "Exploring multi-dimensional spaces: a comparison of latin hypercube and quasi monte carlo sampling techniques," arXiv (2015).

Kuznetsov, V. A., I. A. Makalkin, M. A. Taylor, and A. S. Perelson "Nonlinear dynamics of immunogenic tumors: Parameter estimation and global bifurcation analysis.", Bulletin of Mathematical Biology **56**, 295–321 (1994).

Lai, X. and A. Friedman, "Combination therapy of cancer with cancer vaccine and immune checkpoint inhibitors: A mathematical model.", PLoS ONE **12**, 1–24 (2017).

Lai, X. and A. Friedman, "Combination therapy for melanoma with BRAF/MEK inhibitor and immune checkpoint inhibitor: a mathematical model." BMC Systems Biology **11**, 70 (2017a).

Lai, X., A. Stiff, M. Duggan, R. Wesolowski, W. E. Carson, and A. Friedman, "Modeling combination therapy for breast cancer with BET and immune checkpoint inhibitors," Proceedings of the National Academy of Sciences **115**, 21, 5534–5539 (2018).

Lai, X. and A. Friedman, "How to schedule VEGF and PD-1 inhibitors in combination cancer therapy?." BMC Systems Biology **13**, 1 (2019).

Lai X. and A. Friedman, "Antagonism and negative side-effects in combination therapy for cancer.", DCDS-B **24**, 9 (2019).

Lai X. and A. Friedman, "Mathematical modeling of cancer treatment with radiation and PD-L1 inhibitor.", Science China Mathematics **63**, 465–484 (2020).

Lagarias, J. C., J. A. Reeds, M. H. Wright, and P. E. Wright, "Convergence Properties of the Nelder-Mead Simplex Method in Low Dimensions.", SIAM Journal of Optimization **9**, 1, 112–147 (1998).

Leach, D. R., M. F. Krummel, and J. P. Allison," Enhancement of Antitumor Immunity by CTLA-4 Blockade.", Science **271**, 5256, 1734–1736 (1996).

Lee, P. M., "Bayesian Statistics: An Introduction.," Wiley Publishing (2012).

Li, H. L., S. Li, J. Y. Shao, X. B. Lin, Y. Cao, W. Q. Jiang, R. Y. Liu, P. Zhao, X. F. Zhu, M. S. Zeng, Z. Z. Guan and W. Huang, "Pharmacokinetic and pharmacodynamic study of intratumoral injection of an adenovirus encoding endostatin in patients with advanced tumors", Gene Therapy **15**, 247–256 (2008).

Liu, S.-Y., and Y.-L. Wu. “Ongoing clinical trials of PD-1 and PD-L1 inhibitors for lung cancer in China." Journal of Hematology & Oncology **136**, 10 (2017).

List, T. and D. Neri, “Immunocytokines: a review of molecules in clinical development for cancer therapy.”, Clinical Pharmacology **20**, 5, 29–45 (2013).

Lorenzo, G., M. A. Scott, K. Tew, T. J. R. Hughes, Y. J. Zhange, L. Liu, G. Vilanova, and H. Gomez, “Tissue-scale, personalized modeling and simulation of prostate cancer growth”, PNAS **113**, 7663–7671 (2016).

Luksza, M., N. Riaz, V. Makarov, V. P. Balachandran, M. D. Hellmann, A. Solovyov, N. A. Rizvi, T. Merghoub, A. J. Levine, T. A. Chan, J. D. Wolchok, B. D. Greenbaum. “A neoantigen fitness model predicts tumour response to checkpoint blockade immunotherapy.”, Nature **551**, 517–520 (2017).

McCarthy, E. F. “The toxins of William B. Coley and the treatment of bone and soft-tissue sarcomas”., The Iowa Orthopaedic Journal., **26**, 154–158 (2006).

Mahoney, K. M., P. D. Rennert, and G. J. Freeman. “Combination cancer immunotherapy and new immunomodulatory targets. ” Nature Reviews. Drug Discovery **8**, 561–84 (2015).

Mahoney, K. M., G. J. Freeman, and D. F. McDermott. “The Next Immune-Checkpoint Inhibitors: PD-1/PD-L1 Blockade in Melanoma.” Clinical Therapeutics **37**, 4, 764–782 (2015).

Marino, S., I. B. Hogue, C. J. Ray, and D. E. Kirschner. “A methodology for performing global uncertainty and sensitivity analysis in systems biology.” Journal of Theoretical Biology **254**, 1, 178–196 (2008).

Markert, J. M., M. D. Medlock, S. D. Rabkin, et al., “Conditionally replicating herpes simplex virus mutant, G207 for the treatment of malignant glioma: results of a phase I trial, ” Gene Therapy **7**, 867–874 (2000).

Maute, R. L., S. R. Gordon, A. T. Mayer, M. N. McCracken, A. Natarajane, N. G. Ring, R. Kimura et al., “Engineering high-affinity PD-1 variants for optimized immunotherapy and immuno-PET imaging.” PNAS **112**, 47, E6506–E6514 (2015).

Melcher, A., K. Parato, C. M. Rooney and J. C. Bell, “Thunder and lightning: Immunotherapy and oncolytic viruses collide ”, Molecular Therapy : the Journal of the American Society of Gene Therapy **19**, 1008–1016 (2011).

McDermott, D., C. Lebbe, F. S. Hodi, M. Maio, J. S. Weber, J. D. Wolchok, J. A. Thompson, and C. M. Balch,“Durable benefit and the potential for long-term survival with immunotherapy in advanced melanoma.”, Cancer treatment reviews **40**, 9, 1056–1064 (2014)

McDonagh, M., and E. B. Bell, “The survival and turnover of mature and immature CD8 T cells.” Immunology **84**, 4, 514–520 (1995).

McLean, K.A. and K.B. McAuley, "Mathematical modelling of chemical processes-obtaining the best model predictions and parameter estimates using identifiability and estimability procedures." The Canadian Journal of Chemical Engineering **90**, 2, 351–366 (2012).

Meng, X., N. Qin and H. Huo, "Dynamics analysis of a predator-prey system with harvesting prey and disease in prey species.", Journal of Biological Dynamics **12**, 342–374 (2018).

Murphy, S.A. and A.W. Van Der Vaart, "On profile likelihood." Journal of American and Statistical Association **95**, 449–485 (2000).

Nikolopoulou, E., L. R. Johnson, D. Harris, J. D. Nagy, E. C. Stites and Y. Kuang, "Tumour-immune dynamics with an immune checkpoint inhibitor.", Letters in Biomathematics **5**, S137–S159 (2018).

Nikolopoulou, E., S. E. Eikenberry, J. L. Gevertz and Y. Kuang, "Mathematical modeling of an immune checkpoint inhibitor and its synergy with an immunostimulant", Discrete and Continuous Dynamical Systems - B (2020).

Naidoo J., D. B. Page, B. T. Li, L. C. Connell, K. Schindler, M. E. Lacouture, M. A. Postow, and J. D. Wolchok, "Toxicities of the anti-PD-1 and anti-PD-L1 immune checkpoint antibodies.", Annals of Oncology : Official Journal of the European Society for Medical Oncology **26**, 12 (2015).

Novozhilov, A. S., F. S. Berezovskaya, E.V. Koonin, and G. P. Karev, "Mathematical modeling of tumor therapy with oncolytic viruses: regimes with complete tumor elimination within the framework of deterministic models.", Biology Direct **1**, 1, (2006).

O'Donnell, J. S., M. J. Smyth, and M. W. L. Teng, "Acquired resistance to anti-PD1 therapy: checkmate to checkpoint blockade?", Genome Medicine **8**, 1:1111 (2016).

Ontah, G. M. Trisilowati and I. Darti,"Dynamic Analysis of a Tumor Treatment Model Using Oncolytic Virus and Chemotherapy with Saturated Infection Rate." IOP Conference Series: Materials Science and Engineering **546**, 3 (2019).

Parra-Guillen, Z. P., A. Janda, P. Alzuguren, P. Berraondo, R. Hernandez-Alcoceba, and I. F. Troconiz, "Target-mediated disposition model describing the dynamics of IL12 and IFNγ after administration of a mifepristone-inducible adenoviral vector for IL-12 expression in mice.", AAPS Journal **15**, 1, 183–194 (2013).

Portz, T. and Y. Kuang, "A mathematical model for the immunotherapy of advanced prostate cancer." World Scientific, 70–85 (2013).

Powles, T., J. P. Eder, G. D. Fine, F. S. Braiteh, Y. Loriot, C. Cruz, J. Bellmunt, H. A. Burris, D. P. Petrylak, S. L. Teng, X. Shen, Z. Boyd, P. S. Hegde, D. S. Chen, and N. J Vogelzang, "MPDL3280A (anti-PD-L1) treatment leads to clinical activity in metastatic bladder cancer.", Nature **515**, 7528, 558–62 (2014).

Press Release: The Nobel Prize in Physiology or Medicine (2018). https://www.nobelprize.org/prizes/medicine/2018/press-release/

Prestwich, R. J., Harrington K. J., Pandha H. S., Vile R. G., Melcher A. A., Errington F.,"Oncolytic viruses: a novel form of immunotherapy." Expert Review of Anticancer Therapy **8**, 10, 1581–1588 (2008).

Radunskaya, A., R. Kim , I. Woods, "Mathematical modeling of tumor immune interactions: a closer look at the role of a PDL1 inhibitor in cancer immunotherapy.", Spora: A Journal of Biomathematics **4**, 1, 25–41 (2018).

Rao, A. and M. R. Patel, "A review of avelumab in locally advanced and metastatic bladder cancer.", Therapeutic Advances in Urology **11** (2019).

Raue, A., C. Kreutz, T. Maiwald, J. Bachmann, M. Schilling, U. Klingmuller, J. Timmer, "Structural and practical identifiability analysis of partially observed dynamical models by exploiting the profile likelihood", Bioinformatics **25**, 15, 923–1929 (2009).

Rius, M. and F. Lyko, "Epigenetic cancer therapy: rationales, targets and drugs." Oncogene **31**, 4257–65 (2012).

Rosewell, S. A, and Suzuki M., "Oncolytic Viruses Partner With T-Cell Therapy for Solid Tumor Treatment.", Frontiers in Immunology **9** 2103.

Russell, L. and K.-W. Peng, "The emerging role of oncolytic virus therapy against cancer.", Chinese clinical oncology **7**, 2, 16 (2018).

Rutter, E. M. and Y. Kuang, "Global Dynamics Of A Model Of Joint Hormone Treatment With Dendritic Cell Vaccine For Prostate Cancer." Discrete and Continuous Dynamical System Series B **22**, 3, 1001–1021 (2017).

Santiago, D. N., J. P. W. Heidbuechel, W. M. Kandell, R. Walker, J. Djeu, C. E. Engeland, D. Abate-Daga, H. Enderling, "Fighting cancer with mathematics and viruses." Viruses **9**, 239 (2017).

Saparata, E. A. and L. G. Pillis, "A Comparison and catalog of intrinsic tumor growth models.", Bulletin of Mathematical Biology **76**, 2010–2024 (2014).

Schalper, K. A., V. A. Venur, and V. Velcheti, "Programmed death-1/programmed death-1 ligand axis as a therapeutic target in oncology: current insights." Journal of Receptor, Ligand and Channel Research **8**, 1–7 (2014).

Serre, R., S. Benzekry, L. Padovani, C. Meille, N. Andre, J. Ciccolini, F. Barlesi, X. Muracciole and D. Barbolosi, "Mathematical modeling of cancer immunotherapy and Its synergy with radiotherapy.", Cancer Research **76** , 17, 4931–4940 (2016).

Sharma, P. and J. P. Allison, "Immune checkpoint targeting in cancer therapy: toward combination strategies with curative potential." Cell **161**, 2, 205–214 (2015).

Sharma, P., S. Hu-Lieskovan, J.A. Wargo, and A. Ribas, "Primary, Adaptive, and Acquired Resistance to Cancer Immunotherapy. " Cell **168**, 707–23 (2017).

Shi, L., S. Chen, L. Yang and Y. Li, "The role of PD-1 and PD-L1 in T-cell immune suppression in patients with hematological malignancies." Journal of Hematology and Oncology **6** (2013).

Shi, S., J. Huang and Y. Kuang, "Global dynamics in a tumor-immune model with an immune checkpoint inhibitor." DCDS-B in review (2020).

Simon, S. and N. Labarriere, "PD-1 expression on tumor-specific T cells: friend or foe for immunotherapy?" Oncoimmunology **7** (2017).

Sivia, D. S. and Skilling, J., "Data analysis: A Bayesian tutorial." Oxford University Press (2006).

Spranger, S., R. M. Spaapen, Y. Zha, J. Williams, Y. Meng, T. T. Ha, and T. F. Gajewski, "Up-Regulation of PD-L1, IDO, and Tregs in the Melanoma Tumor Microenvironment Is Driven by CD8+ T Cells." Science Translation Medicine **5** 200 (2013).

Stéphanou, A., P. Ballet and G. Powathil, "Hybrid Modelling in oncology: success, challenges and hopes.", Mathematical Modelling of Natural Phenomena, EDP Sciences, In press (2019).

Storey, K. M., Lawler S. E., and Jackson T. L, "Modeling Oncolytic Viral Therapy, Immune Checkpoint Inhibition, and the Complex Dynamics of Innate and Adaptive Immunity in Glioblastoma Treatment. ", Front Physiology **1**, 151 (2020).

Szomolay, B., T. D. Eubank, R. D. Roberts, Cl. B. Marsh, and A. Friedman, "Modeling the inhibition of breast cancer growth by GM-CSF." Journal of Theoretical Biology **303**, 141–151 (2012).

Talay, O., C. H. Shen, L. Chen, and J. Chen, "B7-H1 (PD-L1) on T cells is required for T-cell mediated conditioning of dendritic cell maturation." PNAS **106**, 8, 2741–2746 (2009).

Talkington, A. and R. Durett, "Estimating tumor growth rates in vivo." Bulletin of Mathematical Biology **77**, 10, 1943–54 (2015).

Tan, S., K. Liu, Y. Chai, C. W.-H. Zhang, S. Gao, G. F. Gao, and J. Qi, "Distinct PD-L1 binding characteristics of therapeutic monoclonal antibody durvalumab.", Protein and Cell **9**, 135–139 (2018).

Tang, J., J. X. Yu, V. M. Hubbard-Lucey, S. T. Neftelinov, J. P. Hodge and Yunqing Lin, "The clinical trial landscape for PD1/PDL1 immune checkpoint inhibitors.", Nature Reviews Drug Discovery **17** , 854–855 (2018).

Tian J. P., "The replicability of oncolytic virus: defining conditions in tumor virotherapy.", Mathematical Biosciences and Engineering **8**, 3, 841–60 (2011).

Tonsing, C., J. Timmer, and C. Kreutz, "Profile likelihood-based analyses of infectious disease models.", Statistical Methods in Clinical Research **27**, 7 (2018).

Topolian, S. L., F. S. Hodi, J. R. Brahmer, S. N. Gettinger,D. C. Smith, D. F. McDermott, J. D. Powderly et al., "Safety, Activity, and Immune Correlates of Anti-PD-1 Antibody in Cancer." The New England Journal of Medicine **366**, 2443–2454 (2012).

Ventola CL., "Cancer Immunotherapy, Part 3: Challenges and Future Trends. " P & T. **42**, 8, 514–521 (2017).

Venzon, D. J. and S. H. Moolgavkar, "A method for computing profile-likelihood-based confidence intervals." Appl Stat **37**, 87–94 (1988).

Wares, J. R. , J. J. Crivelli, C. Yun, I. Choi,J. L. Gevertz, and P. S. Kim, "Treatment strategies for combining immunostimulatory oncolytic virus therapeutics with dendritic cell injections.", Mathematical Biosciences and Engineering, **12** , 1237–1256 (2015).

Walker, R. and Enderling, H., "From concept to clinic: Mathematically informed immunotherapy." Current Problems in Cancer **40**, 68–83 (2016).

Wang, Y., J. P. Tian, and J. Wei., "Lytic cycle: A dening process in oncolytic virotherapy.", Applied Mathematical Modeling **37**, 8, 5962–5978 (2013).

Wang, Z., Z. Guo, and H. Smith., "A mathematical model of oncolytic virotherapy with time delay.", Mathematical Biosciences and Engineering **16**, 4, 1836–1860 (2019).

Wang, Y., H. Wang, C. Y. Li and F. Yuan,"Effects of rate, volume, and dose of intratumoral infusion on virus dissemination in local gene delivery", Molecular Cancer Therapeutics **5**, 362–366 (2006).

Warner, A. B. and M. A. Postow, "Combination controversies: checkpoint inhibition alone or in combination for the treatment of melanoma?" Oncology **32** , 228–34 (2018).

Wen, T., J. Bukczynski, and T. Watts, "4-1BB ligand-mediated costimulation of human T cells induces CD4 and CD8 T cell expansion, cytokine production, and the development of cytolytic effector function," The Journal of Immunology **168**, 4897–4906 (2002).

Wodarz, D., "Viruses as Antitumor Weapons. " Cancer Research **61**, 8, 3501–3507 (2001).

Wodarz D., N. Komarova, "Towards predictive computational models of oncolytic virus therapy: basis for experimental validation and model selection." PLoS ONE **4**, 1 (2009).

Wong, H. H., N. R. Lemoine, and W. Wang, "Oncolytic viruses for cancer therapy: overcoming the obstacles," Viruses **2**, 1, 78–106 (2010).

Wu, H., H. Zhu, H. Miao and A. S. Perelson, "Parameter identifiability and estimation of HIV/AIDS dynamic models", Bulletin of Mathematical Biology **70**, 3, 785–799 (2008).

Wu, Z., T. Phan, Javier Baez, Y. Kuang and E. J. Kostelich, "Predictability and identifiability assessment of models for prostate cancer under androgen suppression therapy." AIMS **16**, 5, 3512–3536 (2019).

Xu, C., Y. Zhang, P. A. Rolfe, V. M. Hernández, W. Guzman, G. Kradjian, B. Marelli, G. Qin, J. Qi, H. Wang, H. Yu, R. Tighe, K. Lo, J. M. English, L. Radvanyi and Y. Lan, "Combination Therapy with NHS-muIL12 and Avelumab (anti-PD-L1) Enhances antitumor efficacy in preclinical cancer models.", Clinical Cancer Research **23** , 5869–5880 (2017).

Yan,Y., A. B. Kumar, H. Finnes, S. N. Markovic, S. Park, R. S. Dronca, and H. Dong, "Combining immune checkpoint inhibitors with conventional cancer therapy.", Frontiers in immunology **9** (2018).

Yang, J. C., M. Hughes, U. Kammula, R. Royal, R. M. Sherry, S. L. Topalian, K. B. Suri, C. Levy, T. Allen, S. Mavroukakis, I. Lowy, D. E. White, and S. A Rosenberg.,"Ipilimumab (anti-CTLA4 antibody) causes regression of metastatic renal cell cancer associated with enteritis and hypophysitis.", Journal of Immunotherapy **30**, 8, 825–30 (2007).

Youngnak, P., Y. Kozono, H. Kozono, H. Iwai, N. Otsuki, H. Jin, and K. Omura et al., "Differential binding properties of B7-H1 and B7-DC to programmed death-1." Biochemical and Biophysical Research Communications **307**, 3, 672–677 (2003).

Zamarin, D. and M. A. Postow, "Immune checkpoint modulation: rational design of combination strategies.", Pharmacology and Therapeutics **150**, 23–32 (2015).

APPENDIX A

CO-AUTHORS PERMISSIONS

I certify that my co-authors, Lauren Dickman, Duanne Harris, Dr. John Nagy, Dr. Edward Stites and Dr. Yang Kuang have given me permission to include all material in my PhD thesis for Chapter 2.

I certify that my co-authors Dr. Steffen Eikenberry, Dr. Jana Gevertz and Dr. Yang Kuang have given me permission to include all material in my PhD thesis for Chapter 3.

APPENDIX B

JOURNAL PERMISSIONS

Some of the material in Chapter 2 was published in Nikolopoulou *et al.* (2018). I certify that I received copyright permissions from the Journal that published the work, Letters in Biomathematics.

Some of the material in Chapter 3 is published in Nikolopoulou *et al.* (2020). I certify that I have received copyright permission from the Journal that is publishing the work, Discrete and Continuous Dynamical Systems-B.

APPENDIX C

SUPPLEMENTARY MATERIAL FOR CHAPTER 2

C.1 PARAMETER ESTIMATION

The parameter estimations presented below are determined based on a literature review and additional calculations. They are grouped by their appearance in the model equations.

Eq (2.4.14): Based off of BCL_1 tumor cells in the spleen, the growth rate of tumor cells is given by 0.18 day^{-1} (Kuznetsov *et al.*, 1994). A study involving culturing human melanoma cells showed the population doubling of three measured tumor cell lines were 25, 48, and 82 hours (Creasey *et al.*, 1979). Thus, the growth rate of tumor cells can be computed as follows:

$$\frac{\ln(2)}{25/24} \approx 0.67 \text{ day}^{-1}$$
$$\frac{\ln(2)}{82/24} \approx 0.2 \text{ day}^{-1}$$

Hence $\lambda_C = 0.18 - 0.67 \text{ day}^{-1}$.

The carrying capacity of tumor cells can be estimated using the assumption that a tumor reaching 1 gram net weight contains 10^9 cells (Del Monte, 2009). By Szomolay *et al.* (2012), the total capacity of living and dead tumor cells can be estimated to be $9.45 \cdot 10^8$ cells/cm^3. Then

$$\frac{9.45 \cdot 10^8 \text{ cells}}{1 \text{ cm}^3} \cdot \frac{1 \text{ gram}}{10^9 \text{ cells}} = 0.945 \text{ g/cm}^3$$

By Friedman and Hao (2018), the carrying capacity of tumor cells is 0.8 g/cm^3. Hence $C_K = 0.8 - 0.945$ g/cm^3. By (Lai and Friedman, 2017), the killing rates of tumor cells by CD4+ and CD8+ T cells are estimated to be 11.5 $\text{day}^{-1} \cdot \text{cm}^3/\text{g}$ and 46 $\text{day}^{-1} \cdot \text{cm}^3/\text{g}$ respectively. Thus, the killing rate of tumor cells by T cells is $\eta = 11.5 + 46 = 57.5 \text{ day}^{-1} \cdot \text{cm}^3/\text{g}$.

Eq (2.4.15): By Lai and Friedman (2017) the activation rate of CD4+ and CD8+ T cells by IL-2 are both estimated to be 0.25 day^{-1}. Hence, the activation rate of T cells by IL-2 is $\lambda_{TI_2} = 0.25 + 0.25 = 0.5 \text{ day}^{-1}$. Similarly, following the same process for the activation rate of T cells by IL-12, we have $\lambda_{TI_{12}} = 4.66 + 4.15 = 8.81 \text{ day}^{-1}$. We consider the density of naive T cells as $T_N = 4 \cdot 10^{-4} + 2 \cdot 10^{-4} = 6 \cdot 10^{-4}$ g/cm^3, as the density of naive CD4+ and CD8+ T cells are estimated to be $4 \cdot 10^{-4}$ g/cm^3 and $2 \cdot 10^{-4}$ g/cm^3 respectively (Lai and Friedman, 2017).

By Grossman and Berke (1980), the lifetime of T cells is assumed to be 50 days ($d_T = 1/50 = 0.02 \text{ day}^{-1}$). By McDonagh and Bell (1995), the lifespan for CD8+ T cells is given to be 68 days ($d_T = 1/68 = 0.014 \text{ day}^{-1}$). When fit to experimental data of a BCL_1 tumor in the spleens of chimeric mice, the death rate of T cells was estimated as $d_T = 0.0412 \text{ day}^{-1}$ (Kuznetsov *et al.*, 1994). In Eikenberry, Thalhauser,

and Kuang (2009), the death rate of T cells is estimated to be $d_T = 0.0 - 0.05$ day^{-1}. Collecting the findings, we take $d_T = 0.0 - 0.05$ day^{-1}.

Eq (2.4.16): In a Phase 1 study of anti-PD-1 (Brahmer *et al.*, 2010), the serum half-life of PD-1 was found to be 12 to 20 days. By the half-life formula:

$$t_{1/2} = \frac{\ln(2)}{d_A},$$

where d_A is the decay constant. Then

$$d_A = \frac{\ln(2)}{20} - \frac{\ln(2)}{12} = 3.47 \cdot 10^{-2} - 5.78 \cdot 10^{-2} \text{ day}^{-1}.$$

In Schalper, Venur, and Velcheti (2014), the half-lives of several anti-PD-1 drugs are listed. Using the same process as above, the decay constant d_A can be computed. Nivolumab has a dose-dependent half-life, ranging from 12–20 hours ($d_A = 0.83 - 1.39$ day^{-1}). Pembrolizumab has a half-life of around 2–3 weeks ($d_A = 3.3 \cdot 10^{-2} - 5 \cdot 10^{-2}$ day^{-1}). Pidilizumab has a half-life between 9 and 17 days ($d_A = 4.1 \cdot 10^{-2} - 7.7 \cdot 10^{-2}$ day^{-1}). From these findings, we can conclude that

$$d_A = 3.3 \cdot 10^{-2} - 1.39 \text{ day}^{-1}.$$

As in Lai and Friedman (2017), we determine a range for μ_{PA} (blocking rate of PD-1 by anti PD-1) using:

$$\mu_{PA} = \frac{d_A}{9P} = \frac{3.3 \cdot 10^{-2}}{9 \cdot (7.47 \cdot 10^{-10})} - \frac{1.39}{9 \cdot (7.47 \cdot 10^{-10})} = 4.9085 \cdot 10^6 - 2.07 \cdot 10^8 \text{ day}^{-1} \cdot \text{cm}^3/\text{g}.$$

In Cheng *et al.* (2013), experiments found an average of 9282 PD-L1 on a single activated T cell, with a general range of about $8000 - 11500$ PD-L1 on a single activated T cell. Following the same procedure as in (Lai and Friedman, 2017), we estimate ρ_L as follows:

$$\rho_L = 8000 \cdot \frac{m_L}{m_T} - 11500 \cdot \frac{m_L}{m_T},$$

where m_L and m_T are the mass of one PD-L1 protein and the mass of one T cell (T_1 or T_8). We assume that one T cell is approximately 10 microns in diameter, with the same density as water at $39C, 0.9926$ g/cm^3. Then we can calculate the mass of one T cell:

$$m_T = \frac{4\pi(0.005)^3 \text{ cm}^3}{3} \cdot \frac{0.9926 \text{ g}}{\text{cm}^3} \approx 5.24 \cdot 10^{-10} \text{ g}.$$

By Lai and Friedman (2017), the mass of one T cell is estimated to be 10^{-9} g. We can then take $m_T = 5.24 \cdot 10^{-10} - 10^{-9}$ g. Thus,

$$\rho_L = 8000 \cdot \frac{4.45 \cdot 10^{-20}}{10^{-9}} - 11500 \cdot \frac{9.3 \cdot 10^{-20}}{5.2 \cdot 10^{-10}} = 3.56 \cdot 10^{-7} - 1.967 \cdot 10^{-6}.$$

In estimating PD-L1 (L), as done in Lai and Friedman (2017), we have

$$L = \rho_L(T + \epsilon_C C),$$

since PD-L1 is expressed on both tumor cells and tumor cells. As PD-L1 is upregulated on tumor cells (Spranger *et al.*, 2013), we suppose $\epsilon_C \in [1, 100]$. We then calculate the lower bound of L by

$$\begin{aligned} L &= \rho_L(T + \epsilon_C C) = (3.56 \cdot 10^{-7}) \cdot [6 \cdot 10^{-3} + 1 \cdot 0.4] \\ &= 1.445 \cdot 10^{-7} \text{ g/cm}^3 \end{aligned}$$

and the upper bound by

$$\begin{aligned} L &= \rho_L(T + \epsilon_C C) = (1.967 \cdot 10^{-6}) \cdot [6 \cdot 10^{-3} + 100 \cdot 0.4] \\ &= 7.87 \cdot 10^{-5} \text{ g/cm}^3. \end{aligned}$$

Thus we assume $L \approx 2 \cdot 10^{-6}$ g/cm^3 at steady state.

Eq (2.4.17): In Cheng *et al.* (2013), experiments showed an average of 3096 PD-1 on a single activated cell, with a general range of $2000 - 5000$ PD-1 on a single activated cell. Following the same procedure as in Lai and Friedman (2017), we estimate ρ_P as follows:

$$\rho_P = 2000 \cdot \frac{m_P}{m_T} - 5000 \cdot \frac{m_P}{m_T},$$

where m_P and m_T are the mass of one PD-1 protein and the mass of one T cell. By Agata *et al.* (1996), a flow cytometry shows the mass of one PD-1 protein is $m_P = 50 - 55$ kDa ($8.3 \cdot 10^{-20} - 9.13 \cdot 10^{-20}$ g). As outlined above, $m_T = 5.24 \cdot 10^{-10} - 10^{-9}$ g. We then calculate:

$$\rho_P = 2000 \cdot \frac{8.3 \cdot 10^{-20}}{10^{-9}} - 5000 \cdot \frac{9.3 \cdot 10^{-20}}{5.2 \cdot 10^{-10}} = 3.19 \cdot 10^{-7} - 8.49 \cdot 10^{-7}.$$

In estimating γ we seek to balance $(\rho_p - \gamma A)$ in Eq (2.4.17) with the magnitudes observed in simulations. In particular, we consider the magnitude of drug A to be $\approx 10^{-8}$ and $\rho_p \approx 10^{-7}$ as listed in Table C.1. Hence, we estimate $\gamma = 10$ cm^3/g.

Table C.1: Parameters of the Model System (2.4.14)-(2.4.16)

Variable	Meaning	Value	Reference
λ_C	tumor cell growth rate	$0.18 - 0.67$ day^{-1}	(Kuznetsov *et al.*, 1994),(Eikenberry, Thalhauser, and Kuang, 2009),(Creasey *et al.*, 1979),(Lai and Friedman, 2017)
C_K	carrying capacity of tumor cells	$0.8 - 0.945$ g/cm^3	(De Pillis and Radunskaya, 2001),(De Pillis, Radunskaya, and Wiseman, 2005),(De Pillis, Gallegos, and Radunskaya, 2013),(Rutter and Kuang, 2017)
η	kill rate of tumor cells by T cells	57.5 day$^{-1}\cdot$ cm^3/g	(Lai and Friedman, 2017)
$\lambda_{TI_{12}}$	activation rate of T cells by IL-12	8.81 day^{-1}	(Lai and Friedman, 2017)
T_N	density of naive T cells	$6 \cdot 10^{-4}$ g/cm^3	(Lai and Friedman, 2017)
I_{12}	IL-12 concentration	$1.5 \cdot 10^{-10}$ g/cm^3	(Lai and Friedman, 2017)
$K_{I_{12}}$	half-saturation of IL-12	$1.5 \cdot 10^{-10}$ g/cm^3	(Lai and Friedman, 2017)
λ_{TI_2}	activation rate of T cells by IL-2	0.5 day^{-1}	(Lai and Friedman, 2017)
I_2	IL-2 concentration	$2.37 \cdot 10^{-11}$ g/cm^3	(Lai and Friedman, 2017)
K_{I_2}	half-saturation of IL-2	$2.37 \cdot 10^{-11}$ g/cm^3	(Lai and Friedman, 2017)
K_{TQ}	inhibition of function of T cells by PD-1-PD-L1	$1.365 \cdot 10^{-18}$ g/cm^3	(Lai and Friedman, 2017)
ρ_L	expression level of PD-L1 on activated T cells	$3.56 \cdot 10^{-7}$ - $1.967 \cdot 10^{-6}$	(Cheng *et al.*, 2013)
ρ_P	expression level of PD-1 on T cells	$3.19 \cdot 10^{-7}$ - $8.49 \cdot 10^{-7}$	(Cheng *et al.*, 2013; Agata *et al.*, 1996)
ϵ_C	expression of PD-L1 in tumor cells vs. T cells	$1 - 100$	estimated
d_T	death rate of T cells	0.0 – 0.05/day	(Eikenberry, Thalhauser, and Kuang, 2009)

Variable	Meaning	Value	Reference
μ_{PA}	blocking rate of PD-1 by anti-PD-1	$4.9085 \cdot 10^6 - 2.07 \cdot 10^8$ day$^{-1}\cdot$ cm^3/g	(Youngnak *et al.*, 2003; Cheng *et al.*, 2013)
γ_A	source of anti-PD-1	10^{-10} day$^{-1}\cdot$ cm^3/g	(Lai and Friedman, 2017)
d_A	degradation rate of anti-PD-1	$3.3 \cdot 10^{-2} - 1.39$ day^{-1}	(Brahmer *et al.*, 2010; Schalper, Venur, and Velcheti, 2014)
γ	blocking of PD-1 by anti-PD-1	10 cm^3/g	estimated

Table C.2: Parameter values used in simulations for equations (2.4.14)-(2.4.16)).

Variable	Meaning	Value
λ_C	tumor cell growth rate	0.4 day^{-1}
C_K	carrying capacity of tumor cells	0.8 g/cm^3
η	kill rate of tumor cells by T cells	57.5 $\text{day}^{-1}\cdot$ cm^3/g
$\lambda_{TI_{12}}$	activation rate of T cells by IL-12	8.81 day^{-1}
T_N	density of naive T cells	$6 \cdot 10^{-4}$ g/cm^3
I_{12}	IL-12 concentration	$1.5 \cdot 10^{-10}$ g/cm^3
$K_{I_{12}}$	half-saturation of IL-12	$1.5 \cdot 10^{-10}$ g/cm^3
λ_{TI_2}	activation rate of T cells by IL-2	0.5 day^{-1}
I_2	IL-2 concentration	$2.37 \cdot 10^{-11}$ g/cm^3
K_{I_2}	half-saturation of IL-2	$2.37 \cdot 10^{-11}$ g/cm^3
K_{TQ}	inhibition of function of T cells by PD-1-PD-L1	$1.365 \cdot 10^{-18}$ g/cm^3
ρ_L	expression level of PD-L1 on activated T cells	$5 \cdot 10^{-7} \cdot 10^{-6}$
ρ_P	expression level of PD-1 on T cells	$2.47 \cdot 10^{-7}$
ϵ_C	expression of PD-L1 in tumor cells vs. T cells	10
d_T	death rate of T cells	0.05, 0.5 /day
μ_{PA}	blocking rate of PD-1 by anti-PD-1	$6.87 \cdot 10^6$ $\text{day}^{-1}\cdot$ cm^3/g
γ_A	source of anti-PD-1	10^{-10} $\text{day}^{-1}\cdot$ cm^3/g
d_A	degradation rate of anti-PD-1	$4.6 \cdot 10^{-2}$ day^{-1}
γ	blocking of PD-1 by anti-PD-1	10 cm^3/g

APPENDIX D

SUPPLEMENTARY MATERIAL FOR CHAPTER 3

D.1 PARAMETER ESTIMATION

By performing a thorough literature review and additional calculations, we are able to estimate some of the parameters used in the model as follows:

Eq (3.3.3): The kill rate of tumor cells by T cells is estimated by Kuznetsov *et al.* (1994) as $\eta = 1.101 \cdot 10^{-7}$ days^{-1}·cells^{-1}. We consider that on average cytotoxic T cells kill on a magnitude of 2-16 infected cells per day (Halle *et al.*, 2016).

$$\eta = \frac{1.101 \cdot 10^{-7}}{\text{cells} \cdot \text{day}} \cdot 2 \text{ cells} - \frac{1.101 \cdot 10^{-7}}{\text{cells} \cdot \text{day}} \cdot 16 \text{ cells},$$

$$\eta = 2.202 \cdot 10^{-7}\text{day}^{-1} - 17.616 \cdot 10^{-7}\text{day}^{-1}.$$

Eq (3.3.4): According to Parra-Guillen *et al.* (2013) the dissociation constant for IL-12 is 0.018 pmol·mL^{-1} $\approx 1.8 \cdot 10^{-11}$M. Since the dissociation constant is terms of M (molarity) we need to make sure that the units are consistent. We observe the following units for the $\frac{dT}{dt}$ equation:

$$\underbrace{\frac{dT}{dt}}_{\frac{mm^3}{day}} = \left(\underbrace{\delta}_{\frac{mm^3}{day}} + \underbrace{\lambda_{TI_{12}}}_{\frac{1}{day}} \underbrace{T}_{mm^3} \frac{\overbrace{A_2'}^{\frac{mol}{liter}}}{\underbrace{K_{A_2}}_{\frac{mol}{liter}} + \underbrace{A_2'}_{\frac{mol}{liter}}} \right) \cdot \frac{1}{1 + \frac{\overbrace{Q}^{mm^6}}{\underbrace{K_{TQ}}_{mm^6}}} - \underbrace{d_T}_{\frac{1}{day}} \underbrace{T}_{mm^3}.$$

Observing more closely the term:

$$\frac{\overbrace{A_2'}^{\frac{mol}{liter}}}{\underbrace{K_{A2}}_{\frac{mol}{liter}} + \underbrace{A_2'}_{\frac{mol}{liter}}} \text{ where } A_2' = \frac{\frac{A_2}{A_2 \text{ molar mass}}}{\text{tumor volume}}.$$

We note that A_2 is originally given in g and the goal is to convert to molarity ($\frac{\text{mol}}{\text{liter}}$). We first convert to moles as follows :

$$\frac{A_2(g)}{\text{molar mass}(\frac{g}{mol})}.$$

According to Sigma-Aldrich source the molar mass of IL-12 is 75KDa, which is approximately $75,000$ grams per mole. Retrieved from: `https://www.sigmaaldrich.com/content/dam/sigma-aldrich/docs/Sigma/Datasheet/2/i2276dat.pdf`.

$$\frac{A_2(g)}{75,000(\frac{\text{g}}{\text{mol}})} = \frac{A_2}{75,000}\text{mol}.$$

Given moles we can now convert to molarity which we denote by c:

$$c = \frac{n}{v} \text{ where } n = \#\text{ of moles and } v = \text{volume in (liters)},$$

$$c_2 = \frac{\frac{A_2}{75{,}000}}{v}.$$

Regarding v (tumor volume in liters), one can observe from Figure 1A that the tumor volume ranges between $(100 - 1000)\ mm^3 \approx (10^{-4} - 10^{-3})\ l$ depending on the type of treatment administrated.

For simplicity we will assume that the whole portion of the drug targets the tumor volume.

$$c_2 = \frac{\frac{A_2}{75{,}000}}{10^{-4}} - \frac{\frac{A_2}{75{,}000}}{10^{-3}},$$

$$c_2 = \frac{A_2}{75 \cdot 10^7}\frac{\text{mol}}{\text{liter}} - \frac{A_2}{75 \cdot 10^6}\frac{\text{mol}}{\text{liter}}.$$

Eq (3.3.5): According to the American College of Clinical Pharmacology (ACCP) and Rao and Patel (2019), the half life of avelumab is 6.1 days. Hence, the degradation rate constant (d_{A_1}) can be calculated as follows:

$$d_{A_1} = \frac{ln2}{t_{\frac{1}{2}}} = \frac{ln2}{6.1} \approx 0.1136 \text{ days}^{-1}.$$

Eq (3.3.11): In Tan *et al.* (2018) the dissociation constant K_{A_1} is estimated as 0.0467 nM$\approx 4.67 \cdot 10^{-11}$ M.

$$\underbrace{L_{bound}}_{mm^3} = \frac{\overbrace{A_1'}^{\frac{moles}{liter}}}{\underbrace{A_1'}_{\frac{moles}{liter}} + \underbrace{K_{A_1}}_{\frac{moles}{liter}}}(\rho_L(\underbrace{T}_{mm^3} + \epsilon_v \underbrace{V}_{mm^3})), \text{ where } A_1' = \frac{\frac{A_1}{A_1 \text{ molar mass}}}{\text{tumor volume}}.$$

Using a similar argument as for Eq(3.3.4) and with similar calculations we conclude that :

$$c_1 = \frac{A_1}{55 \cdot 10^7}\frac{\text{mol}}{\text{liter}} - \frac{A_1}{55 \cdot 10^6}\frac{\text{mol}}{\text{liter}}.$$

Eq (3.3.6): According to List and Neri (2013) the circulatory half-life of NHS-IL12 in vivo is approximately 24 hours. Hence, the degradation rate constant (d_{A_2}) can be calculated as follows:

$$d_{A_2} = \frac{ln2}{t_{\frac{1}{2}}} = \frac{ln2}{1} \approx 0.69 \text{ days}^{-1}.$$

Table D.1: Parameters and variables (Var.) of the model system (3.3.3)-(3.3.6).

Var.	Meaning	Value	Reference
r	Tumor cell growth rate	0.213 day^{-1}	fitted
η	Kill rate of tumor cells by T cells	1 $\text{mm}^{-3} \cdot \text{day}^{-1}$	fitted
δ	Source of T cell activation	0.02 mm^3 /day	estimated
$\lambda_{TI_{12}}$	Activation rate of T cells by IL-12	8.81 day^{-1}	(Nikolopoulou *et al.*, 2018)
K_{A_2}	Dissociation constant of A_2	$7 \cdot 10^{-14}$ moles/liter	estimated
K_{TQ}	Inhibition of function of T cells by PD-1-PD-L1	10^{-13} mm^6	estimated
d_T	Death rate of T cells	$0 - 0.5$ day^{-1}	(Nikolopoulou *et al.*, 2018)
d_{A_1}	Degradation rate of Anti-PD-L1	0.1136 day^{-1}	(Rao and Patel, 2019)
d_{A_2}	Degradation rate of NHS-muIL12	0.69 day^{-1}	(List and Neri, 2013)
ρ_p	Expression level of PD-1	$3.19 \cdot 10^{-7}$ - $8.49 \cdot 10^{-7}$	(Lai and Friedman, 2017)
ρ_L	Expression level of PD-L1	$3.56 \cdot 10^{-7}$ - $1.967 \cdot 10^{-6}$	(Lai and Friedman, 2017)
K_{A_1}	Dissociation constant of free PD-L1 with anti-PD-L1	10^{-13} mol/liter	estimated
ϵ_v	Expression of PD-L1 in tumor cells vs. T cells	1-100	(Nikolopoulou *et al.*, 2018)
σ	fraction of complex association and dissociation	0.01mm^{-3}	estimated
γ_1	continuous infusion rate of avelumab	$10^{-7} - 9 \cdot 10^{-5}$ g/day	estimated
γ_2	continuous infusion rate of NHS-muIL12	$10^{-9} - 2 \cdot 10^{-6}$ g/day	estimated
c_1	conversion constant for A_1 drug	$55^{-1}10^{-7} - 55^{-1}10^{-6}$	estimated
c_2	conversion constant for A_2 drug	$75^{-1}10^{-7} - 75^{-1}10^{-6}$	estimated

Table D.2: Parameter values used in simulations for equations (3.3.3)-(3.3.6).

Variable	Meaning	Value
r	Tumor cell growth rate	0.213 day^{-1}
η	Kill rate of tumor cells by T cells	1 $\text{mm}^{-3} \cdot \text{day}^{-1}$
δ	Source of activation	0.02 mm^3 /day
$\lambda_{TI_{12}}$	Activation rate of T cells by IL-12	8.81 day^{-1}
K_{A_2}	Dissociation constant of A_2	$7 \cdot 10^{-14}$ moles/liter
K_{TQ}	Inhibition of function of T cells by PD-1-PD-L1	10^{-13} mm^6
d_T	Death rate of T cells	0.05 day^{-1}
d_{A_1}	Degradation rate of Anti-PD-L1	0.1136 day^{-1}
d_{A_2}	Degradation rate of NHS-muIL12	0.69 day^{-1}
ρ_p	Expression level of PD-1	$5.84 \cdot 10^{-7}$
ρ_L	Expression level of PD-L1	$2.7635 \cdot 10^{-7}$
K_{A_1}	Dissociation constant of PD-L1 with anti-PD-L1	10^{-13} mol/liter
ϵ_v	Expression of PD-L1 in tumor cells vs. T cells	50
σ	fraction of complex association and dissociation	0.001 mm^{-3}
γ_1	prescribed infusion rate of avelumab	$10^{-7} - 9 \cdot 10^{-5}$ g/day
γ_2	prescribed infusion rate of NHS-muIL12	$10^{-9} - 2 \cdot 10^{-6}$ g/day
c_1	conversion constant for A_1 drug	$55^{-1}10^{-7}$
c_2	conversion constant for A_2 drug	$75^{-1}10^{-7}$

D.2 SUPPLEMENTARY FIGURES

The following figures support the generation of Figure 3.4.

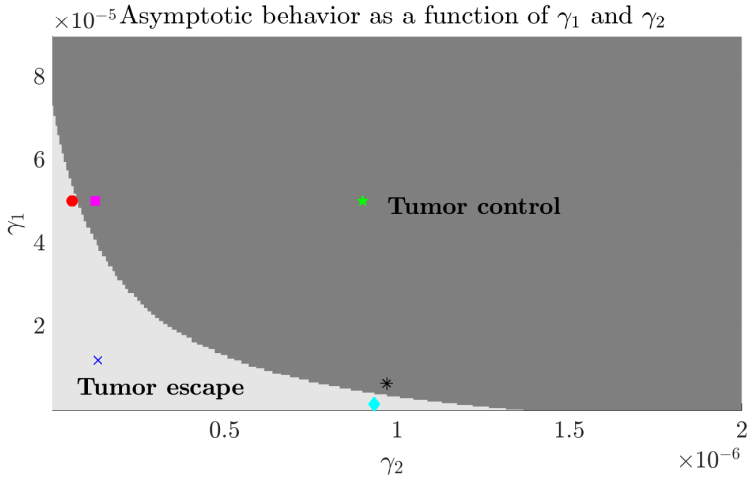

Figure D.1: Surface plot depicting the asymptotic behavior of the full system (3.3.3)-(3.3.6) for combinations of γ_1 (avelumab) and γ_2 (NHS-muIL12) drugs, where both are applied continuously. Based on a threshold, two regions, namely, 'Tumor Control' and 'Tumor Escape' are identified, which are separated by a hyperbolic curve. Six representative points indicated by different markers and colors, are chosen and shown on the plot.

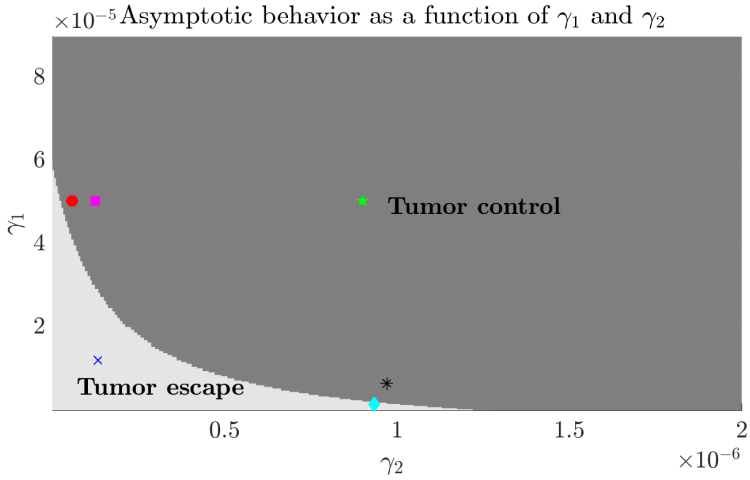

Figure D.2: Surface plot depicting the asymptotic behavior of the limit case system (3.5.22)-(3.5.23) for combinations of γ_1 (avelumab) and γ_2 (NHS-muIL12) drugs, where both are applied continuously. Based on a threshold, two regions, namely, 'Tumor Control' and 'Tumor Escape' are identified, which are separated by a hyperbolic curve. Six representative points indicated by different markers and colors, are chosen and shown on the plot.

APPENDIX E

COMPUTER CODE FOR CHAPTER 3

```
%%%%%%%%%%%%%%%%%%%%%%%%%%%%%% BEGINNING OF CODE %%%%%%%%%%%%%%%%%%%%%%%%%%%%%%%%%%%%%%%%%%%%
% This code demonstrates how to fit the model to data to estimate parameters.
% In the project the parameters r the growth rate and eta the kill rate are
% fitted against the no drug case denoted by mode 1. Data shown in the code
% are extraced by Xu et al. (2017) paper through Webplotdigitizer.

% Written by Elpiniki Nikolopoulou 2019

clear all
clc

%Types of Treatment
mode = 1;                           % 1 = Isotype Control Case

mp   = [ 0.1,    0,     1           %  eta_1 - kill rate of tumor cells by T-cells
         0.2,    0,    inf ];       %  r     - growth rate (r)


mpr  = [   0.001          % 1. sigma        -
           8.81           % 2. lambda_TI12 - activation rate of T cells by IL-12
        7 * 1e-14         % 3. K_A2         - dissociation constant of A_2
           0.05           % 4. d_T          - death rate of T cells
           0.1136         % 5. d_A1         - degradation rate of Anti-PD-L1
           0.69           % 6. d_A2         - degradation rate of NHS-muIL12
       5.84 * 1e-7        % 7. rho_p        - expression level of PD-1
     2.7635 * 1e-7        % 8. rho_l        - expression level of PD-L1
           1e-13          % 9. K_A1         - dissociation constant of A_1
           50             % 10. epsilon     - expression of PD-L1 in tumor cells
          .02             % 11. delta       - source of activation
          1e-13];         % 12. K_TQ        - inhibition of function of T
                                             %cells by PD-1-PD-L1


lb = mp(:,2);            % lower bound
up = mp(:,3);            % upper bound
x0 = mp(:,1);            % Guess of parameters wanted to estimate
options = optimoptions(@fmincon,'Algorithm','interior-point','Display','off');


[min, fval]=fmincon(@(x)error_local(x,mode,mpr),x0,[],[],[],[],lb,up,...
                    [],options);


eta_1 = min(1)
r     = min(2)

[y0,T,V,i_edges,t_edges]     = choose(mode,mpr);
[tout,yout,t_edges,y_edges] = SolveODE_all(y0,t_edges,i_edges,mpr,eta_1,r);

v = yout(:,1); Tc = yout(:,2); A1 = yout(:,3); A2 = yout(:,4);


figure (1)
fitted = plot(tout,v,T,V,'o');
set([fitted],'LineWidth', 3)
legend('fitted curve','data points')
title({'Tumor volume against time'},'Interpreter','latex','fontsize', 20)
xlabel({'Time (days) '},'Interpreter','latex','fontsize', 20)
ylabel({'Tumor Volume $\enspace (mm^3)$ '},'Interpreter','latex','fontsize', 20)
ylim([0 1200])
set(gcf,'position',[550,100,350,550])
set(gca,'FontSize', 20)
set(gca,'TickLabelInterpreter','latex')

% -----------------------------------------------------------------------------
function z = error_local(x,mode,mpr)
```

```
[y0,T,V,i_edges,t_edges] = choose(mode,mpr);
 eta_1 = x(1); r = x(2);

[tout,yout] = SolveODE(y0,t_edges,i_edges,mpr,eta_1,r);
% interpolation
v = yout(:,1);
tout(:);
k = dsearchn(tout(:),T); % Returns the indices k of the closest points of tout to T
v(k);                    % Find solutions for those specific data time points


z = sum(abs((v(k)-V)).^(2));  % minimize this

end

%-------------------------------------------------------------------------
% Function used to define the ode system.

function dydt = f(t,y,mpr,eta_1,r)

    v = y(1); Tc = y(2); A_1 = y(3); A_2 = y(4);      % Define variables

    % Model Parameters

   sigma = mpr(1); lambda_TI12 = mpr(2);  K_A2  = mpr(3); d_T   = mpr(4);
   d_A1  = mpr(5);         d_A2 = mpr(6);  rho_p = mpr(7); rho_l = mpr(8);
   K_A1  = mpr(9);      epsilon = mpr(10); delta=mpr(11);  K_TQ  = mpr(12);



    % Equations

    P    = rho_p * Tc;                          % PD-1 expression
    L_t  = rho_l * (Tc + epsilon * v);          % PD-L1 total expression
    A_1n = A_1 * (1 / (55 * 1e7));
    L_b  = (A_1n / (A_1n + K_A1)) * (rho_l * (Tc + epsilon * v)); % PD-L1 bound
                                                                  % expression
    L_f  = L_t - L_b;                           % PD-L1 free expression
    Q    = sigma * P * L_f ;                    % PD-1-PD-L1 complex expression

    % Ode functions
    A_2n = A_2 * (1 / (75*1e7));
    dv   =  r * v - (eta_1 * Tc * v);                % tumor volume DE
    dTc  = (delta + (lambda_TI12 * Tc * A_2n) / (K_A2 + A_2n))...
           * (1 / (1 + (Q / K_TQ))) - d_T * Tc;      % T-cells DE
    dA_1 =  - d_A1 * A_1;                            % A_1 (avelumab) DE
    dA_2 =  - d_A2 * A_2;                            % A_2 (NHS-muIL12) DE

    dydt = [dv; dTc; dA_1; dA_2];

end

%-------------------------------------------------------------------------
function [t_edges,y_edges] = SolveODE(y0,t_edges,i_edges,mpr,eta_1,r)

options      = odeset();                        % Initial option setting for
                                                % ODE solver

[~,IDX]      = sort(t_edges);
t_edges      = t_edges(IDX);
i_edges      = i_edges(IDX,:);

y_edges      = nan(length(t_edges),length(y0)); % create an empty matrix to
                                                % update initial conditions
                                                % based on the time points
y_edges(1,:) = y0';                             % first row contains initial
```

```
                                                % conditions

for i=1:length(t_edges)-1

    [~,y_temp]      = ode15s(@(t,y)f(t,y,mpr,eta_1,r),[t_edges(i) t_edges(i+1)],...
                             y_edges(i,:)+i_edges(i,:),options);
    y_edges(i   ,:) = y_temp(1,:);
    y_edges(i+1,:) = y_temp(end,:);
end



end


%-------------------------------------------------------------------------------
function [t_all,y_all,t_edges,y_edges] = SolveODE_all(y0,t_edges,i_edges,mpr,eta_1,r)

options      = odeset();              % Initial option setting for ODE solver

[~,IDX]      = sort(t_edges);
t_edges      = t_edges(IDX);
i_edges      = i_edges(IDX,:);

y_edges      = nan(length(t_edges),length(y0));  % create an empty matrix
                  %to update initial conditions based on the time points
y_edges(1,:) = y0';             % first row contains initial conditions

t_all        = [];
y_all        = [];
for i=1:length(t_edges)-1
    %try
    [t_temp,y_temp] = ode15s(@(t,y)f(t,y,mpr,eta_1,r),...
              [t_edges(i) t_edges(i+1)],y_edges(i,:)+i_edges(i,:),options);
    t_all           = [t_all;t_temp];
    y_all           = [y_all;y_temp];
    y_edges(i   ,:) = y_temp(1,:);
    y_edges(i+1,:) = y_temp(end,:);
end

end

function [y0,T,V,i_edges,t_edges] = choose(mode,mpr)
if mode == 1

       y0 = [100; 0.03; 0; 0];

       T = [  0.0001,       2.9364,    6.0471,  10.0347,   13.0612,  17.0977]';
       V = [   100,        182.8576,  267.1761, 443.1102, 675.1583, 1005.3435]';

       t_edges = [ 0    % time points where things occur such as t0,tf,injT,T
                   18   % simulations run up to 18 days based on the data
                   T ]; % data time points

    % perturabation to solution meaning injections
       i_edges = [ 0 0 0 0              % t=0
                   0 0 0 0              % t=18
                   zeros(length(T),4)];  % at data set times T similarly

end

end
```

%%%%%%%%%%%%%%%%%%%%%%%%%%%%%%%% END OF CODE %%%%%%%%%%%%%%%%%%%%%%%%%%%%%%%%

%%%%%%%%%%%%%%%%%%%%%%%%%%%%%%%% BEGINNING OF CODE %%%%%%%%%%%%%%%%%%%%%%%%%%%%%%%%

```
% Inheriting parameters r, eta through fmincon done previously.
% Code to reproduce figures for the remaining cases and mainly for the predictions
% figures.

% Written by Elpiniki Nikolopoulou 2019

clear all
clc

% Types of treatments
% Change of Modes based on the different treatments being administrated
mode = 6;       % 1 = Isotype Control Case
                % 2 = NHS muIL-12 (2\mu g)
                % 3 = NHS muIL-12 (10\mu g)
                % 4 = Avelumab (200\mu g)
                % 5 = Avelumab (200\mu g) + NHS muIL-12 (2\mu g)
                % 6 = Avelumab (200\mu g) + NHS muIL-12 (10\mu g)

% List of parameters
mpr  = [ 1e-13       % 1. K_TQ        - inhibition of function of T
                                         %cells by PD-1-PD-L1
         0.001       % 2. sigma       -
         8.81        % 3. lambda_TI12 - activation rate of T cells by IL-12
         7*1e-14     % 4. K_A2        - dissociation constant of A_2
         0.05        % 5. d_T         - death rate of T cells
         0.1136      % 6. d_A1        - degradation rate of Anti-PD-L1
         0.69        % 7. d_A2        - degradation rate of NHS-muIL12
     5.84 * 1e-7     % 8. rho_p       - expression level of PD-1
     2.7635 * 1e-7   % 9. rho_l       - expression level of PD-L1
        1e-13        % 10. K_A1       - dissociation constant of A_1
         50          % 11. epsilon    - expression of PD-L1 in tumor cells
         .02         % 12. delta      - source of activation
          1          % 13. eta        - kill rate of tumor cells by T cells
       0.213];       % 14.  r         - growth rate of tumor cells


[y0,i_edges,t_edges]         = choose(mode,mpr);
[tout,yout,t_edges,y_edges] = SolveODE_all(y0,t_edges,i_edges,mpr);

v = yout(:,1); Tc = yout(:,2); A1 = yout(:,3); A2 = yout(:,4);

if mode == 2

    T = [ 0.0001,  3.0695,    6.1778,    9.9885,   13.1011,   17.0455]';
    V = [ 100,     209.0725,  247.4396, 357.7861,  543.8542, 739.4961]';

elseif mode == 3

    T = [ 0.0001,  2.9814,    6.0907,   10.0274,    12.9175, 17.0779]';
    V = [ 100,    189.4078,   240.5972, 260.6595,  271.7919, 348.8947]';

elseif mode == 4

    T = [ 0.0001,  3.0682,    6.0018,    9.9845,  13.0524,  17.0862]';
    V = [ 100,   166.4033,  214.6746, 233.2142,  373.1919, 637.7322]';

elseif mode == 5

    T = [ 0.0001, 1.8898,    3.6060,  6.3011,   7.8494,   9.4773, 11.5974,...
          13.6362, 14.9415]';
    V = [ 100,  108.6957,  126.8116, 137.6812, 112.3188, 68.8406, 47.1014,...
          28.9855, 21.7391]';

elseif mode == 6

    T = [ 0.0001, 2.5,    4.7,    6.75,  8.48,  10.35, 12.47, 14.46, 15.8]';
    V = [ 100,   127.35, 138.095, 120.45,77.26, 42.57, 27.73, 18.6,  9.69]';
```

```
end

% Tumor volume plot
subplot(1,3,1)
fitted = plot(tout,v,T,V,'o');
hold on
xline(0,'Color',[0, 0.5, 0],'LineWidth', 3)
xline(0,'--r','LineWidth', 3)
text(0.2,650,'Av','Color',[0, 0.5, 0],'fontsize', 18)
text(0.2,600,'NHS','Color','red','fontsize', 15)
hold on
xline(3,'Color',[0, 0.5, 0],'LineWidth', 3)
text(3.2,650,'Av','Color',[0, 0.5, 0],'fontsize', 18)
hold on
xline(6,'Color',[0, 0.5, 0],'LineWidth', 3)
text(6.2,650,'Av','Color',[0, 0.5, 0]','fontsize', 18)
set([fitted],'LineWidth',3)
legend('fitted curve','data points')
title({'Tumor volume against time'},'Interpreter','latex','fontsize', 18)
xlabel({'Time (days) '},'Interpreter','latex','fontsize', 20)
ylabel({'Tumor Volume $\enspace (mm^3)$ '},'Interpreter','latex','fontsize', 20)
ylim([0 800])
xlim([0 20])
set(gcf,'position',[550,100,350,550])
set(gca,'FontSize', 20)
set(gca,'TickLabelInterpreter','latex')

% A_1 plot
subplot(1,3,2)
drug = plot(tout, A1,'Color',[0, 0.5, 0]');
set([drug],'LineWidth', 3)
xlabel({'Time (days) '},'Interpreter','latex','FontSize', 20)
ylabel({'Avelumab $\enspace (200\mu g)\enspace (A_{1})$'},'Interpreter','latex','
    FontSize', 20)
set(gca,'FontSize', 20)
set(gca,'TickLabelInterpreter','latex')

% A_2 plot
subplot(1,3,3)
drug=plot(tout, A2,'r');
set([drug],'LineWidth', 3)
xlabel({'Time (days) '},'Interpreter','latex','fontsize', 20)
ylabel({'NHS-muIL12 $\enspace (10\mu g) \enspace (A_{2})$'},'Interpreter','latex','
    fontsize', 20)
set(gca,'FontSize', 20)
set(gca,'TickLabelInterpreter','latex')
set(gcf,'position',[650,100,900,700])


% Function used to define the ode system.

function dydt = f(t,y,mpr)

    v = y(1); Tc = y(2); A_1 = y(3); A_2 = y(4);      % Define variables

    % Model Parameters

    K_TQ = mpr(1); sigma    = mpr(2);  lambda_TI12 = mpr(3);
    K_A2 = mpr(4); d_T      = mpr(5);        d_A1  = mpr(6);
    d_A2 = mpr(7); rho_p    = mpr(8);       rho_l  = mpr(9);
    K_A1 = mpr(10);epsilon  = mpr(11);      delta  = mpr(12);
    eta  = mpr(13); r       = mpr(14);

    % Equations
```

```
    P     = rho_p * Tc;                          % PD-1 expression
    L_t   = rho_l * (Tc + epsilon * v);          % PD-L1 total expression
    A_1n = A_1 * (1 / (55 * 1e7));
    L_b   = (A_1n /(A_1n + K_A1)) * (rho_l * (Tc + epsilon * v)); % PD-L1
                                                                  %bound expression
    L_f   = L_t - L_b;                           % PD-L1 free expression
    Q     = sigma * P * L_f ;                    % PD-1-PD-L1 complex expression

    % Ode functions
    A_2n = A_2 * (1 / (75 * 1e7));
    dv    =  r * v - (eta * Tc * v);                                % tumor volume DE
    dTc   = (delta + (lambda_TI12 * Tc * A_2n) / (K_A2 + A_2n)) ...
            * (1 / (1 + (Q / K_TQ))) - d_T * Tc;                    % T-cells DE
    dA_1 = - d_A1 * A_1;                                            % A_1 (avelumab) DE
    dA_2 = - d_A2 * A_2;                                            % A_2 (NHS-muIL12) DE

    dydt = [dv; dTc; dA_1; dA_2];

end



function [t_all,y_all,t_edges,y_edges] = SolveODE_all(y0,t_edges,i_edges,mpr)

options      = odeset();           % Initial option setting for ODE solver

[~,IDX]      = sort(t_edges);
t_edges      = t_edges(IDX);
i_edges      = i_edges(IDX,:);

y_edges      = nan(length(t_edges),length(y0));  % create an empty matrix to
                        %update initial conditions based on the time points
y_edges(1,:) = y0';                % first row contains initial conditions

t_all = [];
y_all = [];
for i=1:length(t_edges)-1

    [t_temp,y_temp] = ode15s(@(t,y)f(t,y,mpr),[t_edges(i) t_edges(i+1)],...
                             y_edges(i,:)+i_edges(i,:),options);
    t_all = [t_all;t_temp];
    y_all = [y_all;y_temp];
    y_edges(i   ,:) = y_temp(1,:);
    y_edges(i+1,:) = y_temp(end,:);

end



end

function [y0,i_edges,t_edges]=choose(mode,mpr)
if mode == 1

       y0 = [ 100; 0.03; 0; 0];

       t_edges = [ 0       % time points where things occur such as t0,tf,injT,T
                  18];


   % perturabation to solution meaning injections
       i_edges = [ 0 0 0 0              % at t=0  we don't have injections
                   0 0 0 0];            % at t=18 we don't have injections


elseif mode == 2           % NHS mulL-12 (2\mu g)
```

```
    y0 = [ 100; 0.03; 0; 0];

    t_edges = [ 0                       % time points where things occur
                                        % such as t0,tf,injT,T
                18];
    % perturabation to solution meaning injections
    i_edges = [ 0 0 0 2e-6              % at t=0  we have A2 drug injection
                0 0 0 0];               % at t=18 we don't have injections


elseif mode == 3        % NHS mulL-12 (10\mu g)

    y0 = [ 100; 0.03; 0; 0];

    t_edges = [ 0       % time points where things occur such as t0,tf,injT,T
                18];


% pertubation to solution meaning injections
   i_edges = [ 0 0 0 10e-6              % at t=0  we have A2 drug injection
               0 0 0 0];                % at t=18 we don't have injections


elseif mode == 4        % Avelumab (200\mu g)

        y0 = [ 100; 0.03; 0; 0];

       t_edges = [ 0    % time points where things occur such as t0,tf,injT,T
                   3
                   6
                  18];

% pertubation to solution meaning injections
      i_edges = [ 0 0 200e-6 0          % at t=0  we have A1 drug injection
                  0 0 200e-6 0          % at t=3  we have A1 drug injection
                  0 0 200e-6 0          % at t=6  we have A1 drug injection
                  0 0  0      0];       % at t=18 we don't have injections


elseif mode == 5        % Avelumab 200e-6 + NHS-muIL12 2e-6

       y0 = [ 100; 0.03; 0; 0];


 t_edges = [ 0          % time points where things occur such as t0,tf,injT,T
             3
             6
            18];

 i_edges = [ 0 0 200e-6 2e-6            % at t=0  we have A1,A2 drug injections
             0 0 200e-6   0             % at t=3  we have A1 drug injection
             0 0 200e-6   0             % at t=6  we have A1 drug injection
             0 0   0      0];           % at t=18 we don't have injections


elseif mode == 6  % Avelumab 200e-6 + NHS-muIL12 10e-6

        y0 = [ 100; 0.03; 0; 0];

       t_edges = [ 0     % time points where things occur such as t0,tf,injT,T
                   3
                   6
                  18];

% pertubation to solution meaning injections
       i_edges = [ 0 0 200e-6 10e-6     % at t=0  we have A1,A2 drug injections
```

```
                    0 0 200e-6 0          % at t=3  we have A1 drug injection
                    0 0 200e-6 0          % at t=6  we have A1 drug injection
                    0 0  0     0];        % at t=18 we don't have injections

end
end
%%%%%%%%%%%%%%%%%%%%%%%%%%%%%%%%%% END OF CODE %%%%%%%%%%%%%%%%%%%%%%%%%%%%%%%%%%

%%%%%%%%%%%%%%%%%%%%%%%%%%%%%% BEGINNING OF CODE %%%%%%%%%%%%%%%%%%%%%%%%%%%%%%%%
% function [] = asymptotic_behavior_full_model()
% This code produces the asymptotic behavior of both drugs in combination
% gamma_1 (Avelumab) and gamma_2 (NHS-muIL12) when applied continuously.
% We use the full ODE system. All the parameters below are determined by
% the data, literature review and intuition as listed in the tables.
% By adjusting the ODE system to the limiting system can produce the
% asympototic behavior for the limiting case.

% Instructions to run this code:
% 1. Set myswitch = 1 to run the code for the entire logspace.
% 2. Create a mat file that contains representative points seen in the synergy plot
% represented by the plot_gamma_points.mat in this code. The values of
% gamma_1 and gamma_2 chosen can be seen in the legend on line 129 in this code.
% Note here that you need to add the z-cordinate which can be either 0 or 1
% for each of the differenent points to enable visibility on the plot.
% 3. Set myswitch = 0 to run specified points in "plot_gamma_points.mat" file

% Written by Elpiniki Nikolopoulou 2019

clear all
clc
format long;

myswitch = 1; % 1 = Run the entire logspace
              % 0 = Run only at specified points in "plot_gamma_points.mat" file


%% Variable initializations and memory allocations
if ~myswitch
    load plot_gamma_points.mat ;
end

mpr = [    1e-13    % 1. K_TQ        - inhibition of function of T cells by PD-1-PD-L1
           0.001    % 2. sigma       - fraction of association/dissociation rate
           8.81     % 3. lambda_TI12 - activation rate of T cells by IL-12
           7e-14    % 4. K_A2        - dissociation constant of A_2
           0.1136   % 5. d_A1        - degradation rate of Anti-PD-L1
           0.69     % 6. d_A2        - degradation rate of NHS-muIL12
         5.84e-7    % 7. rho_p       - expression level of PD-1
         2.7635e-7  % 8. rho_l       - expression level of PD-L1
          1e-13     % 9. K_A1        - dissociation constant of A_1
           50       % 10. epsilon    - expression of PD-L1 in tumor cells vs T cells
           0.02     % 11. delta      - source of activation
           1        % 12. eta        - kill rate of tumor cells by T cells
           0.213    % 13. r          - growth rate of tumor cells
           0.05     % 14. d_T        - death of T cells
    ];

    y0       = [100 0.03 0 0];  % initial conditions

    inc      = [0:1:220]';
    time     = [inc] ;      % time points 0-220
    limit    = [190:1:220]; % last 30 time points
    gamma_1  = logspace(-7,log10(9e-5),201);
    gamma_2  = logspace(-9,log10(2e-6),201);

    fprintf('gamma1 a b: %g %g\n',gamma_1(1),gamma_1(end));
```

```
    fprintf('gamma2 a b: %g %g\n',gamma_2(1),gamma_2(end));

    threshold = 100;                % set threshold same as initial condition

    figure(1)
    hold on
    ttt          =  0;
    escape_table = zeros(length(gamma_1),length(gamma_2));
    Ng1          = length(gamma_1);

%% Main code for system solving

    for i = 1:Ng1
        tic
        if (i > 1)
            fprintf('Init --- Loop %d of %d (time %g --- est: %g)\n',i,Ng1,...
                    ttt,(Ng1-i+1)*ttt);
        else
            fprintf('Init --- Loop %d of %d\n',i,Ng1);
        end

        for j = 1:length(gamma_2)

           if myswitch % calculate solution for each combination of gamma_1
                       % and gamma_2 in entire logspace
               [tout,yout] = ode15s(@(t,y)f(t,y,mpr,gamma_1(i),gamma_2(j)),...
                                                    time,y0);
               plot(tout, yout(:,1))
               % create binary table to plot the 3D surface later on
               if max(yout(limit,1)) > threshold  % if solution at the last
                                                  % time points> threshold
                     escape_table(i,j) = 1;       % place 1 in the escape table
                         matrix
               end

           else % calculate solution only for specified gamma_1
                % and gamma_2 points in the saved variable

            Marker={'o','*','s','p','d','x','o'};

               if gamma_1(i) == points(1).Position(2) ...
                   && gamma_2(j) == points(1).Position(1)

                   [tout,yout]= ode15s(@(t,y)f(t,y,mpr,gamma_1(i),gamma_2(j)),...
                                                    time,y0);
                   plot(tout,yout(:,1),'-k*','Linewidth',2,'MarkerSize',10,...
                        'MarkerIndices',1:10:length(tout));

               elseif gamma_1(i) == points(2).Position(2) ...
                       && gamma_2(j) == points(2).Position(1)

                   [tout,yout] = ode15s(@(t,y)f(t,y,mpr,gamma_1(i),gamma_2(j)),...
                                                    time,y0);
                   plot(tout,yout(:,1),'-ms','Linewidth',2,'MarkerSize',10,...
                        'MarkerIndices',1:10:length(tout),'MarkerFaceColor','m');

               elseif gamma_1(i) == points(3).Position(2) ...
                      && gamma_2(j) == points(3).Position(1)

                   [tout,yout] = ode15s(@(t,y)f(t,y,mpr,gamma_1(i),gamma_2(j)),...
                                                    time,y0);
                   plot(tout,yout(:,1),'-gp','Linewidth',2,'MarkerSize',10,...
                        'MarkerIndices',1:10:length(tout));

               elseif gamma_1(i) == points(4).Position(2) ...
                       && gamma_2(j) == points(4).Position(1)
                   [tout,yout] = ode15s(@(t,y)f(t,y,mpr,gamma_1(i),gamma_2(j)),...
```

```
                                                time,y0);
                    plot(tout,yout(:,1),'-cd','Linewidth',2,'MarkerSize',10,...
                        'MarkerIndices',1:10:length(tout),'MarkerFaceColor','c');

                elseif gamma_1(i) == points(5).Position(2) ...
                        && gamma_2(j) == points(5).Position(1)

                    [tout,yout] = ode15s(@(t,y)f(t,y,mpr,gamma_1(i),gamma_2(j)),...
                                                time,y0);
                    plot(tout,yout(:,1),'-bx','Linewidth',2,'MarkerSize',10,...
                        'MarkerIndices',1:10:length(tout));

                elseif gamma_1(i) == points(6).Position(2) ...
                        && gamma_2(j) == points(6).Position(1)

                    [tout,yout] = ode15s(@(t,y)f(t,y,mpr,gamma_1(i),gamma_2(j)),...
                                               time,y0);
                    plot(tout,yout(:,1),'-ro','Linewidth',2,'MarkerSize',10,...
                        'MarkerIndices',1:10:length(tout),'MarkerFaceColor','r');

                else
                    ;
                end
            end

        end
        ttt = toc;
    end

% Prepare figures
    title('Combination treatment (Avelumab and NHS-muIL12)','Interpreter',...
        'latex','fontsize', 20)
    xlabel('Time (days)','Interpreter','latex','fontsize', 20)
    ylabel('Tumor Volume (mm$$^3$$)','Interpreter','latex','fontsize', 20)
    yline(100,'--','Threshold','Fontsize',20,'Linewidth',3,'Interpreter',...
        'latex','fontsize', 20);
    ylim([0 2e3])
    set(gcf,'position',[100,100,740,400])
    set(gca,'FontSize',20)
    set(gca,'TickLabelInterpreter','latex')
    size(gamma_1);
    size(gamma_2);
    size(squeeze(escape_table(:,:,1)));
    legend('\gamma_1 = 9.35\times10^{-7}, \gamma_2 = 1.52\times10^{-6}',...
           '\gamma_1 = 9.71\times10^{-7}, \gamma_2 = 6.55\times10^{-6}',...
           '\gamma_1 = 1.35\times10^{-7}, \gamma_2 = 1.21\times10^{-5}',...
           '\gamma_1 = 5.84\times10^{-8}, \gamma_2 = 5.05\times10^{-5}',...
           '\gamma_1 = 1.25\times10^{-7}, \gamma_2 = 5.05\times10^{-5}',...
           '\gamma_1 = 9\times10^{-7},       \gamma_2 = 5.05\times10^{-5}')

    legend boxoff
    full = squeeze(escape_table(:,:));
    % Once code is done we save the results in "paper.mat"
    if myswitch
        save('paper.mat');
    end

%end %enable if function instead of script

% ------------------------------------------------------------------------
function [dydt] = f(t,y,mpr,gamma_1,gamma_2)

    v=y(1); Tc=y(2); A_1=y(3); A_2=y(4);        % Define variables

    % Model Parameters

    K_TQ     = mpr(1);   sigma = mpr(2);   lambda_TI12  = mpr(3);
```

```
    K_A2    = mpr(4);  d_A1   = mpr(5);          d_A2  = mpr(6);
    rho_p   = mpr(7);  rho_l  = mpr(8);          K_A1  = mpr(9);
    epsilon = mpr(10); delta  = mpr(11);         eta   = mpr(12);
     r      = mpr(13); d_T    = mpr(14);



    % Equations

    P    = rho_p * Tc;                    % PD-1 expression
    L_t  = rho_l * (Tc + epsilon * v);    % PD-L1 total expression
    A_1n = A_1 * (1 / (55 * 1e7));
    L_b  = (A_1n/(A_1n + K_A1)) * (rho_l * (Tc + epsilon * v)); % PD-L1 bound
        expression
    L_f  = L_t - L_b;                     % PD-L1 free expression
    Q    = sigma * P * L_f;               % PD-1-PD-L1 complex expression
    A_2n = A_2 * (1 /( 75 * 1e7));

    % Ode functions
    dv   = r * v - (eta * Tc * v);                                  % tumor volume DE
    dTc  = (delta + (lambda_TI12 * Tc * A_2n) / (K_A2 + A_2n))...
           * (1 / (1 + (Q / K_TQ))) - d_T * Tc;                     % T-cells DE
    dA_1 = gamma_1 - d_A1 * A_1;                                    % A_1 (avelumab) DE
    dA_2 = gamma_2 - d_A2 * A_2;                                    % A_2 (NHS-muIL12) DE

    dydt = [dv; dTc; dA_1; dA_2];

end
%%%%%%%%%%%%%%%%%%%%%%%%%%%%%%%%% END OF CODE %%%%%%%%%%%%%%%%%%%%%%%%%%%%%%%%%

%%%%%%%%%%%%%%%%%%%%%%%%%%%%%%% BEGINNING OF CODE %%%%%%%%%%%%%%%%%%%%%%%%%%%%%%%
% This code produces the synergy plot for the full model case. As before by
% loading the correspondig mat files from the code above can produce
% the synergy plot for the limiting case.

% Written by Elpiniki Nikolopoulou 2019

%% User defined inputs
% Load your results to be plotted

load('paper.mat')    % mat file saved from asymptotic behavior code
% Load the variable of the points you picked to be evaluated

load('plot_gamma_points.mat') % specific points selected to be ploted
close all

%% Plot section for asymptotic surface plot
    figure_asy = figure(2), surf(gamma_2,gamma_1,squeeze(escape_table(:,:)));
    shading flat   % mesh line segment and face has a constant color

    % allocate textboxes on the surface plot
    dim = [.15 .0002 .2 .225];  % dim [x y w h]
    str = ['\bf Tumor escape'];
    annotation('textbox',dim,'String',str,'FontSize',20,'Interpreter',...
               'latex','FitBoxToText','on','EdgeColor','none');

    dim = [.5 .3 .3 .3];  % dim [x y w h]
    str =['\bf Tumor control'];
    annotation('textbox',dim,'String',str,'FontSize',20,'Interpreter',...
               'latex','FitBoxToText','on','EdgeColor','none');

    %colorbar
    axis tight
    title('Asymptotic behavior as a function of $$\gamma_1 $$ and $$\gamma_2 $$ ',...
          'Interpreter','latex','fontsize', 6)
    ylabel({'$$\gamma_1 $$'},'Interpreter','latex','fontsize', 20)
```

```
    xlabel({'$$\gamma_2 $$ '},'Interpreter','latex','fontsize', 20)
    view(0,90)     % change to top view

    for k = 1:length(points)
          Color  = {'r','k','m','g','c','b','r'};
          Marker = {'o','*','s','p','d','x','o'};
          hold on;
          plot3(points(k).Position(1),points(k).Position(2),1,[Color{mod(k,6)+1},...
                Marker{mod(k,6)+1}],'Markersize',9,'MarkerFaceColor',Color{mod(k,6)
                    +1})
    end

    set(gcf,'position',[100,100,740,400])
    set(gca,'FontSize',20)
    set(gca,'TickLabelInterpreter','latex')
% create custom grayscale map
    map = [0.5  0.5  0.5
           0.9  0.9  0.9];
    colormap(map)
    %colormap summer


%% Plot section for logarithmic surface plot
%     figure(3), surf(log10(gamma_2),log10(gamma_1),squeeze(escape_table(:,:)))
%     shading flat   % mesh line segment and face has a constant color
%
%    % allocate textboxes on the surface plot
%     axis tight
%     title('Logarithmic behavior of $$\gamma_1 $$ and $$\gamma_2 $$ ',...
%           'Interpreter','latex','fontsize',14)
%     ylabel({'$$\gamma_1 $$'},'Interpreter','latex','fontsize',20)
%     xlabel({'$$\gamma_2 $$ '},'Interpreter','latex','fontsize',20)
%     view(0,90)     % change to top view
%     set(gcf,'position',[650,100,740,400])
%     set(gca,'FontSize',20)
%     set(gca,'TickLabelInterpreter','latex')
%     colormap summer
%%%%%%%%%%%%%%%%%%%%%%%%%%%%%%%%%% END OF CODE %%%%%%%%%%%%%%%%%%%%%%%%%%%%%%%%%%
```